Neurochemistry of the Hepatic Encephalopathy

By

Anna Hadjihambi*✦

Supervised by

Professor Rajiv Jalan*

& Professor Alexander V Gourine✦

*UCL Institute for Liver and Digestive Health, Division of Medicine

✦Centre for Cardiovascular and Metabolic Neuroscience, Department of Neuroscience, Physiology and Pharmacology, Division of Biosciences

Submitted for a Doctorate of Philosophy in Neuroscience

UNIVERSITY COLLEGE LONDON

I, Anna Hadjihambi confirm that the work presented in this thesis is my own. Where information has been derived from other sources, I confirm that this has been indicated in the thesis.

Anna Hadjihambi

15th of September, 2017

Abstract

The pathogenesis of hepatic encephalopathy (HE) in cirrhosis is multifactorial and the role of ammonia remains controversial. Experimental studies conducted in animal (rat) models of HE, in combination with pharmacological approaches, were used to test the hypothesis that during HE, chronic exposure to elevated ammonia concentrations alters cerebral oxygenation, compromises lactate transport between astrocytes and neurons, and impairs uptake of neurotransmitters. It was also hypothesised that HE impairs glymphatic clearance mechanisms, either as a cause or a consequence of the disease, which exacerbates the detrimental central nervous effects of the accumulated toxins. The results of the experiments described in this thesis suggest that in HE: a) ammonia compromises cerebral oxygenation, but does not affect cerebrovascular reactivity, b) ammonia mediates cortical hemichannel dysfunction and impairs channel-mediated lactate release, potentially interfering with the astrocyte-neuron lactate shuttle, c) hyperammonemia results in a significant increase in cortical extracellular glutamate concentration, which is exacerbated under hypoxic conditions, and d) efficacy of glymphatic clearance is affected in discrete regions of the brain, which aligns with specific cognitive/behavioral impairments. These findings provide the first evidence of a critical pathophysiological role of ammonia in inducing neuronal energy deficit in HE due to impaired cerebral oxygenation, compromised hemichannel-mediated lactate transport between astrocytes and neurons and affected glymphatic clearance.

Impact statement

The work presented in this PhD thesis demonstrates novel data regarding the understanding of the neurochemistry of hepatic encephalopathy and the mechanism behind it. This PhD has been a collaboration between two departments; the Liver and Digestive Health as well as Neuroscience, Physiology and Pharmacology. This interdisciplinary research allowed us to investigate the proposed hypothesis using a different approach, focusing mainly on the neuroscience aspect of the disease. The reported results give new insights into the mechanism of the pathophysiology and treatment of hepatic encephalopathy. Subsequently, it will allow other scientists and clinicians to study these mechanisms further, as well as consider new approaches in terms of diagnosis, prevention and treatment.

The methods used in this study are novel in the field of hepatic encephalopathy and they will potentially encourage collaboration between hepatologist and neuroscientist, which will bring new ideas to the field. I have also presented this work (oral and poster presentations) in several international meetings, networked with other scientists, and had the opportunity to mentor undergraduate students and teach them the experimental techniques applied in this study. Finally, this PhD has equipped me with sufficient experience that enables me to share my knowledge through teaching and writing fellowships, which is the stepping-stone to continue contributing to high impact research.

Acknowledgments

Rajiv Jalan and Alex Gourine have been great supervisors during this PhD. I am very grateful for the opportunities Rajiv has provided me with in terms of publishing, as well as the trust and freedom he gave me with experiments. I am extremely grateful for the constant support and encouragement Alex has provided me with. I am also thankful for Alex's encouragement in applying for this PhD and every advice he gave me. I have been very lucky to work in Alex's laboratory for the past 5 years and I am very thankful for everyone's help and support. I am also thankful for everyone at the Liver and Digestive health group, especially Rocio, Winston, Graziella, Gautam and Abe.

Special thanks to my family and my friends Curtis Acti, Lilya Andrianova, Marie Holt and the neurogeeks who really helped me come this far. I would also like to thank all my friends who kept me going during this PhD especially Chrisina Elia for her artistic advice. Elena Flouri has been an absolute star with proof reading this thesis. Thanks to everyone else who invested time in this work.

Thanks to Dr. Patrick Hosford who has been next to me, helping me and inspiring me the past 3 years. Thanks to Dr. Svetlana Mastitskaya who has been a great support system through the years. Also thanks to Dr. Isabel Christie and Dr. Alla Korsak who was always happy to help me and comfort me.

Publications

Hadjihambi, A., Harrison, I. F., Arias. N., Gallego-Durán, R., Hosford, P. S., Davies, N., Habtesion, A., Lythgoe, M. F., Gourine, A. V. & Jalan, R. Impaired Brain Glymphatic Flow in Chronic Liver Disease. BioRxiv pre-printer.

Hadjihambi, A., Arias. N., Sheikh, M. & Jalan, R. 2017. Hepatic Encephalopathy – A critical current review. *Hepatology International*.

Hadjihambi, A., Arias. N. & Jalan, R. 2017. Hepatic Encephalopathy. *SA Hepatology*. In press

Hadjihambi, A., De Chiara, F., Hosford, P. S., Habtetion, A., Karagianis, A., Davies, H., Gourine, A. V. & Jalan, R. 2017. Ammonia mediates cortical hemichannel dysfunction in rodent models of chronic liver disease. *Hepatology*, 65, 1306-1318

Karagiannis, A., Sylantyev, S., Hadjihambi, A., Hosford, P. S., Kasparove, S & Gourine, A. V. 2016. Hemichannel-mediated release of lactate. *J Cereb Blood Flow Metab*, 36, 1202-11.

Hadjihambi, A. & Jalan, R. 2015. Hepatic encephalopathy: New treatments. *Clinical Liver Disease*, 5, 109-111.

Hadjihambi, A., Khetan, V. & Jalan, R. 2014. Pharmacotherapy for hyperammonemia. *Expert Opin Pharmacother*, 15, 1685-95

Hadjihambi, A., Rose, C. F. & Jalan, R. 2014. Novel insights into ammonia-mediated neurotoxicity pointing to potential new therapeutic strategies. *Hepatology*, 60, 1101-3.

Conference proceedings

Hadjihambi, A.,* Hosford, P. S.,* Davies, N., Habtesion, A., Jalan, R. & Gourine, A. V (2017). Ammonia mediates impaired cerebral oxygenation in an animal model of hepatic encephalopathy. *Poster presentation at EASL.*

Hadjihambi, A.,* Harrison, I. F.,* Arias. N., Gallego-Durán, R., Hosford, P. S., Davies, N., Habtesion, A., Lythgoe, M. F., Gourine, A. V. & Jalan, R. (2017) Impaired Brain Glymphatic Flow in Chronic Liver Disease. *Poster presentation as EASL.*

Hadjihambi, A., De Chiara, F., Hosford, P. S., Habtetion, A., Karagianis, A., Davies, H., Gourine, A. V. & Jalan, R. 2017. Ammonia mediates cortical hemichannel dysfunction in rodent models of chronic liver disease. *Oral presentation at ISHEN.*

Hadjihambi, A.,* Harrison, I. F.,* Arias. N., Gallego-Durán, R., Hosford, P. S., Davies, N., Habtesion, A., Lythgoe, M. F., Gourine, A. & Jalan, R. (2017) Impaired Brain Glymphatic Flow in Chronic Liver Disease. *Poster presentation as ISHEN.*

Hadjihambi, A., De Chiara, F., Hosford, P. S., Habtetion, A., Karagianis, A., Davies, H., Gourine, A. V. & Jalan, R. (2016). Understanding how liver disease impairs brain function. *Oral presentation at the China-UK glial club 2016.*

Hadjihambi, A., De Chiara, F., Hosford, P. S., Habtetion, A., Karagianis, A., Davies, H., Gourine, A. V. & Jalan, R. (2016). Hepatic encephalopathy is associated with impaired hemichannel mediated release of lactate in the cerebral cortex. *Poster presentation at SfN*

Hadjihambi, A., De Chiara, F., Hosford, P. S., Habtetion, A., Karagianis, A., Davies, H., Gourine, A. V. & Jalan, R. (2016). Ammonia mediates cortical hemichannel dysfunction in rodent models of chronic liver disease. *Oral presentation at Gap Junction Meeting 2016.*

Hadjihambi, A., De Chiara, F., Hosford, P. S., Habtetion, A., Karagianis, A., Davies, H., Gourine, A. V. & Jalan, R. (2016). Alterations in the CNS hemichannel functionality and neurochemical phenotype during the pathogenesis of Hepatic Encephalopathy. *Poster presentation at EASL 2016*

Hadjihambi, A., De Chiara, Habtetion, A., Davies, H., Gourine, A. V. & Jalan, R. (2015). Role of connexins in the pathogenesis of Hepatic encephalopathy. *Poster presentation at the Gordon conference*

Hadjihambi, A., De Chiara, Habtetion, A., Davies, H., Gourine, A. V. & Jalan, R. (2015). Changes in the CNS connexin 43 expression and function in the pathogenesis of Hepatic encephalopathy. *Poster presentation at EASL*

Hadjihambi, A., Gourine, A. V. & Jalan, R. (2014). Role of connexins in the pathogenesis of Hepatic encephalopathy. *Poster presentation at EASL.*

Hadjihambi, A., Gourine, A. V. & Jalan, R. (2014). Neurochemistry of the Hepatic encephalopathy. *Oral presentation at the School of Astrocytes Italy.*

Abbreviations

aCSF	Artificial cerebrospinal fluid
ACTZ	Acetazolamide
ALF	Acute liver failure
Alz	Alzheimer
AQP4	Aquaporin-4
BBB	Blood brain barrier
BDL	Bile duct ligated
Ca^{2+}	Calcium
Cl^-	Chloride
CBF	Cerebral blood flow
CBX	Carbenoxolone
CBXF	Carboxyfluorescein
CLD	Chronic liver disease
$CMRO_2$	Cerebral metabolic rate of oxygen
CNS	Central nervous system
COX-2	Cyclooxygenase-2

CSF	Cerebrospinal fluid
EAAT	Excitatory amino acid transporters
EMG	Electromyogram
eNOS	Endothelial nitric oxide synthase
GABA	Gamma-aminobutyric acid
GFAP	Glial fibrillary acidic protein
GJ	Gap junctions
GLUT-1	Glucose transporter 1
GS	Glutamine synthetase
HA	Hyperammonemia
HE	Hepatic encephalopathy
IC	Intracellular
ICP	Intracranial pressure
IL-1	Interleukin-1
iNOS	Inducible nitric oxide synthase
IP3	Inositol triphosphate
ISF	Interstitial fluid
K^+	Potassium
KO	Knock-out

LPS	Lipopolysaccharide
MAP	Mean arterial blood pressure
MCTs	Monocarboxylate transporters
mHE	Minimal HE
Na^+	Sodium
NH_3	Ammonia
NH_4^+	Ammonium ion
NMDA	N-Methyl-D-aspartate
NO	Nitric oxide
NPPB	5-Nitro-2-(3-phenylpropylamino) benzoic acid
OP	Ornithine phenylacetate
PAG	Phosphate-activated glutaminase
PBS	Phosphate buffered saline
PET	Positron emission tomography
PFA	Paraformaldehyde
PGE_2	Prostaglandin E_2
PO_2	Partial pressure of oxygen
ROI	Region of interest
ROS	Reactive oxygen species

RT-qPCR	Quantitative real-time PCR
SEM	Standard error mean
SIRS	Systemic inflammatory response syndrome
TNF-α	Tumor necrosis factor
VSMC	Vascular smooth muscle cells
4-CIN	α-Cyano-4-hydroxycinnamic acid

Table of Contents

Table of Figures

Table of Tables

Chapter 1: Background

1.0 Introduction

The liver is responsible for many bodily functions of complex organisms characterising its vital role in life. When liver failure occurs, severe complications arise making the understanding of the pathophysiology of liver disease critical. Liver failure is classified as acute (ALF) or chronic liver disease (CLD), while a new category has recently been introduced known as acute-on-chronic liver failure (Jalan et al., 2014). ALF is the acute liver injury (hepatocellular necrosis) occurring within hours up to 6 months after the onset of jaundice (O'Grady et al., 1993, Bosoi and Rose, 2013a). ALF is more frequently caused by drug intoxication and hepatotoxicity, with the main cause in the UK and the US being acetaminophen overdose. Moreover, acute viral hepatitis (A/B) and autoimmune hepatitis can also be responsible for ALF, while a large proportion of aetiologies are still to be identified (O'Grady et al., 1993, Bosoi and Rose, 2013a). On the other hand, CLD occurs due to a chronic deterioration of the liver function by a persistent, long-term hepatic insult. The time course of this disease is longer, 10-30 years, with the result of development of cirrhosis. This is mainly caused by chronic viral hepatitis, long term alcohol consumption as well as accumulation of fat deposits in the liver (non-alcoholic fatty liver disease, non-alcoholic steatohepatitis) (Rosselli et al., 2013, Bosoi and Rose, 2013a).

1.1 Hepatic encephalopathy: Pathogenesis

The liver and the brain interact greatly, with the most important function of the liver being the removal of toxic substances (including neurotoxins such as ammonia and manganese) from the blood (Butterworth, 2002). As a result, a dysfunction in the liver can easily disrupt the brain function and result in what we know as hepatic encephalopathy (HE). HE is defined as “brain dysfunction caused by liver insufficiency and/or porto-systemic shunting manifesting as a wide spectrum of neurological or psychiatric abnormalities ranging from subclinical alterations to coma” (American Association for the Study of Liver and European Association for the Study of the, 2014). The clinical symptoms, as indicated by the above definition, are widely variable extending from subtle impairment in mental state, fine motor and psychomotor functions to coma. The progression and development of HE is believed to occur due to various distinct pathophysiological mechanisms such as inflammation (Jalan et al., 2004b), oxidative stress (Bosoi and Rose, 2013b), impaired blood brain barrier (BBB) permeability (Haussinger et al., 2000), impaired energy metabolism of the brain (Rama Rao and Norenberg, 2012) and (the most common) the neurotoxic effects of high ammonia concentrations (Shawcross and Jalan, 2005). Some of these factors, summarised on Figure 1 will be further discussed in the following sections with more emphasis on the role of ammonia, as it has been the main focus of this project.

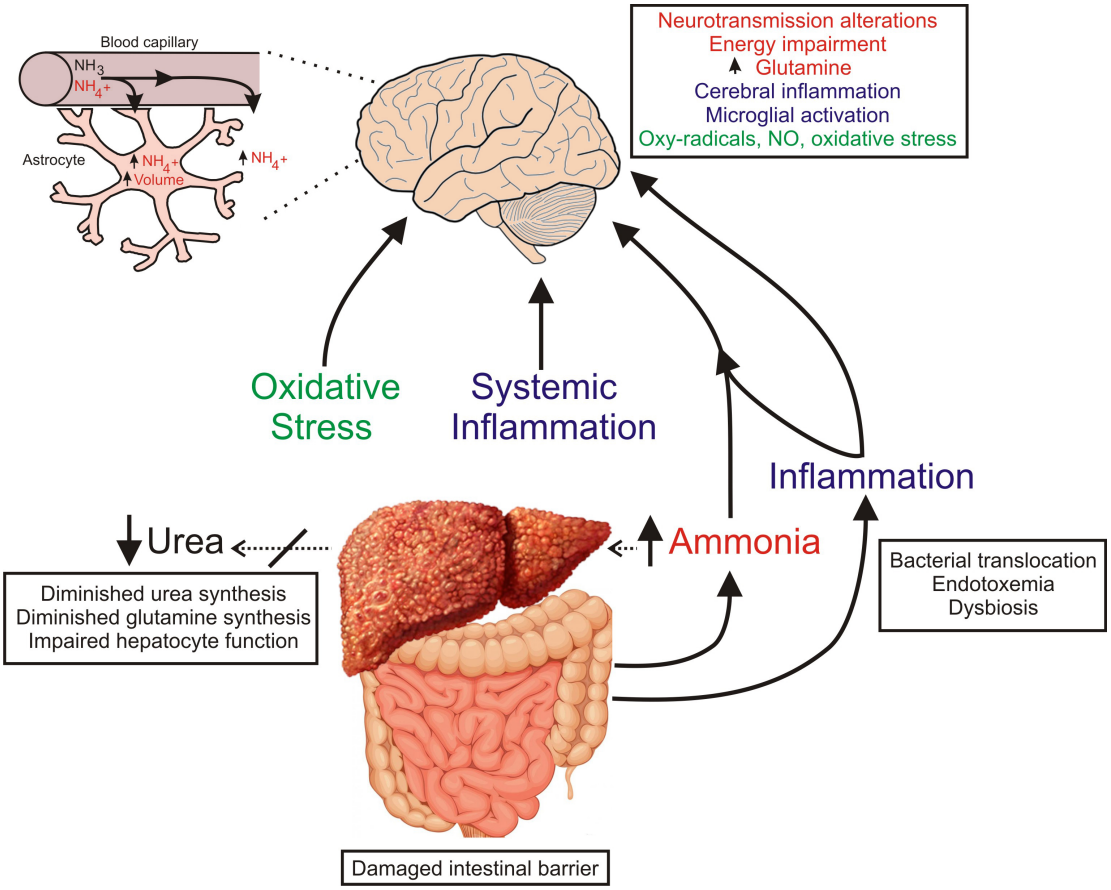

Figure 1: Factors contributing to the pathogenesis of HE. Factors contributing to the pathogenesis of HE with emphasis on the systemic effects of ammonia and inflammation developing due to liver disease. NO: nitric oxide; NH_3: ammonia; NH_4^+: ammonium ions

1.1.1 Ammonia

Ammonia is a ubiquitous by-product of nitrogen metabolism and several metabolic disorders may develop due to its accumulation (Burton, 2000, Hadjihambi et al., 2014a). The primary source of ammonia production is the gut. This takes place in the enterocytes and the ammonia-generating intestinal bacteria through the enzyme phosphate-activated glutaminase (PAG), catalysing deamination of glutamine to glutamate (Kato et al., 1992). Most ammonia is normally detoxified by the liver through the urea cycle (Bosoi and Rose, 2013a, Cooper and Plum, 1987). Further metabolism takes place in a smaller scale in the muscles, heart, kidneys and the brain (Wakim-Fleming, 2011).

Ammonia exists in equilibrium with the ionic (NH_4^+) and gas form (NH_3), crossing all plasma membranes by passive diffusion. Neurons produce as much NH_4^+ as they do glutamate (both linked to the glutamate-glutamine cycle discussed later) (Schousboe et al., 2013, Lerchundi et al., 2015). Brain tissue ammonia increases within seconds of neuronal activity and it is quickly captured by astrocytes. Due to the similar ionic properties of NH_4^+ with potassium (K^+), in terms of charge and diameter, NH_4^+ crosses biological membranes through K^+ channels, as well as K^+ cotransporters [sodium (Na^+)/K^+, H^+/K^+ ATPase and Na^+-K^+-Cl^- cotransporters] (Moser, 1987, Nagaraja and Brookes, 1998) (Brookes, 2000, Marcaggi and Coles, 2001). Due to the permeability of ammonia across the BBB, toxic concentrations can easily be reached in the brain when systemic concentrations arise above normal (Bosoi and Rose, 2009). Furthermore, ammonia can influence the passage of various branched

chain and aromatic amino acids which can eventually result in impaired serotonergic and glutametergic neurotransmission (Skowronska et al., 2012, Cauli et al., 2009).

During liver disease, hyperammonemia develops due to urea cycle defects and increases in gut bacterial translocation (unknown mechanisms). Studies by Felipo et al. (Felipo and Butterworth, 2002a) have also shown that children with congenital urea cycle enzyme defects have a high serum ammonia concentration, which leads to severe neurological symptoms, seizure and coma if left untreated, resembling the symptoms of HE.

The development of hyperammonemia in HE received considerable attention in the early 18th century with the experiments of Pavlov, Nencki and Zaleski using dogs that underwent portacaval fistula surgery, developing neuropsychiatric changes, with worsening of symptoms when the dogs were fed with meat (Hahn M, 1893). This led to the term “meat intoxication syndrome”. In 1991, direct evidence for the role of ammonia in the pathogenesis of HE was obtained by Lockwood et al., (Lockwood et al., 1991), with the use of radiolabeled nitrogen in positron emission tomography (PET) imaging studies of patients with severe liver disease and minimal HE (mHE) (Prakash and Mullen, 2010). Several studies since then have suggested that in ALF, the arterial ammonia concentration correlates with intracranial pressure (ICP), severity of clinical presentation and death by brain herniation (Jalan et al., 2004b, Clemmesen et al., 1999, Bernal et al., 2007, Bosoi and Rose, 2013a). On the other hand, in CLD (approximately 10% of the patients) direct correlation between ammonia and severity of HE is not consistently observed. Examples include

comatose patients with normal arterial ammonia concentrations (Nicolao et al., 2003, He Y, 2011), suggesting the involvement of other factors in the pathogenesis of HE.

Despite the lack of correlation with severity of HE, elevated ammonia has detrimental consequences in the brain, such as depression of synaptic transmission (Cordoba et al., 2003, Butterworth, 2000). Furthermore, neurons exposed to elevated ammonia (or K^+) levels, have increased intracellular chloride (Cl^-) content, which can result in neuronal disinhibition (Benjamin et al., 1978, Dzhala et al., 2010). During health, the enzyme glutamine synthetase (GS), which is abundant in the liver, incorporates ammonia into glutamate (in equimolar concentrations), forming glutamine and consuming ATP. However, when liver failure occurs, this pathway is unavailable, and therefore other organs expressing GS such as muscles, kidney and brain, become the primary ammonia-detoxifying pathway (Rose, 2012, Olde Damink et al., 2009). Astrocytes are the only cells in the brain that express this enzyme. It is therefore believed that due to glutamine being an osmolite, its accumulation results in volume changes in astrocytes referred to as “swelling”, leading to cerebral oedema and increased ICP (Norenberg, 1977) (Haussinger et al., 2000).

Ammonia also appears to have a direct effect on astrocytes. A decrease in glial fibrillary acidic protein (GFAP) (Sobel et al., 1981), glycogen, altered protein phosphorylation, cyclic adenosine monophosphate levels and impairment in uptake of K^+, myo-inositol as well as calcium (Ca^{2+}) has been reported. *In vitro* culture studies by Rama Rao et al., (Rama Rao et al., 2003) suggested that high concentrations of ammonia could increase the astrocytic expression of glucose

transporter 1 (GLUT-1) (Belanger et al., 2006) and aquaporin-4 (AQP4), the main water channel in the brain, two systems central to cerebral volume regulation (Nicchia et al., 2005).

1.1.2 Inflammation

The effects of increased ammonia alone cannot explain all of the neurological changes that characterize HE. In 2000, Rolando and his colleagues (Rolando et al., 2000) suggested that in ALF patients, the presence of a systemic inflammatory response syndrome (SIRS), characterised by the abnormal regulation of cytokines, associated with manifestations such as high body temperature, heart rate, tachypnea and abnormal white blood cells, resulted in a poorer neurological outcome. Cerebral inflammation has been demonstrated to contribute to the development of HE (Butterworth, 2011, Jalan et al., 2004b) while the study of Shawcross et al., (Shawcross et al., 2004), indicated that inflammatory mediators, such as proinflammatory cytokines and nitric oxide (NO), worsens the neuropsychological effects of hyperammonemia in patients with cirrhosis. In this study, resolution of the inflammation was associated with improvement in the mental state, despite the same degree of liver dysfunction and plasma ammonia concentration, highlighting the importance of inflammation in the neuropsychological phenotype of HE.

Furthermore, in ALF patients, serum proinflammatory cytokines have shown to be correlated with brain oedema and high ICP (Gupta et al., 2010, Jalan et al., 2004b). A similar phenotype has been reported in animal models of HE. In these animals,

hypothermia and antibiotic treatment indicated beneficial effects in brain oedema attenuation as well as decrease in serum and cerebral cytokines (Jiang et al., 2009b, Jiang et al., 2009a). Similarly, Bémeur et al., (Bemeur et al., 2010) demonstrated that brain oedema development was suppressed in interleukin-1 (IL-1) (IL-1β and IL-1 receptor type 1) and tumor necrosis factor (TNF-α) knock-out (KO) ALF mice. The link between inflammation and brain oedema has also been observed in CLD (Montoliu et al., 2009) indicating serum proinflammatory cytokines TNF-α, IL-6 and IL-8 being higher in cirrhotic patients with mHE than those without HE, agreeing with the findings of Shawcross et al., (Shawcross et al., 2007).

It is now clear that the systemic immune system communicates with the brain in response to infection and inflammation (Hosoi et al., 2002). The exact mechanism by which inflammation modulates the neuropsychological response to hyperammonemia is still unknown. Cytokines may modulate ammonia diffusion within the central nervous system (CNS) since the release of IL-6, TNF-α, and IL-1β during inflammation increases the BBB permeability (de Vries et al., 1996), as well as ammonia diffusion across astrocytes (Duchini et al., 1996). Finally, the astrocytic release of TNF-α and glutamate further activate microglia (Bezzi et al., 2001), and can lead to neuronal death (Glass et al., 2010, McCoy and Tansey, 2008).

Impaired neurotransmission has also been associated with microglial activation and increased cerebral cytokine synthesis has been reported in animal models of HE (Rodrigo et al., 2010). Additionally, Zemtsova et al., (Zemtsova et al., 2011) using *in vitro* and *in vivo* evidence, as well as postmortem brain tissue, indicated that

ammonia directly activates primary rat microglial (induction of activation marker proteins, such as Iba-1) and stimulates microglial migration (characteristic of activated phenotype). Ammonia also up-regulates the synthesis of reactive oxygen species (ROS) proposing the involvement of microglia in inducing oxidative stress, but has no effect on glutamate release, induction of inducible nitric oxide synthase (iNOS), cyclooxygenase-2 (COX-2; source of proinflammatory prostanoids) and synthesis of prostaglandins and proinflammatory cytokines. This study suggests that microglia become activated by ammonia but do not reflect the fully reactive microglia phenotype. This has also been shown in the cerebral cortex from patients with cirrhosis and HE but not in cirrhotic patients without HE, proposing that the reported phenotype is a feature of HE but not cirrhosis itself (Zemtsova et al., 2011).

1.1.4 Brain oedema and energy metabolism

One characteristic of HE is brain oedema, defined as the excess accumulation of fluid in the intracellular or extracellular space of the brain (Bosoi and Rose, 2013a). This can lead to increased ICP, mainly seen in ALF and less frequently in CLD patients, which can result in brainstem herniation and death (Jalan et al., 2004a, Larsen et al., 1996). Brain oedema can arise either due to cytotoxic, alterations in cellular metabolism, or vasogenic mechanisms, which involve the breakdown of the BBB. However, instead of a severe oedema observed in ALF, mild cytotoxic or no oedema, is seen in CLD (Felipo and Butterworth, 2002b). The variability of results reported in these studies regarding brain oedema in CLD is probably due to the differences in animal models used (Jayakumar et al., 2013).

In ALF unlike CLD, the deficiency of energy metabolism associated with brain oedema has been described. This energy dysfunction is believed to be due to a compromised tricarboxylic acid cycle enzyme, α-ketoglutarate dehydrogenase activity, limited anaplerotic flux and saturated capacity of astrocytes to detoxify ammonium by glutamine synthesis, increased lactate synthesis as well as mitochondrial permeability transition induced by oxidative stress (Rama Rao and Norenberg, 2012, Zwingmann, 2007). At later stages of the disease, several mechanisms have been proposed where ammonia detoxification increases glutamine concentrations intracellularly, which could secondarily impact energy metabolism through an initial osmotic stress, while changes in the glutamate-glutamine cycle follow.

1.2 Astrocytes

Astrocytes are one of the most numerous glial cells in the brain (Pope, 1978). Until recently, their function was thought to be restricted to the provision of structural and metabolic support to neurons. However, we are now able to appreciate their plasticity and active role in the control of neuronal activity and information processing (Navarrete et al., 2012, Sofroniew and Vinters, 2010). Astrocytes are divided in two main subtypes, fibrous (white matter) and protoplasmic (grey matter), according to their anatomical location and cellular morphology (Ramon Y, 1909). A common characteristic of astrocytes is their fine branching processes (Bushong et al., 2002), which allows them to make extensive contacts with parenchymal and pial blood vessels and therefore be involved in cerebral blood flow (CBF) regulation (Attwell et

al., 2010) and control of brain energy metabolism (Sofroniew and Vinters, 2010). Furthermore, astrocytes are estimated to contact several hundred dendrites from multiple neurons and enwrap about 100,000 synapses (Halassa et al., 2007b, Sofroniew and Vinters, 2010, Bushong et al., 2002) a concept known as the "tripartite synapse" (pre-post synaptic terminal and glial process) (Araque et al., 1999, Haydon et al., 2009). This property allows astrocytes to be involved in processes such as glial transmission; release of glutamate, ATP/adenosine, D-Serine and more, as well as neurotransmitter recycling (uptake and enzymatic processing) to avoid neurotoxicity at periods of high neuronal activity (Halassa et al., 2007a, Sofroniew and Vinters, 2010, Henneberger et al., 2010). Furthermore, astrocytes are believed to be actively involved in K^+ buffering (ion and pH synaptic homeostasis) (Kofuji and Newman, 2004, Wallraff et al., 2006) and supply of lactate (astrocyte-neuron lactate shuttle) (Magistretti, 2011, Tsacopoulos and Magistretti, 1996) to neurons when in demand.

Unlike neurons, astrocytes are not electrically excitable. However, they form multicellular networks coupled by gap junctions (GJ) and communicate via intracellular Ca^{2+} excitability (Cornell-Bell et al., 1990). These Ca^{2+} transients can pass between astrocytes and across large networks of cells allowing long distance communication with other astrocytes. The vast number of receptors and transporters that astrocytes express reflects their importance in the brain. These including AQP4, K^+ and glucose transporters, neurotransmitter transporters for glutamate and GABA, that serve to maintain healthy concentrations in the synaptic space, as well as purinergic receptors and hemichannels formed by connexins (S. R. McIver, 2013, Sofroniew and Vinters, 2010). Moreover, astrocytic end-feet are believed to be

contributing to the cellular constituent of BBB (Haussinger et al., 2000, Ballabh et al., 2004).

There is remarkable heterogeneity in astrocyte population, between different species and brain regions in terms of their receptor expression, GJ coupling, membrane currents and morphology (Matyash and Kettenmann, 2010). However, the plasticity and complexity of these cells during disease, damage or neuronal activity is remarkable, which has made them an interesting target for research. Figure 2 summarises the astrocytic functions in the healthy brain.

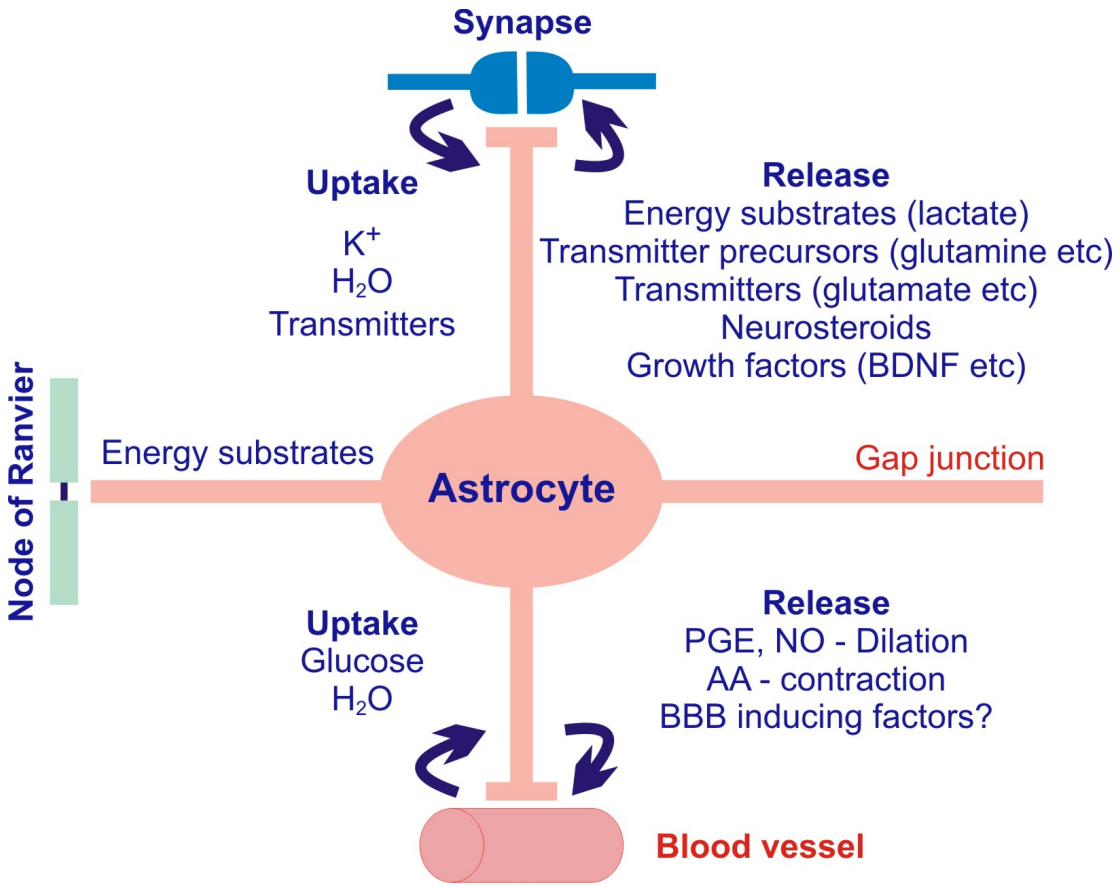

Figure 2: A schematic summarising the astrocytic function in healthy central nervous system. Modified from (Sofroniew and Vinters, 2010)

1.2.1 Astrocytes and their role in HE: Is astrocytic "swelling" the main problem?

During the course of the disease, once the ammonia disposal capacity of the kidney is exceeded, the astrocytes become the major source of detoxification via the enzyme GS (Dejong et al., 1993). Furthermore, being an important constituent of the BBB, allowing trans-astrocytic transport of substances from the blood to the brain, astrocytes could be responsible for alterations in BBB permeability (Haussinger et al., 2000).

Interestingly, most of the research in the field has been focused on the anatomical alterations of astrocytes, referred to as "swelling". Is this however the main problem when it comes to the development and progression of the disease?

Traditionally, it was believed that astrocytes swell due to the increase in intracellular glutamine (more profoundly in ALF), contributing to the neurological phenotype observed. Swelling in most cells leads to transport changes designed to cause shrinkage of the cells back to the normal levels, a process known as "regulatory volume decrease". These alterations in terms of transport can be due to stretch-activated ion channels (Kimelberg et al., 1990). Oligodendrocytes, unlike astrocytes, were rarely found to swell under pathological conditions *in situ*, as demonstrated by the electrophysiological studies of Kimelberg and colleagues (Kimelberg et al., 1990). In the same study, it was observed that astrocytic cell-cell coupling decreased when the swelling-like phenotype was detected. This can therefore have major

effects on the functionality of astrocytes as it can reduce spatial buffering of K^+ and other substances aimed for removal from the CNS. However, these studies have been undertaken in 1990s and a great amount of knowledge has been gained since then.

Despite all the critical research being carried out on the astrocytic swelling phenotype in the pathogenesis of HE, a recent study by Rangroo Thrane et al., (Rangroo Thrane et al., 2013) challenged the hypothesis of astrocyte swelling and brain oedema contributing to the onset of ammonia-induced neurological dysfunctions. In this study, they examined the direct effect of ammonia on intact nervous tissue, avoiding the adaptive changes arising due to chronic exposure (such as that seen in CLD), as well as any ammonia-independent pathology accompanying liver disease. While current literature suggests that astrocyte swelling underlies ammonia neurotoxicity seen in HE, most work done in this area consisted mainly of *in vitro* (cultures-artefact of young age) preparations exposed to high doses of ammonia and post-mortem studies in late stages of HE. Rangroo Thrane and colleagues using *in vivo* two-photon imaging observed transient astrocyte shrinkage after i.p ammonia injection, lasting from 10 to 30 minutes post infusion. This observation contradicts previous hypotheses on astrocytic swelling due to hyperammonemia (Hadjihambi et al., 2014b), although time scale at which swelling was measured in other studies was not always specified.

Work by Butterworth (Butterworth, 2002) has suggested that reducing ammonia influx into astrocytes by inhibiting GS, in order to prevent swelling, could improve

clinical outcomes. However, in awake animals this treatment worsened the neurological phenotype by increasing the overall $[NH_4^+]_o$ and $[K^+]_o$ load on neurons, as these were no longer buffered by astrocytes (Rangroo Thrane et al., 2013). However, ammonia may not be the only mechanism by which astrocyte swelling is triggered in HE. The same phenotype has also been observed *in vitro* under the influence of some neurotransmitters (Bender and Norenberg, 1998, Kimelberg HK, 1993), benzodiazepines (Bender and Norenberg, 1998, Norenberg, 1998), TNF-α (Bender AS, 1992) and hyponatremia (independent predictor of overt HE increasing the risk by a factor of eight) (Wakim-Fleming, 2011, Schliess et al., 1996, H. K. Kimelberg, 1993).

Finally, the changes seen in astrocytes cannot easily be defined as swelling but more as a form of astrogliosis. An example of this, is the Alzheimer type II astrocytosis seen in later stages of CLD, which involves large cells with enlarged nuclei and cytoplasm, margination of chromatin, mitochondrial and rough endoplasmic reticulum (Norenberg, 1977).

1.2.2 Astrocyte-neuron communication

Through the years, the importance of astrocyte-neuronal communication has been established. Understanding the role of astrocytes beyond their metabolic and structural support to neurons but also in the modulation of neuronal excitation, as well as their involvement in the control of breathing (Gourine et al., 2010), memory (Henneberger et al., 2010) and other processes has been a breakthrough. In

contrast to the well-established alterations of astrocyte morphology, neuronal changes have generally been considered to be absent or insufficient to explain the neurological features of HE. Histopathologic studies from patients indicate selective loss of dopamine D_2 receptor density (globus pallidus/putamen), loss of serotonin $5HT_{1A}$ sites (cortical/hippocampal), pseudolaminar cortical necrosis and neuronal cell loss (basal ganglia, thalamus and cerebellum) (Butterworth, 2007) (Chen et al., 2014). However, the extent of neuronal cell death in the brains of patients and animal models of HE, is considerably less than what would be predicted, suggesting the involvement of other cells, such as astrocytes, in protecting the neurons during the development of the disease. This underlines the importance of studying the astrocyte-neuron communication with the aim of further understanding how astrocytic dysfunction contributes to the neuropsychiatric complications arising due to the disease.

1.2.3 Astrocyte-neuron lactate shuttle

Brain information processing requires constant and sufficient supply of oxygen and metabolic substrates. Astrocytes store glycogen (the only cells that have this feature) and represent an important source of lactate, which contributes to the extracellular pool of readily available metabolic substrates taken up by neurons to fuel their activity (Pellerin and Magistretti, 1994, Cataldo and Broadwell, 1986). As suggested by the astrocyte-neuron lactate shuttle, lactate produced by astrocytes is released into the extracellular space where it's taken up by neurons (Pellerin and Magistretti, 1994, Pellerin and Magistretti, 2012). This mechanism is believed to exist for the

supply of lactate as one (even primary) fuel to meet metabolic demands of active neurons (Patet et al., 2015). Furthermore, *in vivo* studies exist proposing the idea that lactate release reduces the glutamate induced neurotoxicity and exerts a neuroprotective effect (Ros et al., 2001). While previously, lactate transport across the cell membranes was thought to be achieved solely via operation of monocarboxylate transporters (MCTs), a recent study (Karagiannis et al., 2016) demonstrated the role of connexin hemichannels (discussed in more detail in section 1.3) as equally important conduits of lactate transport across the membrane.

1.2.4 Brain lactate and liver disease

Recent data has indicated that physiological levels of ammonia applied to astrocytes in mixed cortical cultures and in the somatosensory cortex of anesthetised rats, cause an acute rise in cytosolic lactate followed by its release (Lerchundi et al., 2015). This is believed to be due to mitochondrial matrix acidification resulting in a strong inhibition of mitochondrial pyruvate uptake and consequently lactate production and release. Increased brain lactate synthesis has been reported in hyperammonemic conditions such as ALF (Rose, 2010), due to the inhibition of the tricarboxylic acid cycle enzyme α-ketoglutarate dehydrogenase, reflecting a reduction in oxidative metabolism and impaired energy metabolism (Rose et al., 2007, Lai and Cooper, 1986).

In animal models of ALF and ALF patients, an increase in brain lactate has consistently been reported. Concentrations of lactate in CSF are also elevated in

cirrhotic and CLD patients but only in severe cases of HE (>grade 2) (Yao et al., 1987). Additionally, the study by Bosoi et al., (Bosoi et al., 2014) revealed for the first time in the setting of CLD that increased cerebral lactate (recorded using NMR spectroscopy) is associated to the pathogenesis of brain oedema (cytotoxic). Furthermore, an *ex vivo* study in 6 weeks bile duct ligated (BDL) rats (a clinically relevant model of CLD) showed that a rise in lactate (1.7 fold), and not glutamine, played an important role in the pathogenesis of brain oedema (Bosoi et al., 2014). In contrast, Rackayoya et al. (Rackayova et al., 2016) reported no significant elevation of lactate in rats 8 weeks following BDL, which is a very severe model of HE. These observations are contradictory and the variability may be explained by the different techniques used in each study. Since it is believed that brain oedema in liver disease is mainly cytotoxic, these results imply that the observed increase in total brain lactate is due to its intracellular accumulation.

Despite the existing evidence, it remains unknown whether significant changes in brain lactate metabolism develop in conditions of long-term CNS exposure to increased ammonia concentrations, such as that seen during CLD or HE.

1.2.5 Brain glutamate and liver disease

A glutamate-glutamine metabolic cycle exists between astrocytes and neurons and its role is to metabolize the glutamate that has been released from neurons, preventing over excitation (Cooper, 2001). Glutamate released by presynaptic neurons induces signalling through glutamate receptors. The excess is then cleared up by astrocytic excitatory amino acid transporters (EAAT), converting it to glutamine

by GS and preventing glutamate accumulation (Bosoi and Rose, 2013a, Kimelberg, 2005). An increase in extracellular glutamate has previously been documented in rats with portocaval anastomosis, associated with severe HE (Oria et al., 2012), while extracellular glutamate recorded using microdialysis, in rats with ALF, increases as a function of the deterioration of neurological status (Michalak et al., 1996). This increase in extracellular glutamate concentrations has been described to occur as a result of decreased mRNA and protein expression of astrocytic glutamate transporters (Suarez et al., 2000). Additionally, human studies have also shown increased glutamate in the CSF of patients with liver cirrhosis and HE (Weiss et al., 2016, Watanabe et al., 1984). In CLD, decreased uptake of glutamate, rather than altered transporter expression, has been reported in various preparations (Schmidt et al., 1990), while several studies have discussed the potential role of other factors such as oxidative stress (Blanc et al., 1998b) or manganese (Rose et al., 1999) in interfering with glutamate transport even in the absence of changes in transporter expression (Vaquero and Butterworth, 2006).

Added to the alterations in glutamate uptake, studies in cultured astrocytes suggest that acute ammonia application leads to increased glutamate release involving a pH-mediated, Ca^{2+}-dependent mechanism (Rose, 2002, Rose et al., 2005). Further studies proposed that astrocyte swelling is associated with prostanoid-dependent glutamate exocytosis, which triggers an oxidative/nitrosative stress response by way of N-methyl-D-aspartate (NMDA) receptors (Gorg et al., 2010), and induces tyrosine nitration on key astrocytic proteins, as well as RNA oxidations (in neurons and astrocytes) (Gorg et al., 2008, Schliess et al., 2002). This can result in alterations on local postsynaptic protein synthesis and gene transcription. Furthermore, densities of

the high affinity glutamate receptor, NMDA has been reported to show significant reduction in cerebral cortex, hippocampus and basal ganglia structures of portacaval-shunted rats (Peterson et al., 1990), while a decrease in the activity of NMDA receptor-induced production of cyclic guanosine monophosphate has also been observed (Erceg et al., 2005).

Adding to the reported changes in the glutamate-mediated neurotransmission, as previously discussed by Albrecht et al., (Albrecht and Jones, 1999) in HE associated with CLD, there is an imbalance between excitatory and inhibitory neurotransmission. As suggested by Rangroo Thrane et al., (Rangroo Thrane et al., 2013) compromises of the inhibitory neurotransmitter, gamma-aminobutyric acid (GABA), arising due to elevated ammonia concentrations, could be partly responsible for the altered levels of consciousness occurring in HE. Finally, ammonia also affects other neurotransmitter systems including the synthesis of histamine, serotonin, dopamine and noradrenaline in the brain (Oja et al., 2017).

1.2.6 Astrocyte: functional oxygen sensors and their role in neurovascular coupling

Oxygen is essential for all complex forms of life and the brain is highly vulnerable to oxygen deprivation. The existence of a functional CNS oxygen sensor has been supported by several studies, with evidence showing that the brainstem, the respiratory and cardiovascular control circuits, are sensitive to oxygen changes (Sun and Reis, 1994, Marina et al., 2015). The cellular identity and molecular mechanism

of these sensors was unknown, until a recent study by Angelova et al., (Angelova et al., 2015) identified astrocytes as functional oxygen sensors.

As previously discussed, the anatomical location of astrocytes places them at a strategic advantage to detect both synaptic activity and changes in vascular partial pressure of oxygen (PO_2). Remarkably, PO_2 threshold of astroglial activation is lower than that of the carotid body glomus cells (peripheral chemoreceptors), residing approximately 10 mmHg below normal brain oxygen levels of approximately 25 mmHg (Marina et al., 2015, Zhang et al., 2015). This activation of astrocytes occurs in the absence of peripheral oxygen sensing, suggesting that their role involves both contributing and preserving significant components of the homeostatic respiratory response during hypoxia (however this remains highly controversial, for a recent review see (Gourine and Funk, 2017)). The proposed sensory mechanism of these cells (shown in cultured cells, brain slices and *in vivo*) involves mitochondrial depolarisation. This, in combination with the increased rate in ROS production and lipid peroxidation leads to an activation of phospholipace C, inositol triphosphate (IP3) receptor and recruitment of Ca^{2+} from internal stores. Finally, the rise in $[Ca^{2+}]_i$ results in vesicular ATP release (Gourine et al., 2005). Detection of low PO_2 by brainstem astrocytes stimulate networks of respiratory neurons and contribute to the overall respiratory response to hypoxia, ensuring appropriate oxygenation of arterial blood. Other mechanisms, such as ryanodine receptor activation by ROS cannot be excluded (Green et al., 2002).

The neurovascular unit is a conceptual model encompassing the anatomical and metabolic interactions between neurons, vascular components [endothelial cells, pericytes, vascular smooth muscle cells (VSMC)] and glial cells (astrocytes, microglia) in the brain (Venkat et al., 2016). In order to sustain neuronal function, the "neurovascular coupling" mechanism has evolved in the brain, resulting in hemodynamic responses, which induce vasodilation and increase CBF to the regions of active neurons (known as functional hyperaemia). While a significant controversy exists in literature regarding the cells mediating this effect, available *in vitro* and *in vivo* evidence indicate astrocytes (and pericytes) as essential contributors in vasomotor responses, participating in both vasodilation and vasoconstriction (Attwell et al., 2010, Belanger et al., 2011). Ca^{2+} transients in astrocytes resulting in metabotropic glutamate receptor activation, activates cytosolic phospholipase A_2, triggering the formation of arachidonic acid, which is then converted into vasodilating agents such as prostaglandin E_2 (PGE_2) (Attwell et al., 2010, Belanger et al., 2011). Alternatively, arachidonic acid can diffuse in VSMC and cause vasoconstriction after its conversion in 20-Hydroxyeicosatetraenoic acid (Belanger et al., 2011). Interestingly, studies exist indicating that vasodilation and vasoconstriction may be dictated by the release of metabolic substances, such as lactate, which depend on the metabolic state of the brain (Gordon et al., 2008). It is suggested that under conditions of low oxygen, astrocytic Ca^{2+} concentration is elevated and extracellular lactate and adenosine increases. High external lactate hinders PGE_2 clearance and increases extracellular PGE_2, which causes an astrocytic-mediated vasodilation.

While the neurovascular unit and therefore the cerebral perfusion and oxygenation are controlled by various mechanisms, it can be compromised under pathological conditions (Ostergaard et al., 2014). In patients with cirrhosis and HE, cerebral metabolic rate of oxygen ($CMRO_2$) and CBF are believed to be reduced, compared to patients with cirrhosis without HE and in healthy individuals (Dam et al., 2013), while post-mortem examinations revealed altered vasculature in severely affected brains, such as proliferation of capillaries (probably due to increased vascular resistance) (Butterworth, 2007). Additionally, several studies indicated a preserved cerebral autoregulation (the ability to maintain a constant blood flow despite changes in perfusion pressure) in most patients with cirrhosis (~77%) but it is impaired in severe cases of HE (Strauss et al., 2000). However, the degree of brain hypoxia and the mechanisms underlying any alterations occurring in HE remain unknown.

1.3 Connexin Hemichannels

As previously discussed, astrocytes are extensively coupled by GJ, allowing a direct passage of molecules between cells. GJ channels spin two plasma membranes and consist of two hemichannels (connexons), one from each cell. Each hemichannel is formed by six connexin subunits (Figure 3A-C), and is permeable to small molecules up to 1-1.5kD (Sohl and Willecke, 2004). Their role involves electrical conductance (essential in neurons) and metabolic assistance, transferring ions, glucose, ATP, amino acids, signalling molecules (Giaume et al., 2010, Giaume et al., 2013). Astrocytic GJ communication is believed to be modulated by cytokines, growth factors, neurotransmitters, NO and other factors, making them a subject to change

under certain conditions, such as neuronal injury (Rouach et al., 2000, Blanc et al., 1998a).

Connexins consist of 4 transmembrane helices (M1-M4) (Figure 3A). The N- and C-terminal ends are intracellular. The primary sequence of the intracellular loop is not well conserved, while the C-terminal sequence varies a lot between connexins with connexin-26 being ~20 amino acids and connexin-43 being 150 amino acids long (Fiori et al., 2014). A number of connexins have been identified, with their expression pattern varying between cell types, brain regions and developmental stage. Neurons express connexin-26, connexin-30, connexin-36, connexin-45 and connexin-47 (Rouach et al., 2002), while astrocytes predominantly express connexin-43, connexin-26, connexin-30, connexin-40, connexin-45 and connexin-46 (Giaume et al., 2012), with connexin-43 and connexin-30 being the most abundant astrocytic connexins (Giaume et al., 2010). Across connexin isoforms, there is a variation in unitary conductance (most hemichannels have a fixed negative charge in the pore therefore cation selective) and permeability characteristics that have likely evolved according to the requirements of the tissue in which they are expressed. Moreover, their plasticity allows them to compensate for the loss or down regulation of other connexins as revealed by several KO models (Sohl and Willecke, 2004).

Connexins can also exist as functional hemichannels allowing the exchange of ions and signalling molecules between the intra and the extracellular milieu (Giaume et al., 2010, Rouach et al., 2000) (Figure 3B). Under normal physiological conditions, hemichannels are either closed (Contreras et al., 2003) or in a flickering state (Figure

3D) (Bukauskas and Peracchia, 1997). Maintaining a controlled gating is very important to preserve a normal cell function. Hemichannels are therefore constantly under the control of several factors such as membrane potential, pH, posttranslational modification (phosphorylation, ubiquitination, S-nitrosylation), mechanical stimulations and intracellular/extracellular [Ca^{2+}] (Giaume et al., 2013, Retamal, 2014). A summary of the conditions, which trigger opening and closing of hemichannels is listed in Table 1. In certain pathological conditions, such as epilepsy and ischemia, significant changes in astrocyte structure and function may occur, which are associated with changes in hemichannel activity, affecting coupling within the astroglial networks and their communication with other brain cells (Giaume et al., 2010). Facilitated opening of hemichannels has been shown to correlate with cell death by loss of osmoregulation, excitotoxicity and spread of inflammation (Kim et al., 2017). While the exact gating mechanism of hemichannels is still unclear, the ball and chain mechanism is proposed to explain the closure of connexin-43 hemichannels in response to intracellular acidification. The C-terminal domain acts as a ball that interacts with the intracellular cytoplasmic loop occluding the pore (Fiori et al., 2014). Finally, the N-terminal region is believed to act in a similar way for voltage gating of hemichannels, while calmodulin domains on the C-terminal allow gating of the hemichannels by changes in [Ca^{2+}] (Fiori et al., 2014).

Open conformation	**Close conformation**
<1.4 mM $[Ca^{2+}]_o$	Negative membrane potential
Increase ROS	Low pH
Mechanical stress	Phosphorylation (predominantly Ser368)
TNF- α, IFN- γ and IL-1β	IL-6
Ischemia and hypoxia	High $[Mg^{2+}]$
Hypercapnia (Connexin-26 act as CO_2 sensors)	Lanthanum, Cobalt and Nickel
Quinine/quinide	Gadolinium, Carbenoxolone and NPPB
NO (through N-nitrosylation)	**Chronic hyperammonemia?**

Table 1*:* Conditions/factors, which facilitate opening and closing of connexin hemichannels. In red bold writing is one of the hypotheses, which is addressed in this study. Information was gathered from (Giaume et al., 2013, Retamal, 2014) (Fiori et al., 2014, de Wolf et al., 2017, Saez et al., 2013, Trexler et al., 1999, Willebrords et al., 2016, Batra et al., 2012). ROS: reactive oxygen species, NO: nitric oxide, TNF- α: Tumor necrosis factor alpha, IFN- γ: Interferon gamma, IL-1β: Interleukin 1 beta, NO: nitric oxide, NPPB: 5-Nitro-2-(3-phenylpropylamino)benzoic acid.

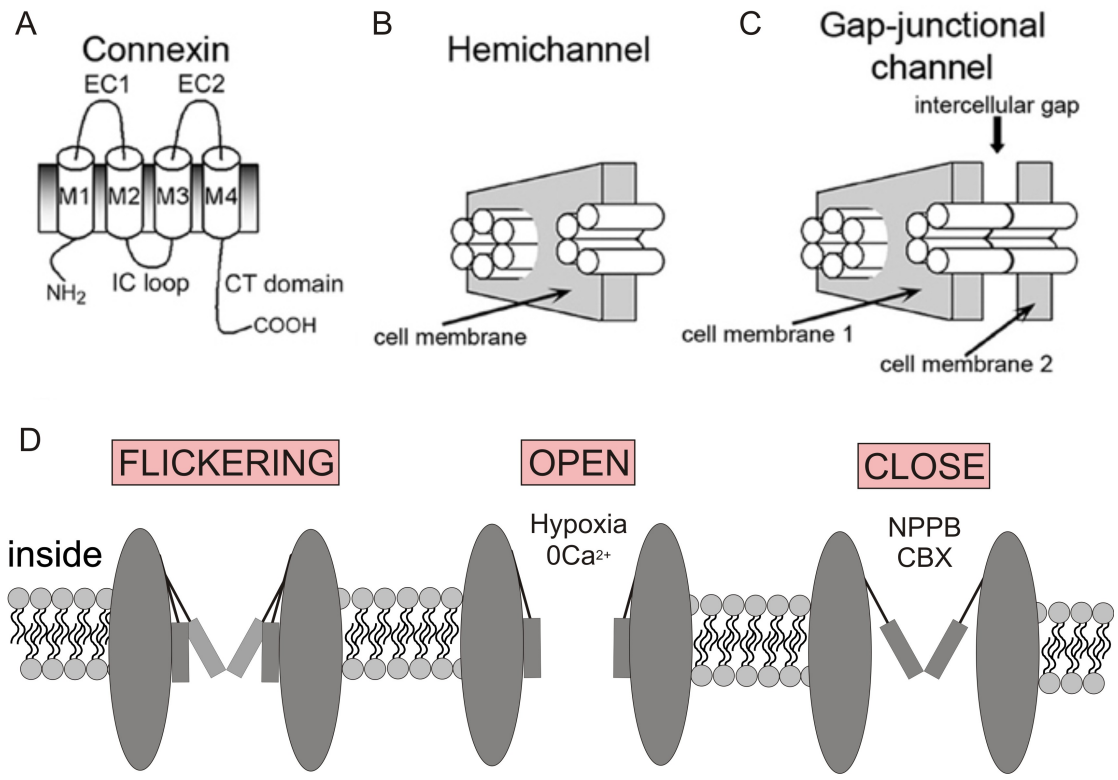

Figure 3: Connexin, hemichannel and gap junction channel representation. A. Schematic illustrating the 4 transmembrane domains (M1-M4) of a connexin channel. The intracellular sequences (N-terminal region, intracellular (IC) loop and the C-terminal domain) are involved in channel gating. **B.** Schematic drawing of a connexin hemichannel made of six connexins. **C.** Schematic indicating the formation of gap junction channels, consisting of two hemichannels, one from each cell. **D.** Schematic of hemichannel gating configuration at baseline conditions, at exposure to stimuli such as hypoxia and/or 0 $[Ca^{2+}]_o$ as well as in the presence of connexin hemichannel blockers such as 5-Nitro-2-(3-phenylpropylamino)benzoic acid (NPPB) and Carbenoxolone (CBX). Modified from (Bao et al., 2005, Fiori et al., 2014)

1.4 The glymphatic system: waste clearance pathway of the brain

As discussed above, there is evidence that many potentially noxious substances and metabolites such as lactate, glutamate, neurosteroids, bile acids and various drugs accumulate in the cerebral interstitial fluid (ISF) and cerebrospinal fluid (CSF) of HE patients (Weiss et al., 2016). It is however still unclear why this build-up of toxins occurs.

In the peripheral tissues, the lymphatic system accounts for clearance of ISF and solutes, a critical process, which ensures tissue homeostasis. Despite the brain being characterized by a high metabolic rate and the exquisite sensitivity of neurons and glia to alterations in the extracellular environment, the brain was believed to be devoid of a lymphatic drainage system. However, recent studies have identified a brain-wide paravascular clearance pathway that facilitates the efficient removal of interstitial proteins, peptides and other molecules from the brain (Iliff et al., 2013a, Iliff et al., 2012). These studies showed that subarachnoid CSF recirculates through the brain parenchyma along paravascular spaces surrounding penetrating arteries, exchanging with the surrounding ISF to facilitate the clearance of interstitial solutes via convective bulk flow. Paravascular CSF-ISF exchange and solute clearance is dependent upon water transport via astrocytic AQP4 channels, which are localized predominantly on perivascular astrocytic end-feet. ISF and its constituents in turn are cleared along paravascular spaces surrounding large calibre cerebral veins, which then reach the recently discovered CNS lymphatic vessels (Louveau et al., 2015) and eventually enter systemic circulation. This pathway has been termed the

“glymphatic system” due to its dependence on glial water channels, summarized in Figure 4 and its adoption of a clearance function similar to peripheral lymphatic system.

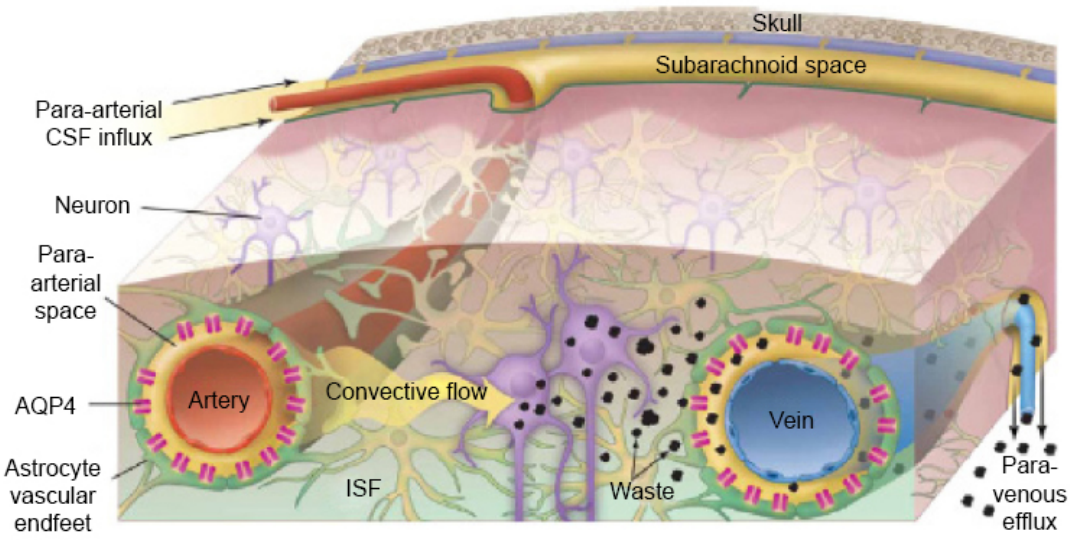

Figure 4: Brain glymphatic system. The perivascular drainage pathway moves waste into the periarterial space and towards the subarachnoid space in the direction opposite to blood flow. The water component of cerebrospinal fluid (CSF) crosses astrocytic aquaporin 4 (AQP4) channels to enter the brain parenchyma. CSF - interstitial fluid (ISF) exchange takes place within the brain parenchyma via convective flow. CSF - ISF then moves into the perivenous space of deep-draining veins. Effluxed waste can then recirculate with the CSF, or be absorbed into the newly discovered CNS lymphatic vessels (Louveau et al., 2015) and eventually enter systemic circulation. Arrows indicate direction of flow. Modified from (Nedergaard, 2013).

The glymphatic system plays an essential role in ensuring healthy function of the brain. In addition to clearing the brain, it may also contribute to the distribution of growth factors, neuromodulators, and other solutes, while failure of the glymphatic system may have important pathophysiological consequences, such as those seen in the aging brain (Kress et al., 2014) and Alzheimer's disease (Iliff et al., 2012, Peng et al., 2016).

It is well known that sleep improves memory and helps regulate the metabolism of the body (intrinsically connected to hormonal regulation such as growth hormone, leptin, ghrelin and more), while prolonged sleep deprivation impairs cognitive performance, elevates stress and is a common cause of seizures. A recent study has proposed that during sleep, glymphatic activity is dramatically enhanced while its function is suppressed during wakefulness. It has been suggested that a key function of sleep is to support the activity of the glymphatic system and clearance of potentially neurotoxic waste substances produced during wakefulness (Xie et al., 2013). Interestingly, CLD and HE are always accompanied by dyssomnia (Bajaj et al., 2011). mHE patients suffer from poor sleep quality, take longer time to fall asleep, exhibit lower sleep efficiency and slow daytime functional disturbances (Liu et al., 2015). Aside from anxiety and depression, other psychiatric factors tend to have a negative impact on sleep quality, which results in a vicious cycle and further health deterioration. The efficacy of the glymphatic system has not been investigated yet in the context of HE and studies of this type might be able to provide invaluable information regarding the diagnosis and treatment of HE patients.

1.5 Main Hypothesis and Aims

Experimental studies described in this thesis tested the hypothesis that during the development of HE, chronic exposure to elevated ammonia concentrations alters cerebral oxygenation, compromises lactate transport between astrocytes and neurons and affects uptake of neurotransmitters. It was also hypothesised that HE impairs glymphatic clearance mechanisms, either as a cause or a consequence of the disease, which contributes to the cognitive impairment.

In vivo whole animal (rat) and *in vitro* experimental models were used to address the following specific aims:

1. To determine whether cerebral oxygenation is impaired in HE and, if so, explore the potential underlying mechanisms (**Chapter 2**);
2. To determine whether in HE, the actions of high ammonia alter brain extracellular lactate concentration and, if so, study the potential underlying mechanisms (**Chapter 3**);
3. To determine whether in HE the actions of high ammonia alter brain extracellular glutamate concentration (**Chapter 4**);
4. To evaluate the efficacy of brain glymphatic clearance pathway in HE and determine the potential cognitive/behavioural consequences of impaired glymphatic flow (**Chapter 5**).

Chapter 2: Ammonia triggers impaired cerebral oxygenation in an animal model of chronic liver disease with minimal hepatic encephalopathy.

2.0 Introduction

Despite only ~2% of total body weight, the brain receives ~15% of cardiac output and is responsible for 20% of the body's total oxygen and glucose consumption (Kisler et al., 2017, Attwell et al., 2010). Mechanisms within the brain have evolved to control blood flow to active areas in order to match metabolic supply and demand, known as neurovascular coupling (Attwell et al., 2010). Due to the limited energy reserve in the brain, if CBF is interrupted then neuronal functionality ceases within seconds (Moskowitz et al., 2010). Long-term impairment of this mechanism has been linked to the development and/or progression of the cognitive impairment in aging and Alzheimer's disease (Lourenco et al., 2015). Additionally, acute impairment can have long-term consequences on neurological function (Khot and Tirschwell, 2006). Clearly, maintaining appropriate CBF is essential for supporting neuronal function and therefore, cognition.

The precise mechanisms controlling neurovascular coupling have not yet been fully elucidated however, studies have shown that a group of cells known as the neurovascular unit (neurons, astrocytes, and endothelial cells) function in concert to ensure blood supply is delivered to active areas. Astrocytes, and pericytes at the

capillary level, are also thought to mediate communication between neurons and blood vessels (Attwell et al., 2010, Iadecola, 2004, Hall et al., 2014, Mishra et al., 2016).

In patients with liver cirrhosis and HE, $CMRO_2$ and CBF are believed to decrease, compared to patients with cirrhosis without HE and healthy controls (Dam et al., 2013). Additionally, several studies indicate a preserved cerebral autoregulation in most patients with cirrhosis (~77%), which is impaired in more severe cases of HE (Strauss et al., 2000). Results from functional magnetic resonance studies also revealed that patients with HE have abnormal activation in several brain regions when performing selected cognitive tasks, proposing a possibly uncoupled neurovascular unit (Zhang et al., 2007). These changes may bring the brain into a general dysmetabolic state. In such state of low activity and low oxygen consumption, mechanisms are likely to be triggered resulting in decreased oxygen delivery (less demand less supply) and therefore further brain atrophy. However, the precise level of brain tissue oxygenation and the mechanisms behind any alterations occurring due to the disease, are still unknown.

Studies showing impaired $CMRO_2$ and CBF did not observe a correlation with arterial ammonia concentration or cerebral metabolic rate of ammonia (Iversen et al., 2009). The results of these studies do not support a direct effect of hyperammonemia on brain oxidative metabolism but do not preclude other or indirect roles of ammonia.

This study determined whether cerebral tissue oxygen tension and CO_2 cerebrovascular reactivity are altered in animal models of HE. Ornithine phenylacetate (OP, OCR-002; Ocera Therapeutics, CA, USA) has been shown to reduce ammonia concentration (in plasma and brain) in animal models of cirrhosis and ALF (Jalan et al., 2007). OP treatment was found to be associated with a significant reduction in the severity of brain swelling (Jalan et al., 2007), improvement in neurophysiological function (Oria et al., 2012) and reduction in intracranial pressure (Ytrebo et al., 2009). Therefore, OP was applied in this study as an experimental ammonia-lowering treatment. The data obtained demonstrate that, in HE, ammonia actions contribute to the compromised cerebral oxygenation but have no effect on cerebrovascular reactivity to CO_2. The cause of the low basal brain tissue PO_2 remains unknown however; compromised cerebral perfusion could be a contributing factor.

2.1 Materials and Methods

All the experiments were performed in accordance with the Animals (Scientific Procedures) Act 1986 (ASPA) revised according to the European Directive 2010/63/EU and the UK Home Office (Scientific Procedures) Act (1986) with project approval from the Institutional Animal Care and Use Committee.

2.1.1 Animal models

Male Sprague-Dawley rats (body weight ~350-400g) were obtained from a commercial supplier (Charles Rivers Laboratories, Inc.).

BDL surgery: Under general anaesthesia (5% isoflurane in oxygen for induction, 2% isoflurane in air for maintenance) 24 rats underwent triple ligation of the bile duct via a small laparotomy to induce chronic liver injury and were studied 28 days after the surgery (Harry et al., 1999).

Sham surgery: Under general anaesthesia (5% isoflurane in oxygen for induction, 2% isoflurane in air for maintenance) 21 rats underwent sham surgery. Via a small laparotomy, the bile duct was detected and exposed for several seconds, prior closure of the incision. Sham-operated animals were studied 28 days after the surgery.

OP treatment: 3 weeks after the surgery, 6 BDL and 7 Sham-operated rats were given twice daily intraperitoneal injections of combined L-ornithine and phenylacetate (0.3g/kg; OP) ~7 hours apart for 5 days – a dosing regimen that has previously been shown to effectively reduce plasma ammonia concentration (Davies et al., 2009). The rats were studied on day 28 post BDL surgery, within 3 hours of the last OP injection.

Blood and brain tissue were collected under terminal isoflurane anaesthesia. Plasma biochemistry was performed using a Cobas Integra II system (Roche Diagnostics).

2.1.2 Measurement of brain tissue PO_2

Sham (n=14), BDL (n=18), Sham-OP treated (n=7) and BDL-OP treated (n=6) rats were anesthetized with α-chloralose (100mg kg^{-1}), instrumented for arterial blood pressure recording and artificially ventilated. Arterial PO_2 was maintained within the physiological range by adjusting the rate and/or stroke volume of the ventilator. Cerebral tissue PO_2 was monitored by optical fluorescence (Oxylite™, Oxford Optronics). The sensor is based on optical fluorescence technology that allows real-time detection of PO_2. After a limited craniotomy, oxygen sensors were placed in the somatosensory cortex (0.5–1 mm below the cortical surface) and sealed from the air. Tissue PO_2 was recorded at baseline and during systemic hypercapnia (10% CO_2; 5 min).

2.1.3 Pharmacological interventions

It has been previously reported that systemic arterial blood pressure is lower in conscious BDL animals at 4 weeks post ligation (Estrela et al., 2016). It was also noted that under anaesthesia, BDL animals have a significantly lower mean arterial pressure (MAP) than Sham controls. In order to control for the effects of lower perfusion pressure, an alpha1-adrenoceptor agonist, phenylephrine (PE) was used to increase systemic blood pressure in the BDL animals equal to that of Sham controls. PE was infused at a rate of 5-10μg min^{-1} to maintain a MAP of ~100 mmHg for a period of approximately 10mins.

In order to investigate the role of cerebral perfusion in brain oxygenation during liver disease, the carbonic anhydrase inhibitor acetazolamide (ACTZ) was used. ACTZ increases CBF (Vorstrup et al., 1984) (by decreasing pH-protons cause smooth muscle relaxation) and cerebral oxygenation, which confer some of its therapeutic benefits (Wang et al., 2015). It is also used prophylactically to prevent acute altitude sickness. Sham-operated and BDL animals received 10mg kg^{1} (i.v.) ACTZ (in 100% DMSO) after a baseline PO_2 was recorded.

2.1.4 *Statistical analysis*

For the analysis of differences in blood PO_2/PCO_2 and brain PO_2 between animal groups, Kruskal-Wallis test followed by Dunn's multiple comparison post-hoc test

was applied. The analysis of pharmacological interventions and CO_2 reactivity was performed using one-way ANOVA for comparison between the animal groups (comparing changes of PO_2 due to drug/CO_2 application) and paired sample t-test for comparison within groups (evaluating the effect of drug/CO_2 before and after application).

The biochemistry data was analysed using one-way ANOVA. Data are reported as mean±SEM. Differences with p value of <0.05 were considered to be significant. Statistical analysis was performed using OriginPro 9.1 (OriginLab).

2.2 Results

2.2.1 Biochemistry

Plasma biochemistry, including ammonia concentration was assessed in all groups of animals (Table 2). Compared to Sham surgery, BDL resulted in a significant increase in plasma ALT and bilirubin ($p<0.001$), indicating impaired liver function, while albumin and total protein concentrations were significantly decreased ($p<0.001$). Treatment of BDL rats with OP had no effect on these parameters (Table 2). Plasma ammonia concentration was significantly higher in BDL rats when compared to Sham-operated animals ($p<0.001$). Treatment of BDL animals with OP lowered plasma ammonia concentration, which was similar to that measured in Sham-operated animals ($p=0.3$) (Table 2).

Parameters	Sham	BDL	BDL+OP	Sham+OP
N numbers	**22**	**60**	**30**	**7**
Ammonia, µmol/L	56±3	141±1**	61±0.5	50±5
Albumin, g/L	35±4	23±0.2**	23±1	30±2
Total protein, g/L	50±0.3	38±0.3**	42±0.5	53±1
Bilirubin, µmol/L	5±0.5	205±1**	163±2	6±0.5
ALT, U/L	11±0.4	130±0.5**	86±1	13±0.5

Table 2: Plasma biochemistry. ALT: alanine aminotransferase. Data expressed as means±SEM, ** $p<0.001$ compared to Sham group using one-way ANOVA.

2.2.2 Brain tissue PO_2 and cerebrovascular CO_2 reactivity in animal models of HE

Following placement of the oxygen sensor in the cerebral cortex, blood PO_2 and PCO_2 were maintained constant at ~121±2 mmHg and 32±1 mmHg, respectively, in Sham-operated animals (n=14) and 114±3 mmHg, (PO_2, p=0.2) and 33±1 mmHg (PCO_2, p=1), respectively, in BDL animals (n=18), ensuring equal arterial oxygenation (Figure 5A-B).

Once blood gases were stabilized, cerebral PO_2 was obtained at several time points revealing a significantly lower brain PO_2 of 13±2 mmHg ($p<0.001$) in BDL animals compared to Sham-operated controls (26±1 mmHg) (Figure 6).

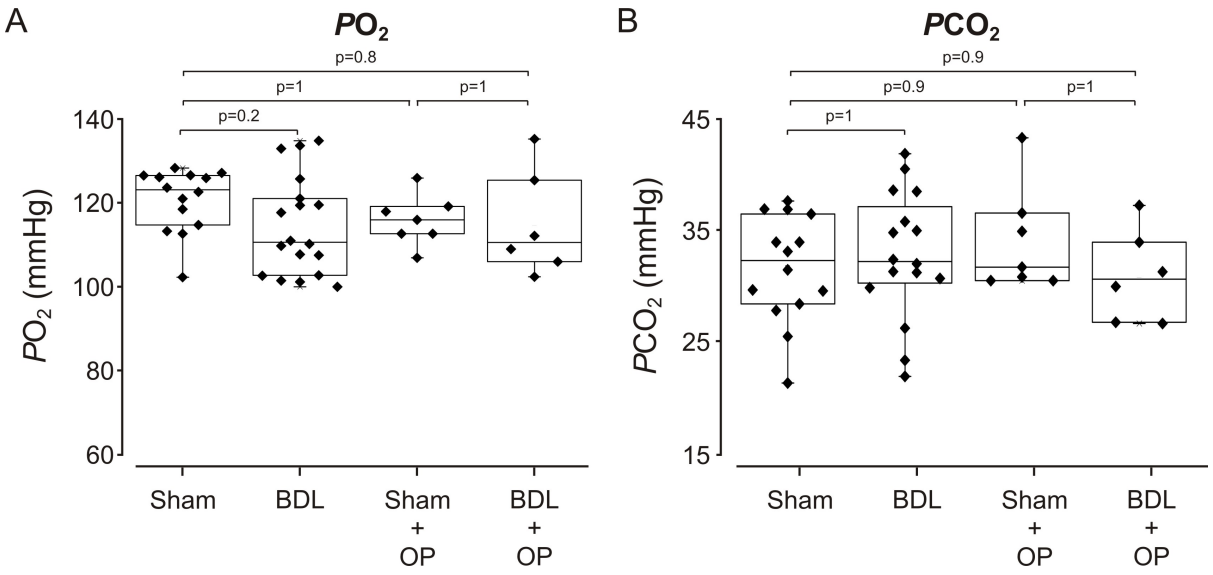

Figure 5: Brain PO_2 and PCO_2 in an animal model of HE. A. Blood PO_2 and **B.** PCO_2 are not significantly different between the animal models.

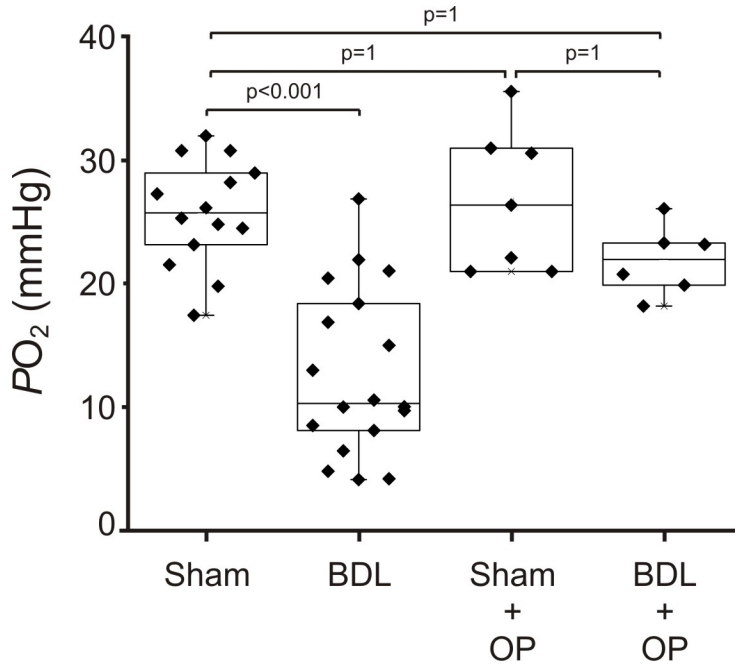

Figure 6: Brain PO_2 in an animal model of HE. Basal PO_2 in the somatosensory cortex is lower in BDL animals but recovers with the ammonia lowering treatment (OP).

In order to evaluate the ability of vessels to respond to a known vasodilatory stimulus, systemic hypercapnia (10% CO_2) was applied. Despite the lower PO_2 baseline, CO_2 reactivity was preserved in BDL animals (n=6), with an increase in PO_2 (by 21±2 mmHg, p=0.6) similar to the one recorded in Sham-operated animals (by 24±2 mmHg, n=8) (Figure 7).

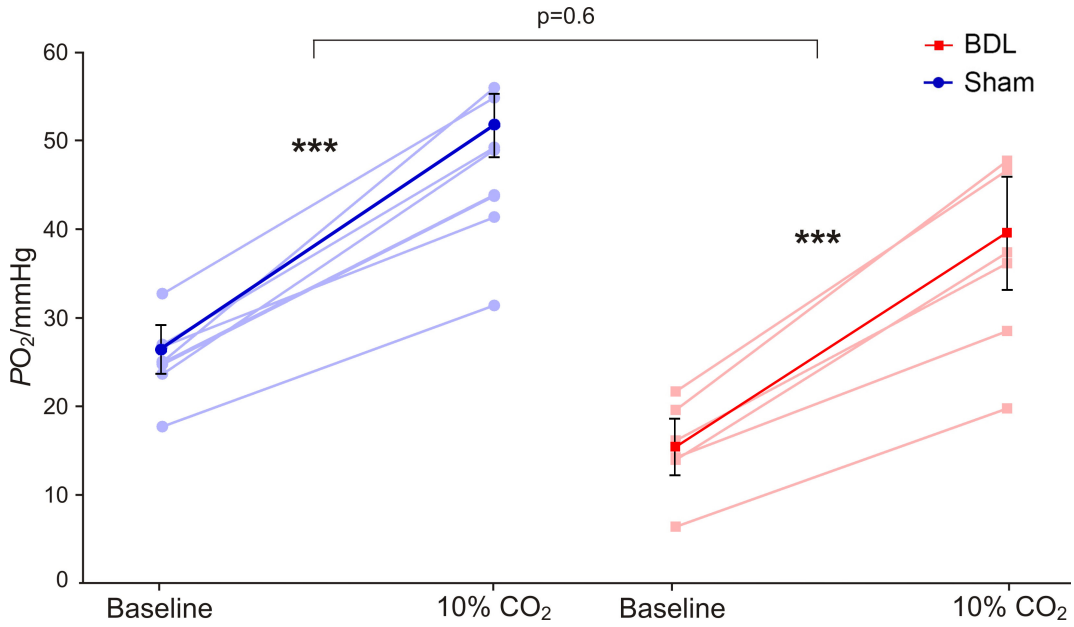

Figure 7: Cerebrovascular reactivity to hypercapnia (10% inspired CO_2) is unchanged in BDL animals when compared to Sham-operated controls, despite lower basal PO_2.

2.2.3 Normalisation of MAP does not restore brain tissue PO_2 but increasing CBF potentially does

While data exists in patients indicating preserved autoregulation, the possibility of low MAP recorded in BDL animals (57±3 mmHg) contributing to the compromised cerebral PO_2, was attempted to be excluded. PE, an α1-adrenergic receptor agonist, was infused i.v, increasing MAP in BDL animals to ~100-120 mmHg, which is the normal blood pressure recorded in healthy control rats under anesthesia (Figure 8). Both animal groups showed a significant increase in brain tissue PO_2 from the corresponding baseline (Figure 8-9), although the overall change in oxygen was significantly lower in the BDL (by 6±1 mmHg, n=6, p=0.02) compared to Sham-operated animals (by 18±6 mmHg, n=6) (Figure 10A). The PO_2 of BDL animals treated with PE was also significantly lower than the PO_2 baseline of Sham-operated animals (p=0.02) suggesting that the intervention did not restore cerebral PO_2 of BDL animals back to normal values.

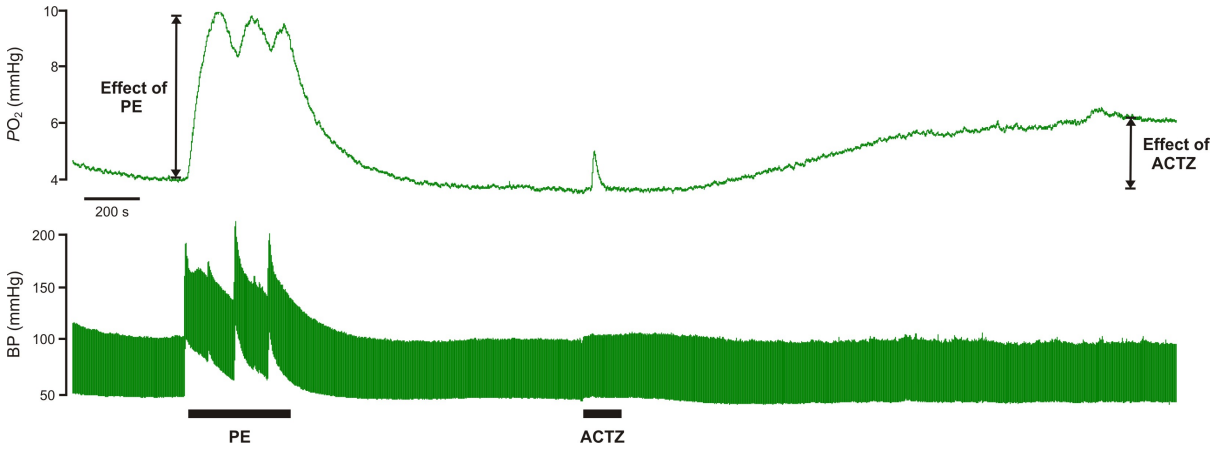

Figure 8: Representative traces from BDL animals indicating cerebral PO_2 and blood pressure before, during and after i.v infusion of PE and ACTZ.

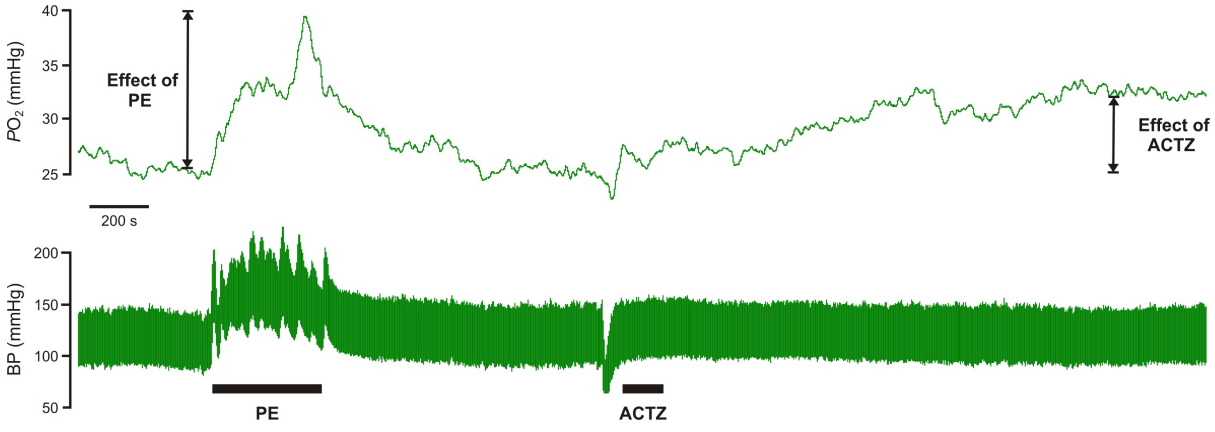

Figure 9: Representative traces from Sham-operated animals indicating cerebral PO_2 and blood pressure before, during and after i.v infusion of PE and ACTZ.

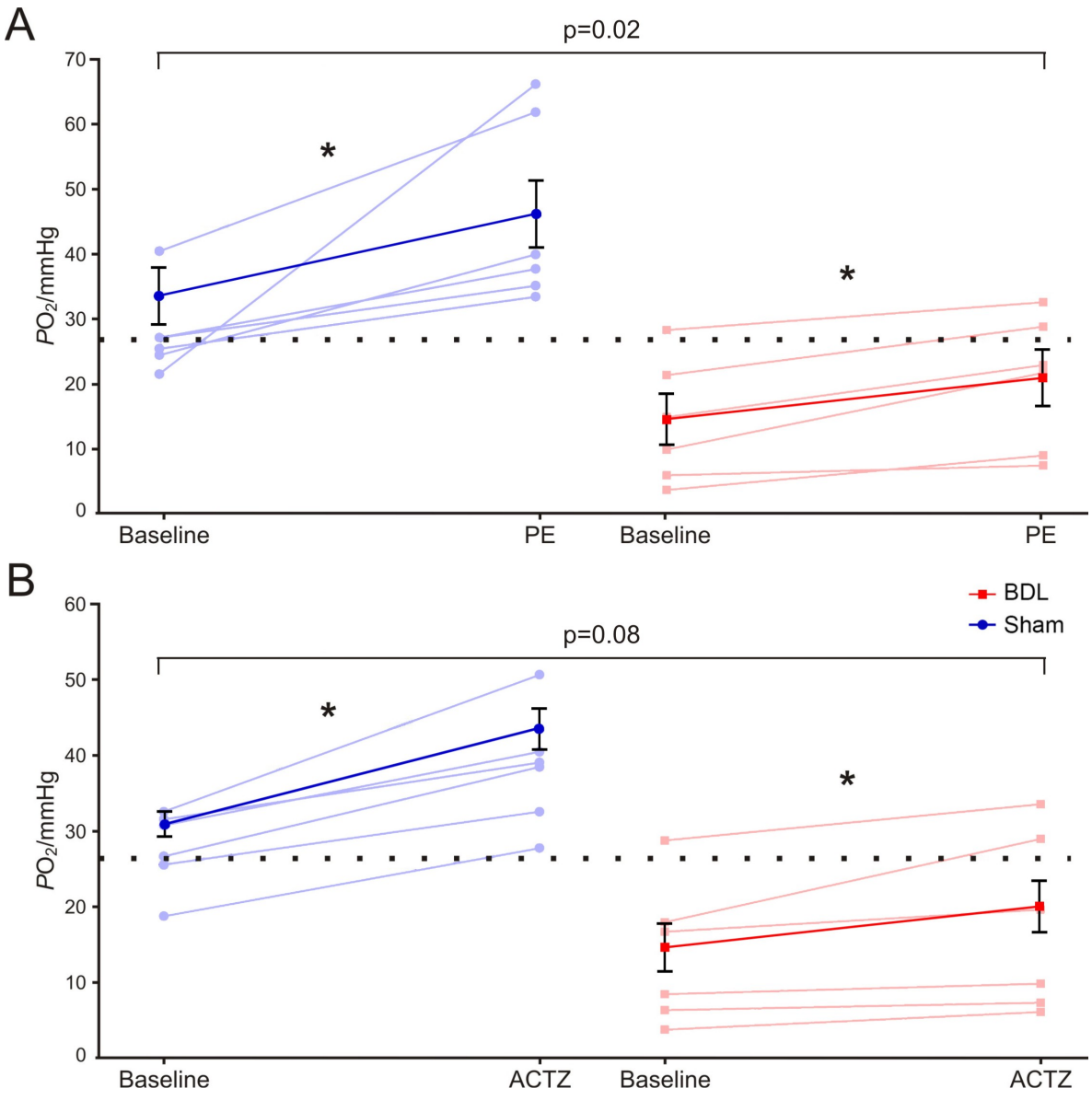

Figure 10: Brain PO_2 is not restored in the BDL animals when MAP is normalised but it improves when CBF is increased. **A.** Summary and individual data illustrating the effect of PE infusion, increasing MAP, on the cortical PO_2 of Sham-operated and BDL rats. **B.** Summary and individual data illustrating the effect of ACTZ infusion, increasing CBF, on the cortical PO_2 of Sham-operated and BDL rats. The dotted line indicates normal brain PO_2 values.

ACTZ, a carbonic anhydrase inhibitor, induces an increase in both CBF and blood volume in the normal brain. According to literature, CBF in patients with HE is compromised. Following a protocol from a previous MRI study performed in Prof. Gourine's laboratory, a concentration of ACTZ known to increase CBF successfully (by 85 ml/100g/min which corresponds to an increase of 102% from baseline CBF) was infused and changes in brain PO_2 were recorded. A significant increase in oxygen from the corresponding baseline was observed in both animal groups with the overall change in oxygen not being significantly different between BDL (5±2 mmHg, n=6, p=0.05) and Sham-operated animals (11±2 mmHg) (Figure 8-9, 10B). ACTZ treatment was potentially effective in normalising the cerebral PO_2 of BDL animals (after treatment), which was not significantly different from the Sham-operated baseline PO_2 before treatment (p=0.08) (Figure 10B).

2.2.4 Ammonia lowering treatment prevents fall of brain tissue PO_2

Daily OP treatments had been shown to decrease systemic and brain ammonia concentrations in BDL animals (Davies et al., 2009). In the experiments described in this thesis, OP treatment of BDL rats significantly improved cerebral PO_2 (22±1 mmHg, n=6, p=1), increasing the oxygen tension to levels similar to that recorded in Sham-OP rats (27±2 mmHg, n=7), when blood PO_2 and PCO_2 were constant (Sham-OP: PO_2: 116±2 mmHg, PCO_2: 34±2 mmHg; BDL-OP: PO_2: 115±5 mmHg, p=1; PCO_2: 31±2 mmHg, p=1) (Figure 5-6).

2.3 Discussion

Brain information processing requires constant and sufficient supply of oxygen and metabolic substrates. Compromised tissue oxygenation can have detrimental effects on all cell types, with the development of severe clinical symptoms in the long term. Several studies have reported compromised CBF and $CMRO_2$ due to HE (rather than cirrhosis) (Dam et al., 2013), with no clear mechanistic insights and contradictory data regarding the role of ammonia.

Several mechanisms exist in the brain ensuring adequate cerebral perfusion such as cerebral autoregulation, which seeks to maintain constant CBF. In this study, cerebral tissue PO_2 was monitored directly, for the first time, using optical fluorescence, in animal models of CLD with mHE. At a constant blood PO_2 and PCO_2, a significantly lower brain tissue PO_2 was recorded in BDL animals compared to Sham-operated rats. While evidence of preserved autoregulation exists in patients with HE, restoring MAP did not normalise cerebral PO_2 in BDL animals, suggesting that the decreased brain oxygenation is not due to relative hypotension. However, increasing CBF acutely using a pharmacological intervention like ACTZ, improved brain tissue PO_2.

While these interventions may provide some information regarding the mechanisms underlying the reported phenotype, precise conclusions cannot be drawn yet. Limitations such as damage caused by the invasiveness of the oxygen electrode cannot be rejected. Additionally, earlier studies have indicated the role of NO as a

modulator of the ACTZ-induced CBF response (Tuettenberg et al., 2001). Interestingly, the NO pathway appears to be compromised in BDL animals due to hyperammonemia (Balasubramaniyan et al., 2012) and it could therefore be a limiting factor in fully restoring cerebral perfusion via ACTZ (PO_2 of treated BDL animals is still on the lower range of normal PO_2). CBF will be further investigated in an MRI study, examining baseline perfusion, effectiveness of ACTZ and sildenafil in increasing CBF as well as integrity of neurovascular coupling in animal models of HE (beyond the scope of this study).

The role of ammonia in interfering with brain oxygenation was also investigated, by treating BDL rats with OP, a drug known to lower systemic and brain ammonia (Davies et al., 2009). OP treatment significantly improved PO_2 of BDL animals, suggesting that ammonia is indeed responsible for the reported phenotype. The exact pathway by which ammonia affects brain oxygenation is unknown, however, a recent study has revealed that hyperammonemia contributes to endothelial nitric oxide synthase (eNOS) downregulation through induction of inflammation and increased production of asymmetric-dimethylarginine, an endogenous inhibitor of eNOS (Balasubramaniyan et al., 2012). NO plays an important role in regulating blood flow and preventing vascular and endothelial dysfunction, which could contribute to HE. Reduction in ammonia with OP restored eNOS activity, improving NO metabolism (Balasubramaniyan et al., 2012).

In BDL animals, electron microscopy studies reported collapsed microvessel with moderate perimicrovessel oedema (Wright et al., 2007), which is possibly a major

contributor in the reduced CBF reported in HE patients. Cytotoxic oedema arising due to hyperammonemia could result in an extrinsic compression of capillaries (a phenotype also seen in kidneys due to ischemia (Johnston and Latta, 1977)) and therefore compromise baseline blood flow. However, a more precise method such as *in vivo* two-photon microscopy should be performed in order to further investigate the cerebrovascular structure of these animals. Additionally, pericytes that are contractile cells on capillaries, which might be involved in CBF regulation (Fernandez-Klett et al., 2010), are believed to die after ischemia-induced constriction (partly due to glutamate) or oxidative stress (Yemisci et al., 2009). These cells die in rigor and produce long-lasting decrease of capillary constriction and blood flow (as well as BBB breakdown) (Hall et al., 2014, Hauck et al., 2004), contributing to neuronal damage, which could also occur during HE and be responsible for the reported phenotype. Pericytes have not been studied extensively in the field of HE and it will therefore be essential to investigate their role in more depth. While the above proposed factors in combination with the impaired NO metabolism, could be resulting in a higher vascular tone, vasodilation due to CO_2 was preserved in BDL animals, suggesting intact cerebrovascular reactivity and capacity for blood vessels to dilate.

Another possible mechanism by which increased ammonia could be compromising brain PO_2 is via impairment of brain energy metabolism. Evidence exists pointing towards lactate as an important energy substrate (further investigated in **Chapter 3**) as well as a mediator of vasodilation (Hein et al., 2006, Gordon et al., 2008). Furthermore, high ammonia concentrations interfere with mitochondrial functionality, by inhibiting enzymes such as α-ketoglutarate dehydrogenase, pyruvate dehydrogenase and isocitrate dehydrogenase, which could profoundly affect the

operational rate of the tricarboxylic acid cycle and subsequently the electron transport chain. Additionally it can interfere with the malate-aspartate shuttle, which is the principal mechanism for the transfer of reducing equivalents from the cytosol into mitochondria for oxidative phosphorylation, and it can therefore alter further the normal operation of the electron transport chain (Rama Rao and Norenberg, 2012). Furthermore, studies using chronic hyperammonemic mice indicated a progressive inhibition of cytochrome C oxidase (complex IV of electron transport chain, ETC) activity and mRNA levels of its subunit II (Rao et al., 1997). Another possible mechanism for impaired energy metabolism in HE and hyperammonemia is the mitochondrial permeability transition pore. This leads to a collapse of the mitochondrial (mainly astrocytic) inner membrane potential that is created by the pumping out of protons by the electron transport chain. Loss of the membrane potential leads to osmotic swelling of the mitochondrial matrix, defective oxidative phosphorylation, decrease of ATP synthesis, and the production of ROS (Rama Rao and Norenberg, 2012). This in combination with a possible impairment in lactate production and release, could be setting the brain in a dysmetabolic state, with alterations in neuronal activity, oxygen consumption and therefore changes in CBF and oxygen supply, which improves when hyperammonemia is resolved. The proposed hypothesis of decrease demand of oxygen by cells followed by decreased supply, suggests that if oxygen is not used then its delivery will be altered accordingly, similar to the Hebbian synapse theory (“if you don’t use it, you lose it”). However, further work is required to support this hypothesis.

In conclusion, the results presented in this Chapter suggest that HE is associated with reduced brain tissue PO_2, which is independent of systemic hypotension, with

ammonia playing a key role. While the exact mechanism of the reported phenotype is still unclear, it is proposed that ammonia acts by diminishing brain metabolic activity and oxygen consumption, as well as increasing vascular tone [via NO, lactate, mitochondrial deficiency (planned to be investigated in more depth), compressed blood vessels] with secondary effects on CBF. The hypoxic conditions reported in this study are sufficient to trigger astrocytic activation, (Angelova et al., 2015) as well as neuronal death (Banasiak and Haddad, 1998) and are hypothesised to contribute to the pathogenesis of HE.

Chapter 3: Ammonia mediates cortical hemichannel dysfunction and impairs lactate release in rodent models of chronic liver disease with minimal hepatic encephalopathy

3.0 Introduction

Several hypotheses regarding the pathogenesis of HE have been proposed and numerous factors have been suggested as key players in HE, including: inflammation (Jalan et al., 2004b), oxidative stress (Bosoi and Rose, 2013b), impaired brain energy metabolism (Rao and Norenberg, 2001) and (the most common one) the neurotoxic effects of ammonia (Shawcross and Jalan, 2005). Recent evidence demonstrated that astroglial lactate production and release in cortical cultures and in the somatosensory cortex of anesthetised rats is facilitated in the presence of ammonia (Lerchundi et al., 2015). This appears to be due to acidification of the mitochondrial matrix resulting in a direct inhibition of mitochondrial pyruvate uptake. Increased brain lactate levels have also been reported in hyperammonemic conditions such as in ALF, which is thought to be due to inhibition of the tricarboxylic acid cycle enzyme α-ketoglutarate dehydrogenase, suggesting a reduction in oxidative metabolism (Rose et al., 2007). Results described in the previous Chapter revealed compromised cerebral PO_2 in animal models of HE, with ammonia playing a key role. Thus, it was then determined whether significant changes in brain lactate metabolism develop in conditions of long-term CNS exposure to increased ammonia concentration, such as that seen during CLD or HE.

Astrocytes, one of the most numerous type of glial cell in the CNS, are thought to play an important role in HE pathogenesis. The astrocytic dysfunction developing during the progression of the disease could precipitate neuronal pathology, leading to neurological impairment. Astrocytes are extensively connected by GJ formed of connexins, which also exist as functional hemichannels allowing effective transfer of ions, metabolic substrates and signalling molecules across the plasma membrane (Bennett et al., 2003). Under normal physiological conditions, hemichannels are either closed (Contreras et al., 2003) or in a flickering state (Bukauskas and Peracchia, 1997). In certain pathological conditions, such as epilepsy and ischemia, significant changes in astroglial structure and function may occur, which are associated with changes in connexin hemichannel function, affecting coupling within the astroglial networks and their communication with other brain cells (Giaume et al., 2010). It is therefore hypothesised, that in HE, connexin hemichannel dysfunction contributes to the development of its neurological features.

There is recent evidence that hemichannels may function as a conduit of lactate transport across the membrane (Karagiannis et al., 2016). Therefore, it was next investigated whether connexin hemichannel expression and hemichannel-mediated release of lactate are altered in animal models of HE. OP (OCR-002; Ocera Therapeutics, CA, USA) was applied in this study, as described in **Chapter 2**, as an experimental ammonia-lowering treatment. The data obtained demonstrate that, in HE, ammonia mediates cortical hemichannel dysfunction associated with a significant reduction in hemichannel-mediated lactate release, whereas no significant alterations are observed in the cerebellum.

3.1 Materials and Methods

All the experiments were performed in accordance with the Animals (Scientific Procedures) Act 1986 (ASPA) revised according to the European Directive 2010/63/EU and the UK Home Office (Scientific Procedures) Act (1986) with project approval from the Institutional Animal Care and Use Committee.

3.1.1 Animal models

Male Sprague-Dawley rats (body weight ~350-400g) were obtained from a commercial supplier (Charles Rivers Laboratories, Inc.).

BDL surgery: 30 rats underwent BDL surgery as described in detail in section 2.1.1.

Non-cirrhotic hyperammonemia condition: 32 rats were administered high ammoniagenic diet (HA). The amino acid recipe used for a stock of ~100g was: 15g leucine, 7.7g phenylalanine, 7g glutamate, 10g alanine, 4.4g proline, 5.8g threonine, 11g aspartate, 5g serine, 4.8g glycine, 3.3g arginine, 9.6g lysine, 8.4g histidine, 3g tyrosine, 1.5g tryptophan and 10.6g valine. 25 g of this mix (mixed 1:5 with standard rodent chow powder) was freshly prepared daily with water in a mash form and rats were given free access to it for 5 days. The recipe approximates the amino acid composition of a rodent haemoglobin (Riggs, 1963), mimicking the effect of

gastrointestinal bleeding, which is known to result in systemic hyperammonemia (Balata et al., 2003).

Ornithine Phenylacetate (OP) treatment: 24 BDL-operated animals were treated with OP as described in detail in section 2.1.1.

Blood and brain tissue were collected under terminal isoflurane anaesthesia. Plasma biochemistry was performed using a Cobas Integra II system (Roche Diagnostics).

3.1.2 *In vitro* slice preparation

Rats were humanely sacrificed by isoflurane inhalation overdose. After cardiac perfusion with chilled (4°C) artificial cerebrospinal fluid (aCSF, 124 mM NaCl, 3 mM KCl, 2 mM $CaCl_2$, 26 mM $NaHCO_3$, 1.25 mM NaH_2PO_4, 1 mM $MgSO_4$, 10 mM D-glucose saturated with 95% O_2, 5% CO_2, pH 7.5, PCO_2 35 mmHg), with an additional 9mM Mg^{2+}, the brain was rapidly removed and placed in a bath of chilled (4-6°C) aCSF. 300 µm coronal cortical and cerebellar slices were cut using a vibrating microtome. The slices were recovered in oxygenated (95% O_2, 5% CO_2) aCSF at room temperature for 30 min.

3.1.3 Quantitative real-time PCR

Quantitative real-time PCR (RT-qPCR) was used to determine the level of connexin RNA expression in the cortex of Sham (n=5) and BDL rats (n=6). 1µg of extracted and purified RNA was reverse transcribed using the QuantiTect Reverse Transciption Kit (Qiagen) as per manufacturer's protocol. PCR reactions were performed in 20µl volumes using the TaqMan Universal Master Mix II with the final volume of 9µl cDNA, equivalent to 1µg RNA, sample template per reaction. PCR reactions were performed in duplicate using the TaqMan assay as detection method and an Applied Biosystems 7500 Real Time PCR system (Applied Biosystems Inc., Austin, TX, USA). Relative quantification values for gene expression were calculated using the comparative ΔΔCt method normalising to Ubiquitin C (Rn01789812_g1, 88 bp amplicon length, Life Technologies). The TaqMan assays used were: connexin-43 (Rn01433957_ml), connexin-36 (Rn00439121_m1), connexin-30 (Rn02042582_s1) and connexin-26 (Rn00691548_m1), all purchased from Thermo Fisher scientific.

3.1.4 Western blot

Proteins (30 µg) extracted from the cortices of 5 Sham-operated, 6 BDL, 6 HA and 5 BDL-OP-treated rats were separated by sodium dodecyl sulphate-polyacrylamide gel electrophoresis on a 4% to 12% Bis-Tris NuPAGE gel (Invitrogen) and transferred to nitrocellulose membranes. Membranes were blocked with 5% Bovine Serum Albumin and incubated with antibodies against connexin-43 (Cell Signaling

Technology, 1:1000), connexin-36 (Santa Cruz, 1:1000), connexin-30 (Invitrogen, 1 μg/mL) and connexin-26 (Thermo Fisher Scientific, 1 μg/mL). Detection of actin (Santa Cruz, 1:1000) was used to control for protein loading. Binding of antibody was detected using a horseradish peroxidase-conjugated secondary antibody (Goat anti-rabbit or goat anti-mouse IgG-HPR, Santa Cruz, 1:10000) where appropriate and the SuperSignal Chemiluminescence Substrate for detection of horseradish peroxidase (Pierce). Densitometric analysis was performed using Kodak 1D image analysis software (Kodak, Rochester, NY).

3.1.5 Measurements of lactate release using microelectrode biosensors

Amperometric enzymatic biosensors were obtained from Sarissa Biomedical (Coventry, UK). The design and operation of the biosensors were described in detail previously (Llaudet et al., 2003, Tian et al., 2009). All sensors were operating against a reference electrode (Ag/AgCl) and had a linear response to lactate within the concentration range recorded in this study (Karagiannis et al., 2016). Further information on the principle of operation and response time is given in Figure 11A-C. To control for the release of non-specific electroactive interferants, a dual recording configuration was used. In every recording, a “null” sensor, lacking enzymes but otherwise identical, was used to measure current changes not associated with lactate oxidase activity, which were then subtracted from the current recorded by the lactate biosensor (Gourine et al., 2002) (Figure 12).

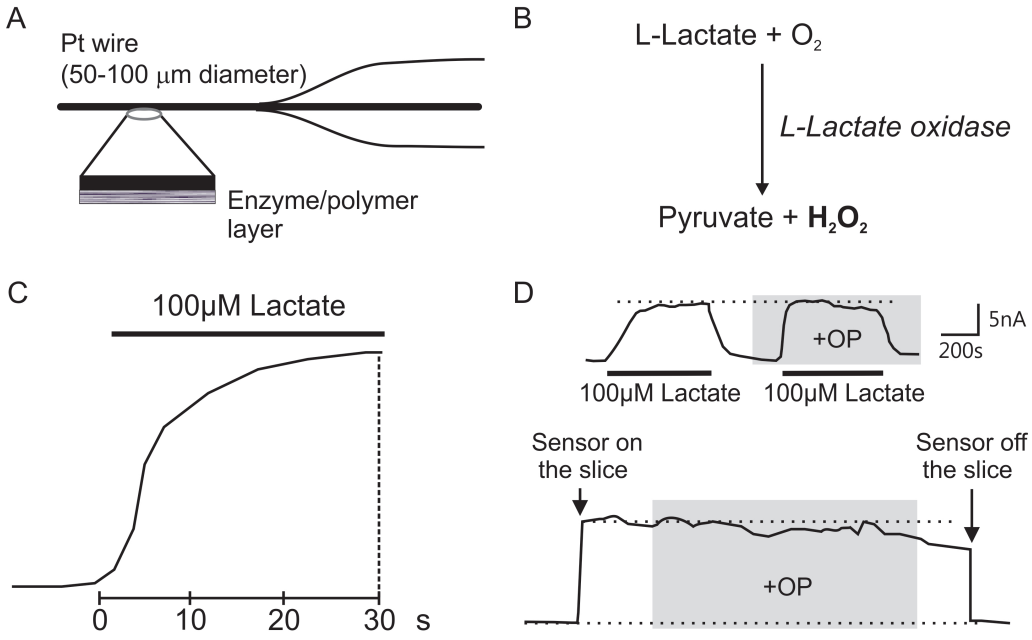

Figure 11: Response time, principles of lactate biosensor operation and the effect of OP on lactate biosensor detection system. A. A schematic drawing of the lactate biosensor assembly showing the enzymatic biolayer, which surrounds the tip of the platinum (Pt) wire. **B.** Enzymatic reaction taking place in the biolayer of the sensor. **C.** Expanded portion of the lactate calibration trace illustrating the response time of the lactate biosensor. Note that the sensor responds immediately when lactate solution is starting to enter the calibration chamber. **D.** Raw traces illustrating lactate biosensor current responses to lactate (100 μM) when calibrated in control artificial cerebrospinal fluid (aCSF), and in the presence of ornithine phenylacetate (OP, 1:50 dilution of the stock solution of 0.1g/ml; concentration applied is similar to the concentration estimated to be reached in a 300 g rat following IP injections). Bottom: Representative trace from the recordings obtained in the cerebral cortex of a BDL rat showing the effect of OP on lactate tone. Grey shading indicates period of OP application.

The sensors were calibrated directly in the slice chamber immediately before and after every recording by application of 100 μM of lactate (Figure 12). To convert changes in the biosensor current to changes in lactate concentration, an average of sensor calibrations before and after the recording were used. For each of the recordings, a slice was transferred into the recording chamber and superfused with aCSF at 35°C (3 ml min^{-1}). Sensors were initially placed in the chamber having no contact with the cortical or cerebellar slice. Once a steady-state baseline was achieved, the sensors were laid flat in direct contact with the surface of the slice (Figure 12), revealing tonic lactate release which stabilised within ~15 min. Hypoxic conditions, known to increase both lactate production due to inhibition of oxidative phosphorylation and the opening probability of connexin hemichannels (Orellana et al., 2010, Karagiannis et al., 2016), were induced for 2-4 min by replacement of oxygen in the medium with nitrogen (perfusion of the chamber with aCSF saturated with 95% N_2/5% CO_2) (Huckstepp et al., 2010). As detection of lactate by the biosensors requires oxygen (Figure 11B) (Turovsky et al., 2015), the effect of hypoxia was determined by measuring the peak lactate release upon re-oxygenation (Figure 12) as described in detail previously (Turovsky et al., 2015, Karagiannis et al., 2016). Once the baseline was restored, Ca^{2+}-free aCSF (with the addition of 1 mM EGTA) was applied for 20 min as the second stimulus known to increase the opening probability of certain membrane channels, including connexin hemichannels (Muller et al., 2002). There is no prior evidence that Ca^{2+}-mediated increases in mitochondrial NADH influence cytosolic NAD^+/NADH homeostasis and therefore lactate production (Marcu et al., 2014). These stimuli were reapplied in the presence of connexin hemichannel blockers carbenoxolone (CBX, 100 μM; Sigma) or 5-Nitro-2-(3-phenylpropylamino)benzoic acid (NPPB, 200 μM, Sigma) and an MCT blocker,

4-CIN (250 mM; Sigma). CBX, NPPB and 4-CIN were previously shown to have no effect on lactate biosensor detection system (Karagiannis et al., 2016).

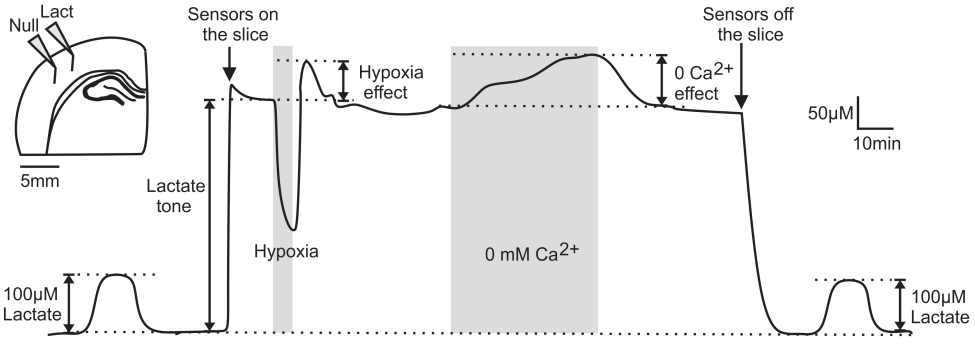

Figure 12: Measuring release of lactate using microelectrode biosensors. Representative example of changes in the net lactate biosensor current (difference in current between lactate and null sensors) during calibration (100 μM lactate), after biosensor placement in direct contact with the surface of the cortical slice (recording tonic lactate release), in response to a hypoxic challenge (perfusion with aCSF saturated with 95% N_2/5% CO_2), and in response to lowering extracellular [Ca^{2+}]. Peak hypoxia-induced lactate release is measured upon reoxygenation. Upper left: Schematic drawing of the dual recording configuration of lactate and null (control) biosensors placed on the surface of the brain slice.

3.1.6 Assessment of connexin-43 hemichannel function by dye loading of transfected HeLa cells

For the assessment of hemichannel functionality (effectiveness of channel opening and closing) 200 µM fluorescent dye carboxyfluorescein (CBXF: 376 Da) was used. Connexin hemichannels are permeable to CBXF and can act as conduits of CBXF transfer across the membrane in accord with the concentration gradient of the dye. When the cells are exposed to a condition that triggers connexin opening (e.g. 0 Ca^{2+} aCSF), CBXF enters the cells. The dye remains in the HeLa cells making them fluorescent under the microscope and the amount of fluorescence correlates with opening of hemichannels. Connexin-43 transfected HeLa cells (on coverslips) were subjected to CBXF for 5 min in Ca^{2+}-free aCSF (positive control) or 5 mM ammonia aCSF. This was then followed by a wash of 30 min in standard aCSF. For analysis, 40 cells were randomly chosen for each condition. Using ImageJ, an ROI was drawn around each cell body and the median pixel intensity for the cell was calculated. Background fluorescence was subtracted (Huckstepp et al., 2010).

3.1.7 Assessment of cortical hemichannel function by dye loading

Cortical slices from Sham-operated, BDL, HA and BDL-OP-treated rats were exposed to control aCSF with an addition of CBXF for 9 min resulting in background connexin-mediated dye loading, followed by perfusion with Ca^{2+}-free aCSF without CBXF for 9 min resulting in CBXF unloading. Ca^{2+}-free aCSF with CBXF was then applied for 4 min increasing the permeability of hemichannels and therefore resulting

in dye loading. Hypoxic conditions (without CBXF) were next applied to unload the slice and also to demonstrate bidirectional permeability of the channel to CBXF (Meigh et al., 2013). The same hypoxic stimulus was then re-applied in the presence of CBXF, resulting in dye loading. After application of each stimulus in the presence of CBXF, a further 5 min perfusion with aCSF containing CBXF, followed by a 10 min wash with normal aCSF was applied, enabling the channels to return to their physiological state. Images were taken using MiCAM-02 imaging system (SciMedia). Using ImageJ software, ROI were drawn around an area of the cerebral cortex (~3cm^2) across layers I-III and the mean pixel intensities for the ROI were calculated. Background fluorescence was subtracted.

3.1.8 ***Statistical analysis***

For the analysis of the RT-qPCR data, the intervals of confidence (95% IC) have been obtained by applying the general formula for the propagation of errors to the initial standard deviations of the duplicates measured for each sample (Chapman et al., 2012). Western blot data were normalised using the protocol of LI-COR Biosciences (Normalisation Accuracy for Western Blotting) and group data were compared using two-way ANOVA with Tukey post hoc test. Data obtained using biosensor recordings were analysed and presented non-parametrically using box and whisker plots (Figures 13-15A, 16A-C). For the comparisons between the experimental groups, Kruskal-Wallis test followed by Dunn's post hoc test was applied. The peak hypoxia- or 0 Ca^{2+}-induced lactate releases are presented as changes in release from the baseline (Figure 12). The effects of connexin blockers

are presented as % changes from the control responses recorded in the absence of the blockers and Wilcoxon signed rank test was applied for comparison. *p* values in Figures 13-15B,C indicate significance level of differences between the control responses and the responses recorded in the presence of the drugs.

Data obtained in dye loading experiments were analysed using two-way ANOVA (Figure 18-19B, data normally distributed) followed by Tukey post hoc test or Wilcoxon signed rank test (Figures 19C-D, data not normally distributed), as appropriate. The biochemistry data was analysed using one-way ANOVA. Data are reported as mean±SEM. Differences with *p* value of <0.05 were considered to be significant. In all the experiments the 'n' number represents the number of animals. Sample sizes were calculated using Gpower 3 v3.1.9.2 (http://www.gpower.hhu.de/en.html) (Faul et al., 2009); using a 'means: Wilcoxon-Mann-Whitney test (two groups)' test, with a desired power of 90% and a significance level of 5%. The effect size varied between groups according to the preliminary data acquired during the study. Statistical analysis was performed using OriginPro 9.1 (OriginLab).

3.2 Results

3.2.1 Biochemistry

Plasma biochemistry and ammonia concentration were assessed in all groups of animals, indicating the same parameters described in **Chapter 2** (Table 2-3). Additionally, rats fed with HA diet had similar plasma biochemistry to control rats. Plasma ammonia concentrations were significantly higher in BDL and HA rats when compared to Sham-operated animals ($p<0.001$) (Table 2-3).

Parameters	**HA**
N numbers	**22**
Ammonia, µmol/L	121±4**
Albumin, g/L	30±0.4
Total protein, g/L	51±1
Bilirubin, µmol/L	4±0.3
ALT, U/L	17±2

Table 3: Plasma biochemistry of hyperammonemic (HA) rats. ALT: alanine aminotransferase. Data expressed as means±SEM, **p<0.001 compared to Sham group using one-way ANOVA.

3.2.2 Release of lactate in the cerebral cortex and cerebellum in animal models of HE

In cortical slices of Sham-operated animals, enzymatic amperometric biosensors detected tonic lactate efflux of 335±10 μM (n=18). Recordings from cortical slices of BDL and HA rats showed lower tonic release of lactate of 203±6 μM (p=0.03, n=18) and 178±8 μM (p=0.005, n=16), respectively (Figure 13A). Increasing the permeability of connexin hemichannels by lowering $[Ca^{2+}]_e$ (0 Ca^{2+} conditions) triggered similar increases in the release of lactate in Sham-operated rats (by 43±3μM, n=15), BDL (by 38±4 μM; p=0.07, n=17) and HA animals (by 54±4 μM; p=0.5, n=16) (Figure 14A). Hypoxia facilitated release of lactate in cortical slices of Sham-operated rats (43±3 μM, n=18), but had no effect on lactate release in slices of BDL (1±0.8 μM; p<0.001, n=18) and HA animals (5±2 μM; p<0.001, n=16) (Figure 15A). These results demonstrated impaired tonic and hypoxia-induced release of lactate in both animal models of HE.

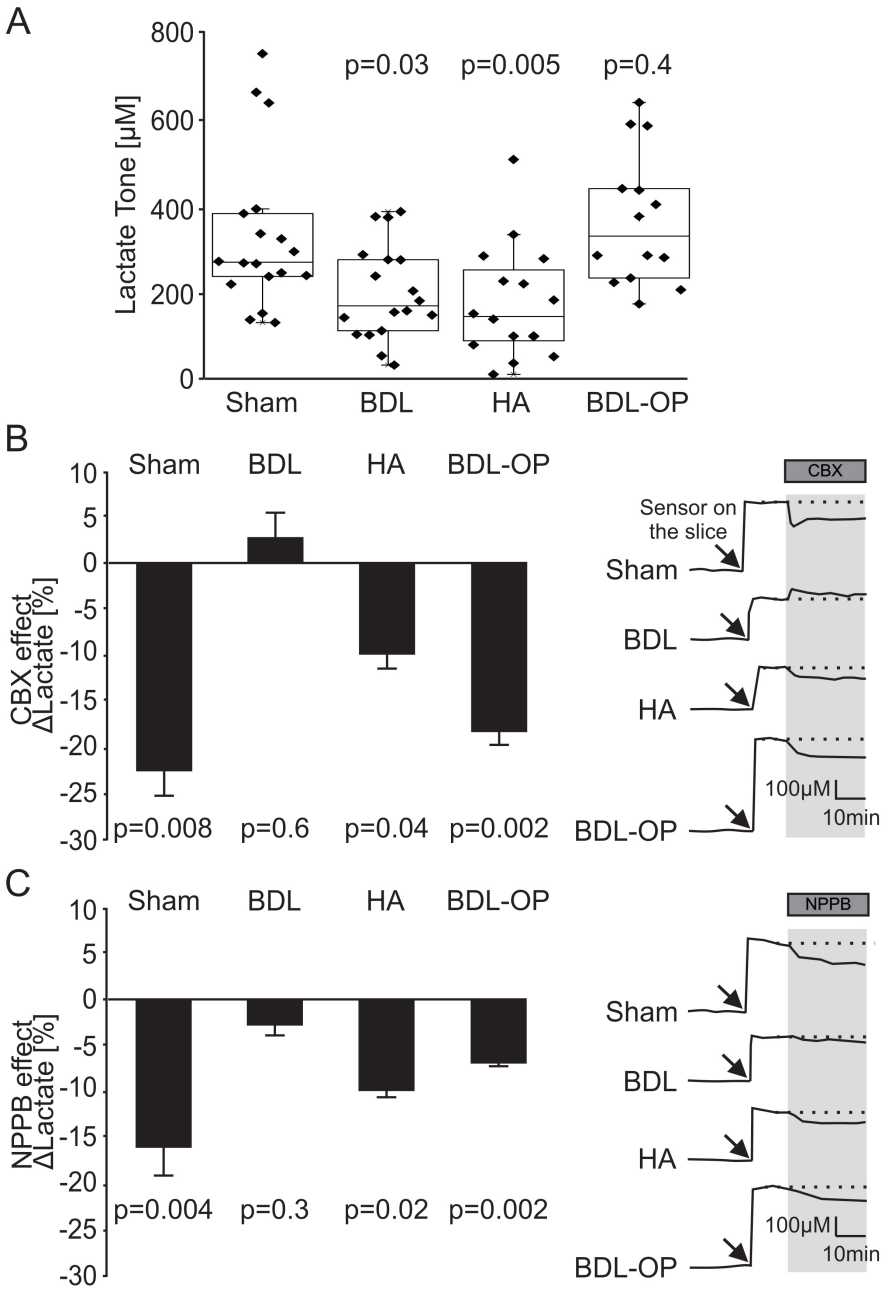

Figure 13: HE is associated with a reduction in hemichannel-mediated release of lactate in the cerebral cortex. A. Summary data illustrating tonic release of lactate in cortical slices of Sham operated, BDL, HA, and BDL-OP treated rats. *p* values indicate differences from Sham-operated rats. **B.** Left: Summary data illustrating the effect of CBX (100 µM) on tonic release of lactate (expressed as percent change from the baseline) in cortical slices of Sham-operated, BDL, HA, and BDL-OP treated rats. Right: Representative recordings of lactate biosensor current showing changes in tonic release of lactate in

response to CBX application. *p* values indicate differences from the respective baseline. **C.** Left: Summary data illustrating the effect of NPPB (200 μM) on tonic release of lactate (expressed as percent change from the baseline) in cortical slices of Sham-operated, BDL, HA, and BDL-OP treated rats. Right: Representative recordings of lactate biosensor current showing changes in tonic release of lactate in response to NPPB application. *p* values indicate differences from the respective baseline.

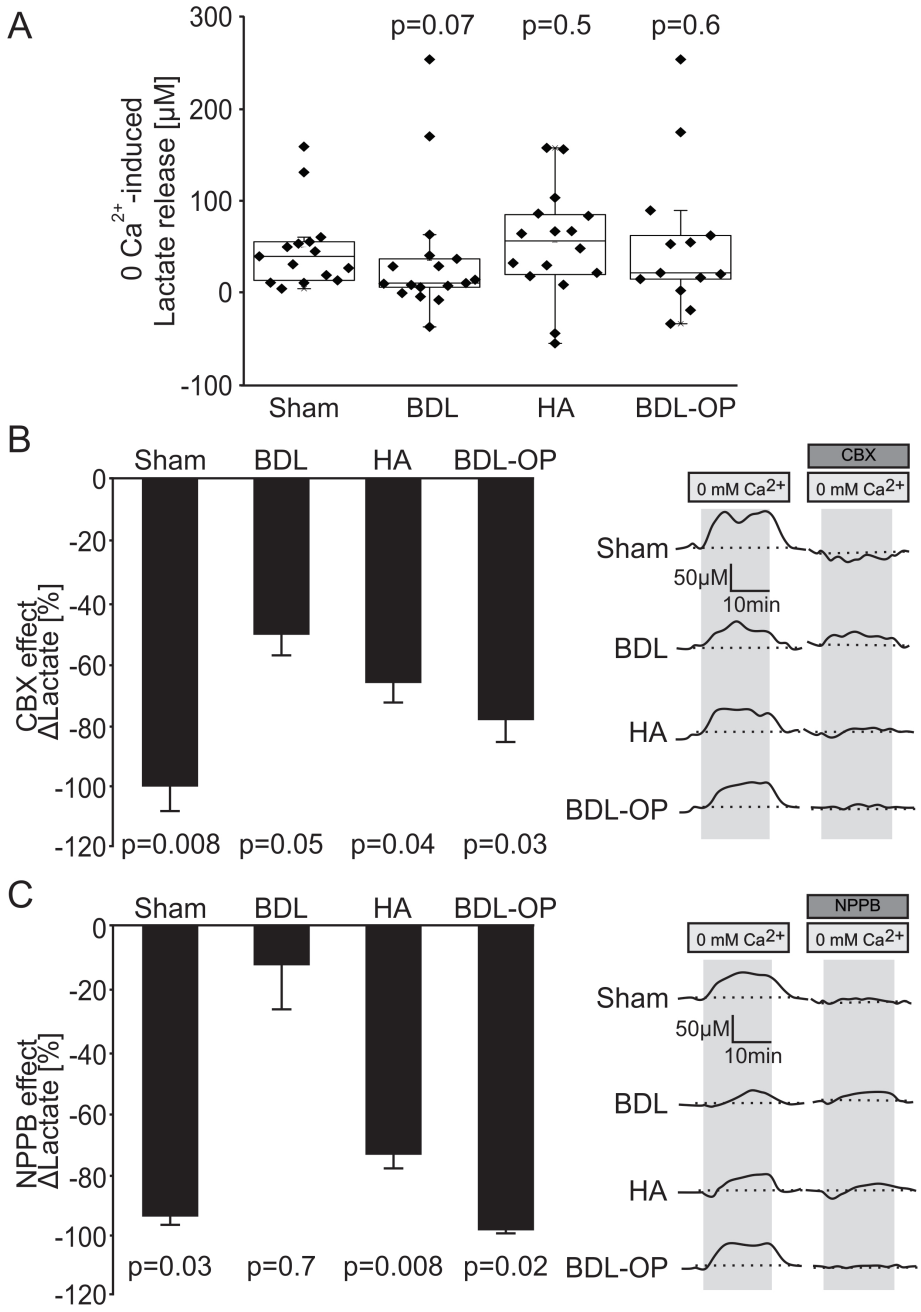

Figure 14: Lactate release in response to lowering extracellular [Ca^{2+}]. A. Summary data illustrating peak changes in lactate release in response to lowering $[Ca^{2+}]_e$ in cortical slices of Sham-operated, BDL, HA, and BDL-OP treated rats. *p* values indicate differences from the responses recorded in Sham-operated rats. **B.** Left: Summary data illustrating the effect of CBX (100 µM) on the release of lactate facilitated in response to 0 $[Ca^{2+}]_e$ (expressed as the percentage of the amount of lactate released in response to 0 $[Ca^{2+}]_e$ in

the absence of CBX) in cortical slices of Sham-operated, BDL, HA, and BDL-OP treated rats. Right: Representative recordings of lactate biosensor current showing the effect of CBX on 0 $[Ca^{2+}]_e$ -induced release of lactate. *p* values indicate differences between the responses recorded in the absence and presence of CBX. **C.** Left: Summary data illustrating the effect of NPPB (200 μM) on the release of lactate facilitated in response to 0 $[Ca^{2+}]_e$ (expressed as the percentage of the amount of lactate released in response to 0 $[Ca^{2+}]_e$ in the absence of NPPB) in cortical slices of Sham-operated, BDL, HA, and BDL-OP treated rats. Right: Representative recordings of lactate biosensor current showing the effect of NPPB on 0 $[Ca^{2+}]_e$ -induced release of lactate. *p* values indicate differences between the responses recorded in the absence and presence of NPPB.

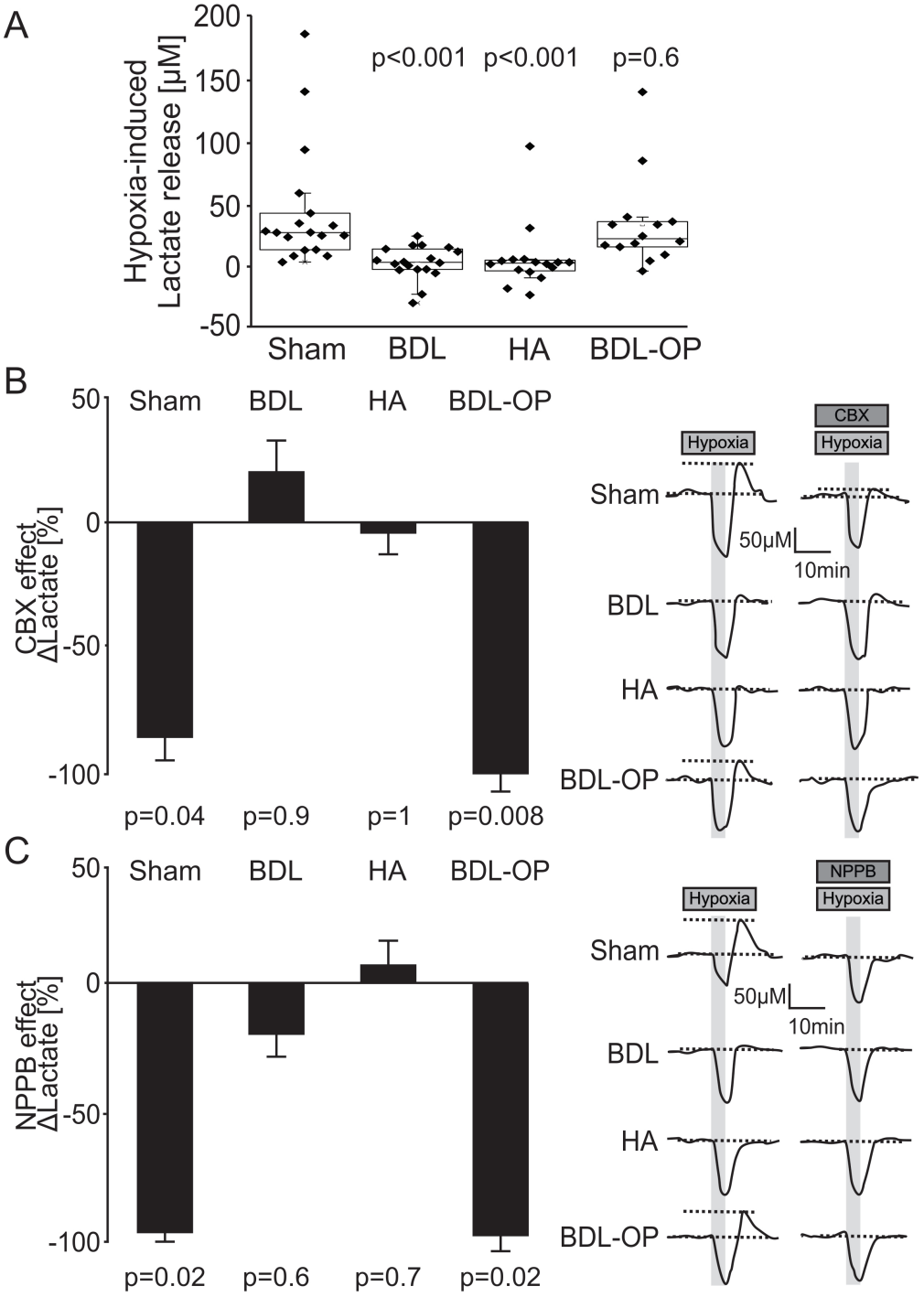

Figure 15: HE is associated with a reduction of hypoxia-induced release of lactate. A. Summary data illustrating peak changes in lactate release in response to hypoxia (aCSF saturated with 95% N_2/5% CO_2) in cortical slices of Sham-operated, BDL, HA, and BDL-OP treated rats. *p* values indicate differences from the responses recorded in Sham-operated rats. **B.** Left: Summary data illustrating the effect of CBX (100 µM) on the release of lactate facilitated in response to hypoxia (expressed as the percentage of the amount of lactate

released in response to hypoxia in the absence of CBX) in cortical slices of Sham-operated, BDL, HA, and BDL-OP treated rats. Right: Representative recordings of lactate biosensor current showing the effect of CBX on hypoxia-induced release of lactate. Decrease in O_2 availability reduces biosensor current followed by a positive signal upon reoxygenation, which is used to estimate hypoxia-induced lactate release. *p* values indicate differences between the responses recorded in the absence and presence of CBX. **C.** Left: Summary data illustrating the effect of NPPB (200 μM) on the release of lactate facilitated in response to hypoxia (expressed as the percentage of the amount of lactate released in response to hypoxia in the absence of NPPB) in cortical slices of Sham-operated, BDL, HA, and BDL-OP treated rats. Right: Representative recordings of lactate biosensor current showing the effect of NPPB on the hypoxia-induced release of lactate. *p* values indicate differences between the responses recorded in the absence and presence of NPPB.

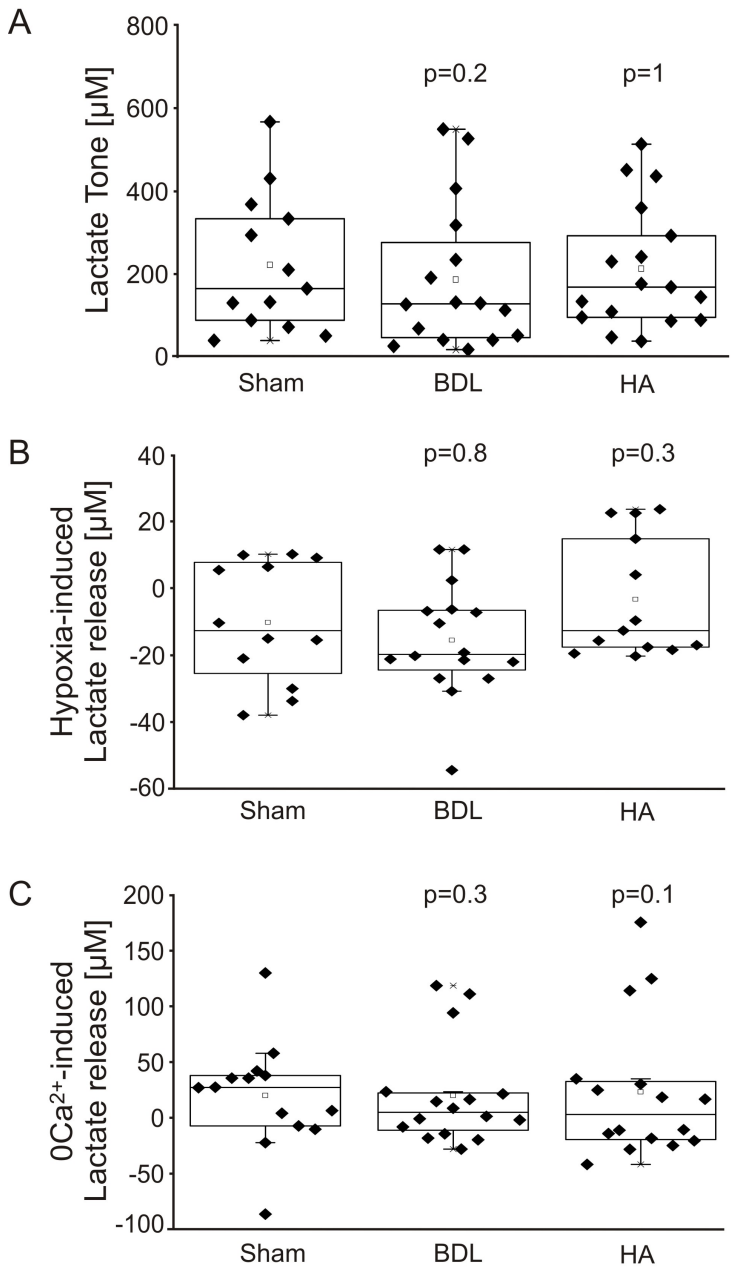

Figure 16: HE is not associated with alterations in lactate release in the cerebellum. A. Summary data illustrating tonic release of lactate in cerebellar slices of Sham-operated, BDL and HA rats. **B.** Summary data illustrating peak changes in lactate release in response to hypoxia (aCSF saturated with 95% N_2/5% CO_2) in cerebellar slices of Sham-operated, BDL and HA rats. **C.** Summary data illustrating peak changes in lactate release in response to lowering $[Ca^{2+}]_e$ in cerebellar slices of Sham-operated, BDL and HA rats. *p* values indicate differences from the Sham-operated rats.

The same protocol was applied to record lactate release in cerebellar slices from Sham, BDL and HA animals. In Sham-operated animals biosensors detected tonic lactate efflux of 221±13 μM (n=13). In BDL and HA rats, the lactate tone recorded was 183±11 μM (n=16, p=0.2) and 211±9 μM (n=17, p=1) respectively, which was not significantly different from the Sham-operated animals (Figure 16A). Hypoxia-induced no lactate release in cerebellar slices of Sham-operated rats (0±2 μM, n=12), and it was not different from the lactate release in slices of BDL (-5±1 μM; p=0.8, n=16) and HA animals (0±2 μM; p=0.3, n=13) (Figure 16B). Finally, increasing the permeability of connexin hemichannels by lowering $[Ca^{2+}]_e$ triggered similar increases in the release of lactate in Sham-operated rats (by 39±13μM, n=13), BDL (by 32±1 μM; p=0.3, n=16) and HA animals (by 28±3 μM; p=0.1, n=16) (Figure 16C). These results demonstrated intact tonic and hemichannel-induced release of lactate in the cerebellum of both animal models of HE.

Due to the cerebellar recordings from BDL and HA not being significantly different from the ones observed in the Sham-operated animals, the rest of the experiments were focused on the cerebral cortex.

3.2.3 Ammonia lowering treatment restores cortical lactate release

Experimental evidence further demonstrated that OP treatment of BDL rats restored tonic (374±11 μM; p=0.4, n=14) and hypoxia-induced (32±3 μM; p=0.6, n=14) lactate release similar to that recorded in cortical slices of Sham-operated animals (Figure 13A, 15A). Direct application of OP on cortical slices of Sham-operated and BDL rats

had no effect on lactate release (Figure 11D). These results strongly suggest that high ammonia levels are responsible for the reduction in lactate release in the cerebral cortex of BDL animals.

3.2.4 Impaired hemichannel function underlies reduced cortical lactate release in animal models of HE

In cortical slices of Sham-operated animals, application of hemichannel blockers CBX (n=9) or NPPB (n=9) resulted in a significant reduction in lactate tone (Figure 15B-C). Hemichannel blockade had no effect on lactate tone in cortical slices of BDL animals (Figure 13B-C). However, hemichannel blockade had an effect on lactate tone recorded in cortical slices of HA animals (CBX: n=10; NPPB: n=8) (Figure 13B-C). CBX and NPPB reduced lactate tone in cortical slices of BDL animals treated with OP (CBX: n=10; NPPB: n=10) (Figure 13B-C).

In cortical slices of Sham-operated (CBX: n=8; NPPB: n=6) and HA animals (CBX: n=10; NPPB: n=8), hemichannel blockade using CBX or NPPB abolished or significantly reduced the amount of lactate release facilitated in Ca^{2+}-free conditions (Figure 14B-C). Smaller effect of hemichannel blockers on 0 Ca^{2+}-induced release of lactate was observed in cortical slices of BDL rats (CBX: n=11; NPPB: n=9) (Figure 14B-C). In conditions of OP treatment, when basal and evoked lactate release were restored in cortical slices of BDL rats, CBX (n=7) and NPPB (n=7) abolished the release of lactate triggered by 0 Ca^{2+} (CBX: n=7; NPPB: n=7); an effect similar to

that observed after application of hemichannel blockers in cortical slices of Sham-operated animals (Figure 14B-C).

Hypoxia-induced release of lactate recorded in cortical slices of Sham-operated animals was also abolished or markedly reduced by connexin hemichannel blockade (CBX: n=9; NPPB: n=7) (Figure 15B-C). CBX and NPPB had no significant effect on the release of lactate induced by hypoxia in cortical slices of BDL (CBX: n=13; NPPB: n=9) and HA rats (CBX: n=10; NPPB: n=12) (Figure 15B-C). In cortical slices of OP-treated BDL rats, the effects of CBX and NPPB were restored. CBX (n=8) and NPPB (n=7) effectively abolished hypoxia-induced lactate release in cortical slices of BDL rats treated with OP (Figure 15B-C).

Application of MCT blocker, α-Cyano-4-hydroxycinnamic acid (4-CIN) had no significant effect on tonic release of lactate in cortical slices of Sham-operated (n=5) and BDL rats (n=5) (Figure 17A-B). Hypoxia-induced lactate release recorded in Sham-operated rats (n=5) was significantly reduced by 4-CIN, as reported previously (Karagiannis et al., 2016). In cortical slices of BDL rats (n=5) the effect of 4-CIN on hypoxia-induced release of lactate was found to be smaller (Figure 17A-B).

These results demonstrate that connexin hemichannel blockade has no effect on the release of lactate in the cerebral cortex of BDL rats. This implies that the function of hemichannels, which act as conduits of lactate release (Karagiannis et al., 2016), is already compromised in the brains of these animals. These data also suggest that

cortical hemichannel dysfunction in the BDL animals is likely to be due to the actions of ammonia.

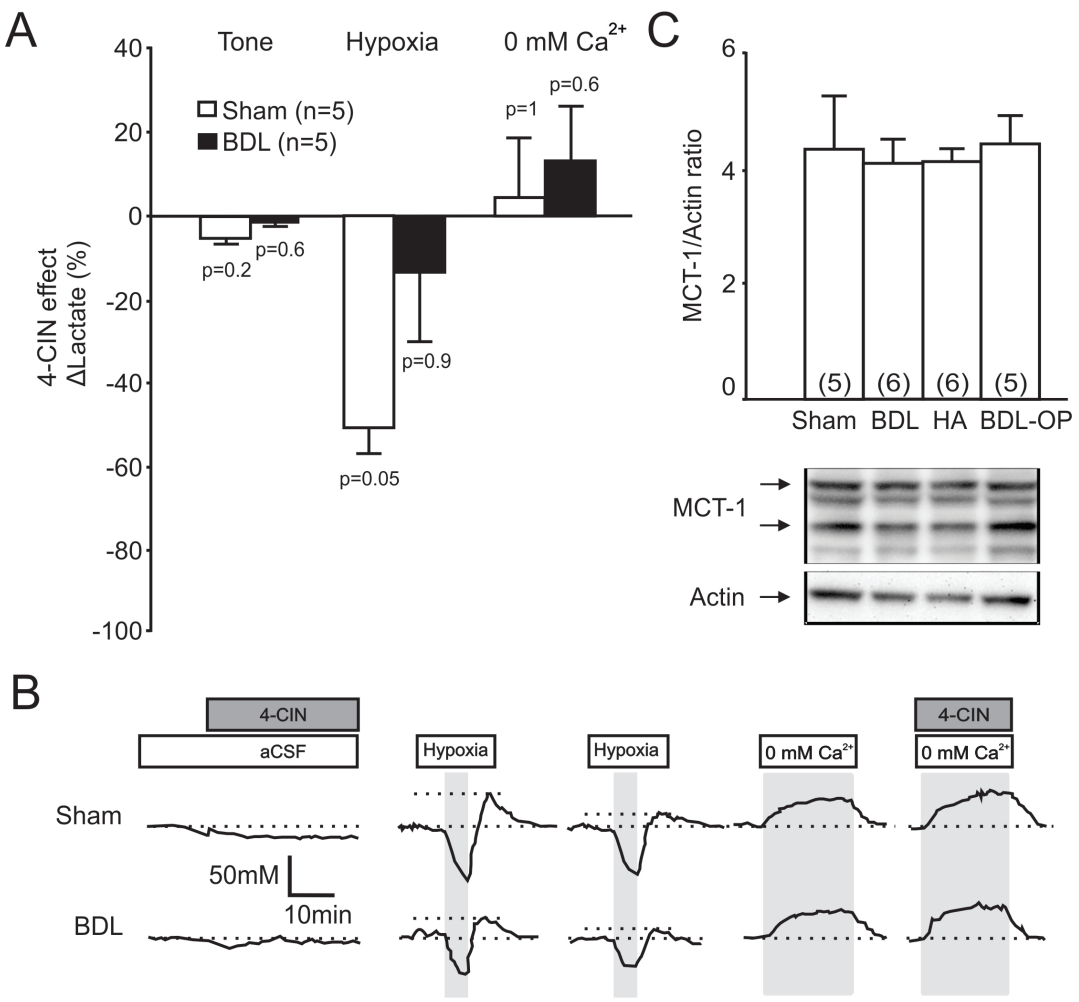

Figure 17: Monocarboxylate transporter (MCT) protein expression and functionality in cortical slices of Sham-operated and BDL rats. A. Summary data illustrating the effect of MCT blocker, 4-CIN (250 μM, Sigma) on tonic release of lactate (expressed as % change from the baseline) and release of lactate facilitated in response to tissue hypoxia and 0 $[Ca^{2+}]_e$ (expressed as the % of the amount of lactate released in response to hypoxia/0 $[Ca^{2+}]_e$ in the absence of 4-CIN) in cortical slices of Sham-operated, BDL, HA and BDL-OP treated rats. *p* values indicate differences between responses recorded in the absence and presence of 4-CIN. **B.** Representative recordings of lactate biosensor current showing the effect of 4-CIN on tonic as well as hypoxia- and 0 $[Ca^{2+}]_e$ -induced release of lactate. **C.** Summary data illustrating means±SEM of the densitometry of MCT-1 protein levels, mainly

expressed in astrocytes (Chemicon International, 0.5 µg/mL) normalised to the expression of Actin, in cell lysates of the cerebral cortices of Sham-operated, BDL, HA and BDL-OP treated rats. Bottom: Representative immunoblots showing MCT-1 protein expression in cerebral cortices of Sham-operated, BDL, HA and BDL-OP treated rats.

3.2.5 Connexin-43 hemichannel-mediated dye loading in transfected HeLa cells exposed to high concentrations of ammonia

HeLa cells transfected to express connexin-43, were kindly provided by Professor Nicholas Dale (Warwick University) for dye loading experiments. These experiments were performed at the beginning of this PhD study and the idea behind this work was to acquire data on whether the increased cerebral concentration of ammonia has an effect on the hemichannel functionality. If this hypothesis is correct then the fluorescence of the HeLa cells incubated with ammonia will be altered.

The results obtained demonstrated that a 3 day incubation of the cells with 5 mM ammonia has an effect on the connexin-43 hemichannel opening as illustrated in Figure 18A. The opening of the channels after incubation with ammonia, exposed to 0 Ca^{2+} stimulus, was significantly lower than in the control cells exposed to the same stimulus (0 Ca^{2+}) (Figure 18B). This observation supports the idea that ammonia may directly alter connexin-43 functionality. Therefore, this hypothesis was further investigated using dye loading in slices of the cerebral cortex from Sham-operated rats and animal models of HE.

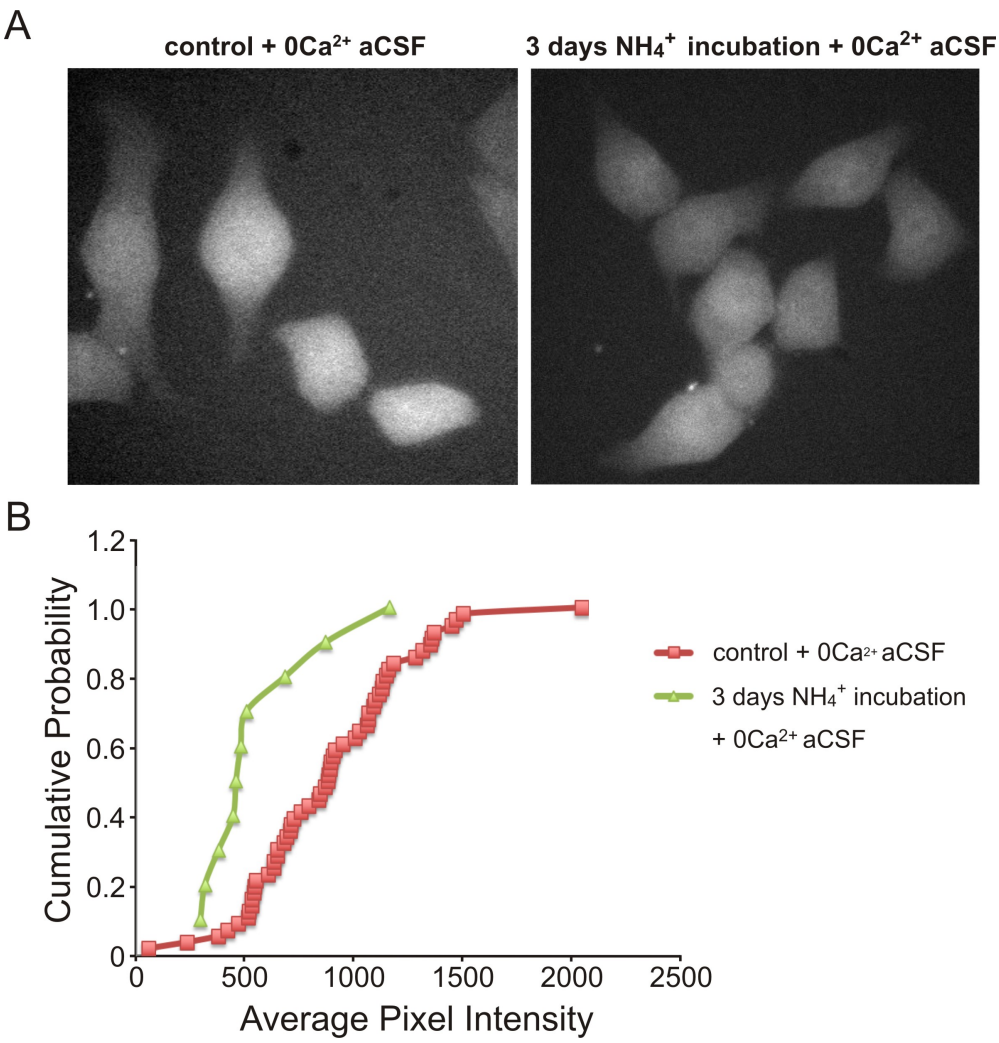

Figure 18: Ammonia impairs connexin-43 mediated dye loading in transfected HeLa cells. A. Dye loading assay demonstrating $0Ca^{2+}$-induced loading of carboxyfluorescein in HeLa cells expressing connexin-43, in the presence and absence of ammonia (NH_4^+) incubation. Cells incubated with ammonia (NH_4^+) for 3 days show lower uptake of the fluorescent dye compared to controls (no incubation). Scale bars 40 µm. **B.** Cumulative probability plots showing the average pixel intensity of connexin-43 transfected control HeLa cells (red) and HeLa cells treated for 3 days with 5 mM ammonia (green) and exposed to 0 Ca^{2+} conditions. Each curve illustrates the averaged pixel intensity recorded from 40 cells.

3.2.6 Hemichannel-mediated dye loading in animal models of HE

Membrane channel-mediated dye loading experiments were next performed in cortical slices to investigate brain hemichannel dysfunction in HE. In cortical slices of Sham-operated rats (n=10), significant background loading (14.3±0.4 A.U) was observed in control conditions when slices were perfused with aCSF containing CBXF (Figure 19A-B). Increasing the permeability of hemichannels by lowering $[Ca^{2+}]_e$ in the absence of CBXF reduced slice fluorescence by 6.4±0.2 A.U. The same stimulus applied in the presence of CBXF significantly increased fluorescence by 16.9±0.6 A.U. Hypoxia-induced opening of hemichannels in the absence of CBXF resulted in dye unloading with fluorescence decreasing by 12.7±0.4 A.U. Addition of CBXF in conditions of hypoxia increased slice fluorescence by 13.9±0.4 A.U (Figure 19B).

In cortical slices of BDL rats (n=10) efficacy of CBXF dye loading and unloading was markedly reduced under all the conditions (Figure 19A-B). Cortical slices from HA rats (n=10) displayed background loading (Figure 19A-B) and 0 Ca^{2+} -induced unloading of 11.2±0.2 A.U (p=0.04) and 4.7±0.08 A.U (p=0.4) respectively (Figure 19A-B). Addition of CBXF in 0 Ca^{2+} conditions increased fluorescence by 11.6±0.2 A.U (p=0.004), similar to that observed in slices of Sham-operated animals. However, the effect of hypoxia was significantly reduced in slices of HA animals (unloading by 7.6±0.1 A.U, p<0.001; loading by 7.8±0.2 A.U, p<0.001) (Figure 19B). In cortical slices of BDL animals treated with OP, hemichannel-mediated CBXF dye

loading and unloading were similar to that observed in slices of Sham-operated animals (Figure 19A-B).

Hemichannel blockade with CBX or NPPB effectively abolished CBXF dye loading and unloading in cortical slices of Sham-operated animals (Figure 19C-D). In cortical slices of BDL and HA rats, CBX and NPPB had no significant effect on dye loading and unloading (Figure 19C-D). In cortical slices of OP-treated BDL rats, the effects of CBX and NPPB on CBXF dye loading and unloading were similar to that observed in Sham-operated animals. (Figure 19C-D). Figures 19C-D illustrate changes in fluorescence (ΔFluorescence) following application of the hemichannel blockers, compared to the respective changes in fluorescence recorded in the absence of the blockers in slices of the same animal. Negative values show decreases in fluorescence while positive values illustrate higher fluorescence levels compared to the controls.

These data show that the background activity and stimuli-evoked opening and closure of connexin hemichannels is impaired in BDL and HA rats. The efficacy of CBXF dye loading (and hence hemichannel functionality) is restored by OP treatment suggesting that the actions of ammonia are responsible for cortical hemichannel dysfunction in HE.

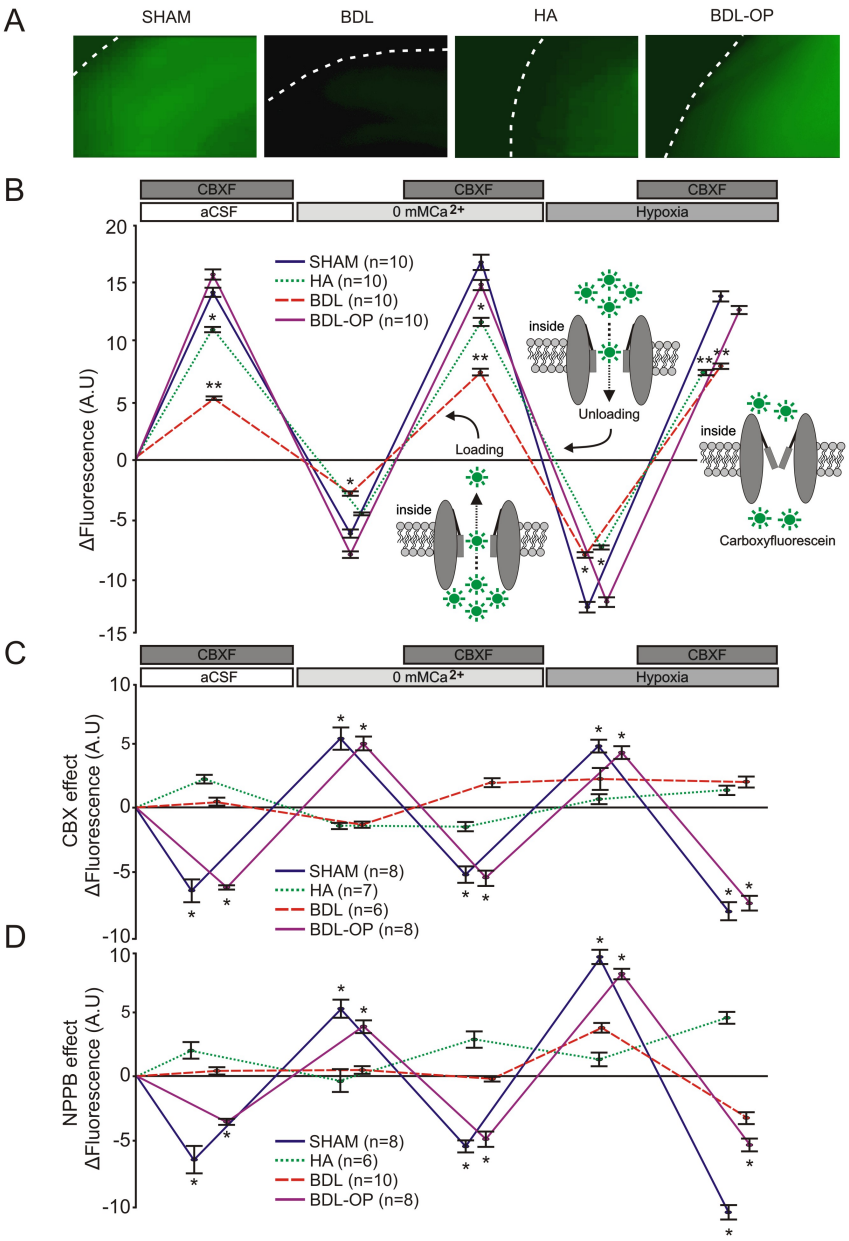

Figure 19: Impaired hemichannel-mediated dye loading reveals cortical hemichannel dysfunction in HE. A. Representative images of background loading with CBXF dye in cortical slices of Sham-operated, BDL, HA, and BDL-OP treated rats. White dashed lines depict the edge of each cortical slice. **B.** Fluorescence intensity changes in cortical slices of Sham-operated, BDL, HA, and BDL-OP treated rats in response to 0 $[Ca^{2+}]_e$ and hypoxia in the absence and presence of CBXF in the medium. Application of 0 $[Ca^{2+}]$ aCSF or hypoxia

in the presence of CBXF resulted in dye loading and an increase in fluorescence, whereas application of these stimuli in the absence of CBXF resulted in dye unloading and a decrease in fluorescence. Insets: Schematic drawings of connexin hemichannel mediated dye loading and unloading. *p<0.05, **p<0.001 versus Sham-operated animals. **C.** Summary data illustrating the effect of CBX (100 μM) on fluorescence intensity changes (ΔFluorescence) in cortical slices of Sham-operated, BDL, HA, and BDL-OP treated rats induced by 0 $[Ca^{2+}]_e$ and hypoxia in the absence and presence of CBXF in the medium. The data are presented as differences in fluorescence after CBX application compared with the respective fluorescence recorded in the absence of CBX. *p<0.05 for the effect of CBX on CBXF loading and unloading. **D.** Summary data illustrating the effect of NPPB (200 μM) on fluorescence intensity changes (ΔFluorescence) in cortical slices of Sham-operated, BDL, HA, and BDL-OP treated rats induced by 0 $[Ca^{2+}]_e$ and hypoxia in the absence and presence of CBF in the medium. The data are presented as differences in fluorescence after NPPB application compared with the respective fluorescence recorded in the absence of NPPB. *p<0.05 for the effect of NPPB on CBXF loading and unloading.

3.2.7 Cortical connexin expression in animal models of HE

The expression of the main astrocytic and neuronal connexins was next evaluated in animal models of HE used in this study. RT-qPCR was performed on mRNA extracted from the cerebral cortices of BDL and Sham-operated animals (Figure 20). The data were normalised against the housekeeping gene Ubiquitin C, which was chosen as the appropriate endogenous control gene after running a TaqMan Array Rat Endogenous Control Plate (Thermo Fisher scientific) testing 32 different genes.

The relative expression of connexin-43, the most abundant astrocytic connexin was similar in the cerebral cortex of BDL rats (1.22, CI 0.23-0.29, n=6) and Sham-operated animals (CI 0.16-0.19, n=5). No difference was observed in connexin-36 (mainly neuronal) expression between the BDL (1.16, CI 0.16-0.19, n=6) and Sham-operated animals (1, CI 0.18-0.22, n=5). Expression of connexin-30, the second main astrocytic connexin was found to be higher in the cortical tissue of BDL animals (1.49, CI 0.25-0.31, n=6) while no difference in connexin-26 expression was found (Sham-operated: 1, CI 0.24-0.32, n=5; BDL: 1.04, CI 0.18-0.21, n=6).

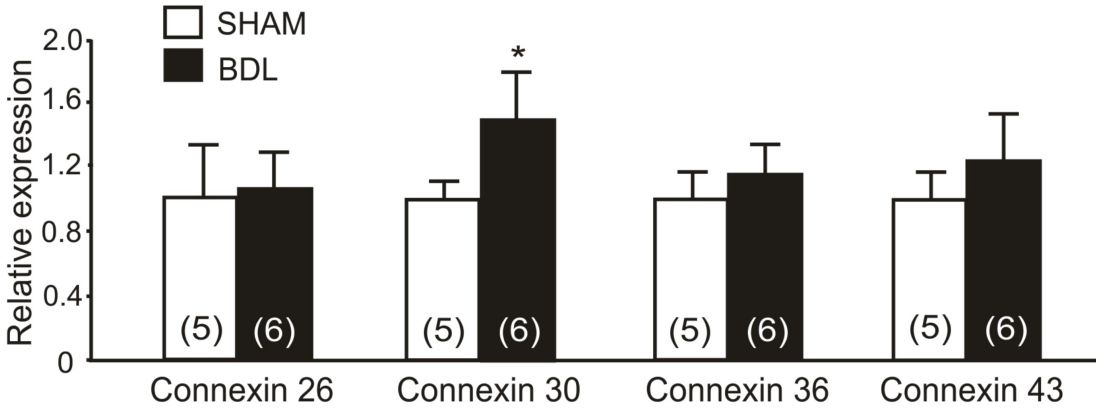

Figure 20: Cortical connexin RNA expression is not reduced in an animal model of HE. Relative expression ($2^{-\Delta\Delta Ct}$) of connexin-43, connexin-36, connexin-30 and connexin-26 mRNA normalised to the housekeeping gene, Ubiquitin C, in the cortex of Sham-operated and BDL animals.

Western blots were next performed on proteins extracted from the cerebral cortices of Sham-operated, BDL, HA and BDL-OP animals (Figure 21). No differences in cortical connexin-43, connexin-36 and connexin-30 expression was observed between Sham-operated, BDL, HA and OP-treated BDL animals. An increase in connexin-26 expression ($p=0.03$) was detected in BDL-OP rats compared to the BDL animals (Figure 21). Expression of MCT-1 was similar in all the experimental groups (Figure 17C).

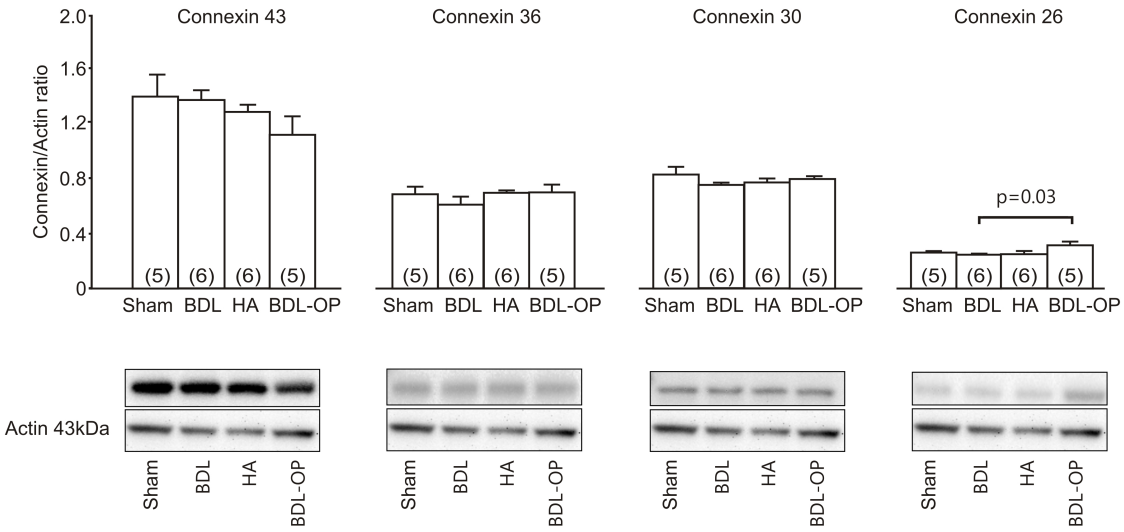

Figure 21: Connexin protein expression in the cortex is not affected in HE. Top: Summary data illustrating means±SEM of the densitometry of connexin-43, connexin-36, connexin-30, and connexin-26 protein expression normalised to the expression of actin in cell lysates of the cerebral cortices of Sham-operated, BDL, HA, and BDL-OP treated rats. **Bottom:** Representative immunoblots showing connexin-43, connexin-36, connexin-30, and connexin-26 protein expression in cerebral cortices of Sham-operated, BDL, HA, and BDL-OP treated rats. The *p* value indicates the difference in expression level between the BDL and BDL-OP treated groups.

3.3 Discussion

Astrocytes represent an important source of lactate, which contributes to the extracellular pool of readily available metabolic substrates taken up by neurons to fuel their activity (Pellerin and Magistretti, 1994). While previously, lactate transport across the cell membranes was thought to be achieved solely via operation of monocarboxylate transporters (MCTs), a recent study (Karagiannis et al., 2016) demonstrated the role of connexin hemichannels as equally important conduits of lactate release.

In animal models of ALF and patients, an increase in brain lactate concentration has consistently been reported (Rose, 2010). Concentrations of lactate in the CSF were also found to be elevated in cirrhotic patients but only in severe cases of HE (Yao et al., 1987). The BDL and HA rats used in these experiments are models of mHE (Butterworth et al., 2009). In contrast to the existing evidence suggesting that brain lactate concentrations are increased in patients with ALF (Bernal, 2010), the experiments described in this thesis demonstrated that the development of HE in rats is associated with a significant reduction in tonic and stimulated release of lactate in the cerebral cortex, whereas no marked changes were observed in the cerebellum. Additionally, hypoxia did not induce lactate release in the cerebellum of Sham-operated or diseased animals. The differences observed in the cortex and cerebellum can be explained by the heterogeneity of astrocytes present in each brain region. Detailed electrophysiological studies have revealed that protoplasmic and fibrous astrocytes in the cortex (as well as astrocytes in different brain regions)

express different levels and types of ion channels, such as K^+ channels, than Bergmann glial in the cerebellum (Butt and Kalsi, 2006, Oberheim et al., 2012). This can result in subtle differences in electrophysiological properties, including resting membrane potentials. While it is still unclear whether heterogeneity exists with regard to the number of functional hemichannels within the different classes of astrocytes, evidence exists indicating regional differences in the shape of astrocytic syncytium and level of coupling by GJ (Kettenmann and Verkhratsky, 2011). Finally, studies have revealed that in the cerebellum, due to the morphology and structural arrangement of Purkinje neurons and astrocytes, Bergmann glial cells are in more intimate arrangement to synapses. This could explain the inability to record a hypoxia-induced lactate release in the cerebellum. It is possible that due to the astrocytes being in such close proximity to synapses, lactate released as a product of the hypoxic stimulus is taken up by neurons more effectively than in the cortex, which results in no recorded increase in extracellular lactate concentration.

In the cortex, blockade of connexin hemichannels was found to be effective in reducing lactate release in Sham-operated and HA animals but was ineffective in BDL rats, suggesting that the reduction in hemichannel-mediated lactate release in BDL animals is due to a combination of pathological factors (e.g. inflammation, oxidative stress).

Increased lactate production by astrocytes appears to be essential for the recovery of synaptic function during re-oxygenation after hypoxia (Schurr et al., 1997). It was found that hypoxia-induced lactate release was significantly lower in the cerebral

cortex of BDL and HA rats compared to control animals and this was unaffected by the hemichannel blockers indicating hemichannel dysfunction. The observed decrease in extracellular lactate is likely due to impaired release from astrocytes although increased neuronal activity and therefore lactate consumption cannot be excluded. The observation of Bosoi et al., (Bosoi et al., 2014) showing higher total brain lactate of BDL rats using NMR spectroscopy seems to contradict the reported data. Bosoi and colleagues suggested that increased lactate contributes to the pathogenesis of brain oedema (cytotoxic), and may imply that the observed increase in total brain lactate is due to its intracellular accumulation. If the rate of lactate production and glymphatic clearance (Lundgaard et al., 2016) is not affected, intracellular retention of lactate would explain higher concentration of this metabolite as measured by NMR spectroscopy (Bosoi et al., 2014) and would be in full agreement with the data showing impairment of hemichannel-mediated release in HE.

High concentration of ammonia can potentially generate significant pH changes, which can have various effects on many pH sensitive membrane channels, including hemichannels. The pH sensitivity of hemichannels is known as the chemical gate, which is the phenomenon of hemichannel blockade when intracellular pH (pH_i) decreases (Duffy et al., 2002). This provides one potential mechanism, which might be responsible for impaired hemichannel-mediated lactate release in HE.

Hemichannel functionality was also examined using the dye loading method. Some differences between the data obtained using biosensor recordings and this technique

could be due to the fact that CBXF is not identical in terms of the molecular structure and size to lactate. Additionally, lactate could be released through specific connexin hemichannels, whereas CBXF is small enough to pass through the majority of hemichannels expressed by both astrocytes and neurons. While induction of hypoxia targets predominantly astroglial hemichannels (Orellana et al., 2010), the rest of the conditions are not cell specific and conclusions on affected cell types cannot be drawn from the results obtained using dye loading experiments.

The experimental stimuli used (0 Ca^{2+} and hypoxia) are known to increase the permeability of hemichannels, possibly by affecting various protein bonds resulting in conformational changes (Muller et al., 2002). Dye loading experiments clearly demonstrated a marked reduction in fluorescent dye uptake and release in cortical slices of BDL and HA rats compared to Sham-operated animals (the differences were more profound when hypoxia was used as a stimulus), suggesting reduced bidirectional permeability of hemichannels in these animal models of HE. Hemichannel blockade had no effect on fluorescent dye uptake in BDL and HA rats providing additional evidence that the function of these channels is already compromised in HE. Ammonium ions may cause structural alterations to the connexin proteins, by interacting with various amino acid side chains, which could affect gating of the channel. However, since hemichannels have a relatively short life cycle and are recycled frequently, the observed changes in hemichannel functionality appear to be reversible with OP treatment.

In CLD, hyperammonemia is believed to impair mitochondrial function and induce astroglial dysfunction, which is associated with altered neurotransmitter recycling leading to neuronal damage (Bosoi and Rose, 2009). Ammonia may also interfere with cell energy metabolism in several ways. There is recent evidence suggesting that in astrocytes, ammonia may divert the flux of pyruvate to lactate production, contributing to the net aerobic lactate production (Lerchundi et al., 2015). However, the effects of chronic ammonia exposure on astrocytes are unknown. The role of ammonia was investigated by treating BDL rats with OP, a drug known to lower systemic and brain ammonia (Davies et al., 2009). OP treatment improved the neurochemical phenotype of BDL animals by restoring the tonic and stimulated connexin hemichannel-mediated lactate release. Furthermore, hemichannel blockade became effective following OP treatment, suggesting that ammonia is indeed responsible for hemichannel dysfunction observed in this model.

Cytotoxic brain oedema observed in BDL animals is attenuated by ammonia-lowering treatments such as the one used in this study (Bosoi et al., 2011, Davies et al., 2009). The effect of cell swelling on hemichannel function is poorly understood. Ye et al., (Ye et al., 2009) showed that astrocytes obtained from connexin-43 knock-out animals developed cell swelling as efficiently as the wild type animals when exposed to a hypotonic solution suggesting that hemichannels do not play a significant role in this process although evidence to the contrary exists (Quist et al., 2000).

On further examination of the expression profile of key astroglial and neuronal connexins in the animal models of HE used in this study, no significant differences were observed. This suggests that HE is associated with altered hemichannel function but not with changes in connexin expression. The upregulated expression of connexin-26 observed in the BDL-OP animals is not prominent enough to explain the marked improvement observed in the lactate measurements and dye loading experiments. Additionally, no changes were observed in the expression of the main astroglial lactate transporter MCT-1 in the models of HE used in this study. No effect of 4-CIN, a MCT blocker, on lactate release was observed in cortical slices of Sham-operated and BDL animals. Hypoxia-induced lactate release in Sham-operated rats was significantly reduced by the application of 4-CIN, as demonstrated in the previous study (Karagiannis et al., 2016).

Depletion of lactate as one of the key readily available metabolic substrates may have important neurological consequences particularly in patients with advanced cirrhosis given the fact that these patients display evidence of cerebral vasoconstriction (Guevara et al., 1998), which is associated with impaired cerebral autoregulation, an important mechanism which ensures constant CBF (Larsen et al., 1995). Clinical consequences of this may be relevant during liver transplantation, where further reductions in CBF have been observed during the anhepatic phase of transplantation and may contribute to post-transplant neurologic dysfunction (Philips et al., 1998). Evidence for critical reduction in cerebral oxygenation was obtained in the majority of patients with acute-on-chronic liver failure who had poor neurologic outcome supporting the hypothesis that the brain energy metabolism is critically compromised in cirrhosis and further perturbations as demonstrated in this Chapter

may be clinically deleterious (Sawhney et al., 2016). The data indicating an impaired hemichannel-mediated lactate release and tissue hypoxia, in combination with these observations could help to explain the severe neurological manifestations in patients with HE. As ammonia is central in causing this dysfunction, the potential clinical implications involve the use of ammonia lowering treatments as the main therapeutic strategy, as well as attempts to increase cerebral oxygenation in order to preserve the neuronal function.

In conclusion, the results of the present study suggest that HE is associated with cortical hemichannel dysfunction, with ammonia playing a key role. The data provide evidence of a potential neuronal energy deficit due to impaired hemichannel-mediated lactate transport between astrocytes and neurons as a possible mechanism underlying pathogenesis of HE.

Chapter 4: Ammonia mediates alterations in cortical extracellular glutamate concentration in rodent models of chronic liver disease with minimal hepatic encephalopathy

4.0 Introduction

Ammonia is a ubiquitous by-product of nitrogen metabolism and the primary source of ammonia production is the gut. This takes place in the enterocytes and the ammonia-generating intestinal bacteria through the enzyme PAG, which catalyses deamination of glutamine to glutamate (Kato et al., 1992). Ammonia is therefore linked to the glutamate-glutamine cycle while its toxicity has been reported to be closely associated with the altered glutamatergic system (Bobermin et al., 2015, Gorg et al., 2010, Montana et al., 2014, Rose, 2006).

Derangements of neurotransmitter systems have been suggested to play a significant role in the pathogenesis of HE (Butterworth, 2014). Glutamate is the major excitatory neurotransmitter in the mammalian brain and alterations in its homeostasis could lead to altered signal transduction as well as deleterious effects on the neurons, since high concentrations of glutamate are neurotoxic (Cooper, 2001). A glutamate-glutamine metabolic cycle exists between astrocytes and neurons and its role is to re-cycle glutamate that has been released from neurons, preventing neuronal over excitation (Cooper, 2001). Under normal conditions, glutamate

released by presynaptic neurons induces signalling through glutamate receptors. Astrocytic glutamate transporters, EAAT1/EEAT2 in humans and GLT-1/GLAST in rodents, take up the excess glutamate and it is then converted to glutamine by the GS enzyme, preventing glutamate accumulation (Bosoi and Rose, 2013a, Kimelberg, 2005). Glutamine is then transported to neurons via glutamine transporters, where it is hydrolysed back to glutamate (Broer and Brookes, 2001).

An increase in extracellular glutamate has been documented in the rat cerebellum following portocaval anastomosis and has been described to occur as a result of decreased expression of astrocytic glutamate transporters, GLT-1 and GLAST (Suarez et al., 2000). Experimental studies described in this Chapter investigated whether glutamate release is altered in the cortex and cerebellum of animal models of CLD with mHE. In order to explore the role of ammonia, OP was applied as an experimental ammonia-lowering treatment (described previously in **Chapter 2**). The data obtained demonstrate that, in CLD, the actions of ammonia lead to a significant elevation of cortical extracellular glutamate, which may contribute to the development and pathogenesis of HE.

4.1 Materials and Methods

All the experiments were performed in accordance with the Animals (Scientific Procedures) Act 1986 (ASPA) revised according to the European Directive 2010/63/EU and the UK Home Office (Scientific Procedures) Act (1986) with project approval from the Institutional Animal Care and Use Committee.

4.1.1 Animal models

The animal models used in this study (BDL, HA and OP-treated BDL rats) have already been described in detail in **Chapter 3**.

4.1.2 *In vitro* slice preparation

In vitro slices were performed as described in section 3.1.2.

4.1.3 Measurements of glutamate release using microelectrode biosensors

Glutamate biosensors were used in the same way as the lactate biosensors, the operation of which is described fully in section 3.1.5. The design and operation of glutamate biosensors were described in detail previously (Tian et al., 2009). All sensors were operating against a reference electrode (Ag/AgCl) and had a linear

response to glutamate within the concentration range recorded in this study (Figure 22).

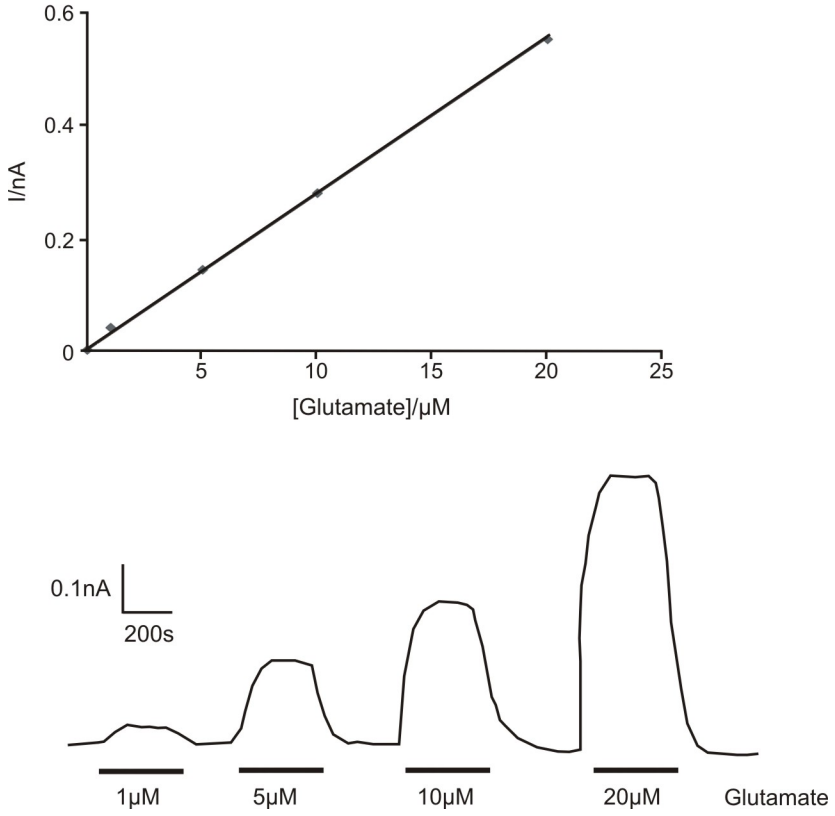

Figure 22: Representative calibration curve and sample responses of the glutamate biosensor showing a linear response to glutamate applied within the concentration range recorded in this study.

To control for the release of non-specific electroactive interferants, a dual recording configuration was used. In every recording, a “null” sensor, lacking enzymes but otherwise identical, was used to measure current changes not associated with glutamate oxidase activity, which were then subtracted from the current recorded by the glutamate biosensor (Gourine et al., 2002, Gourine et al., 2008) (same as lactate recordings in Figure 12).

In these experiments, the sensors were calibrated directly in the slice chamber immediately before and after every recording by application of 10 μM of glutamate. To convert changes in the biosensor current to changes in glutamate concentration, an average of sensor calibrations before and after the recording were used.

4.1.4 Quantitative real-time PCR

The protocol used for the quantitative real-time PCR (RT-qPCR) is described in section 3.1.3. In this experiment, the RNA expression of the astrocytic glutamate transporters, GLT-1 and GLAST, was examined in the cortex of Sham-operated (n=5) and BDL rats (n=6). Relative quantification values for gene expression were calculated using the comparative ΔΔCt method normalising to Ubiquitin C (Rn01789812_g1, 88 bp amplicon length, Life Technologies). The TaqMan assays used in this experiment were: GLT-1 (Rn00564705_m1, 92 bp amplicon length) and GLAST (Rn01402419_g1, 99 bp amplicon length) all purchased from Thermo Fisher scientific.

4.1.5 Western blot

The western blot protocol described in section 3.1.4 was applied for the quantification of GLT-1 protein in the cortices of 5 Sham-operated, 6 BDL and 6 HA rats. Membranes were blocked with 5% Bovine Serum Albumin and incubated with antibodies against GLT-1 (EAAT-2, Abcam, 1:1000). Detection of α-Tubulin (Cell Signaling Technology, 1:1000) was used to control for protein loading. Binding of antibody was detected using a horseradish peroxidase-conjugated secondary antibody (Goat anti-rabbit IgG-HPR, Santa Cruz, 1:10000) and the SuperSignal Chemiluminescence Substrate for detection of horseradish peroxidase (Pierce). Densitometric analysis was performed using Kodak 1D image analysis software (Kodak, Rochester, NY). Due to the inability to obtain a good antibody for GLAST, western blots for this specific protein were not performed.

4.1.6 *Statistical analysis*

Data obtained using biosensor recordings were analysed and presented non-parametrically using box and whisker plots (Figure 23-25A, 26). For the comparisons between the experimental groups, Kruskal-Wallis test followed by Dunn's post hoc test was applied. The peak hypoxia- or 0 Ca^{2+}-induced glutamate releases are presented as changes in the release from the baseline (Figure 24-25, 26B-C).

For the analysis of the RT-qPCR data the intervals of confidence (95% IC) have been obtained by applying the general formula for the propagation of errors to the initial standard deviations of the duplicates measured for each sample (Chapman et al., 2012). Western blot data were normalised using the protocol of LI-COR Biosciences (Normalisation Accuracy for Western Blotting) and group data were compared using two-way ANOVA with Tukey post hoc test.

4.2 Results

4.2.1 Biochemistry

Plasma biochemistry and ammonia concentration were assessed in all groups of animals, indicating the same changes as described in **Chapter 2** (Table 2-3). Rats fed with HA diet had similar plasma biochemistry to control rats. Plasma ammonia concentrations were significantly higher in both BDL and HA rats when compared to Sham-operated animals ($p<0.001$) (Table 2-3).

4.2.2 Release of glutamate in the cerebral cortex and cerebellum in animal models of HE

In cortical slices of Sham-operated animals, enzymatic amperometric biosensors detected tonic glutamate efflux of 0.9±0.06 μM, (n=27). Recordings from cortical slices of BDL and HA rats showed markedly higher tonic release of glutamate of 5.7±0.3 μM ($p<0.001$, n=28) and 7.3±0.4 μM ($p<0.001$, n=26) respectively (Figure 23).

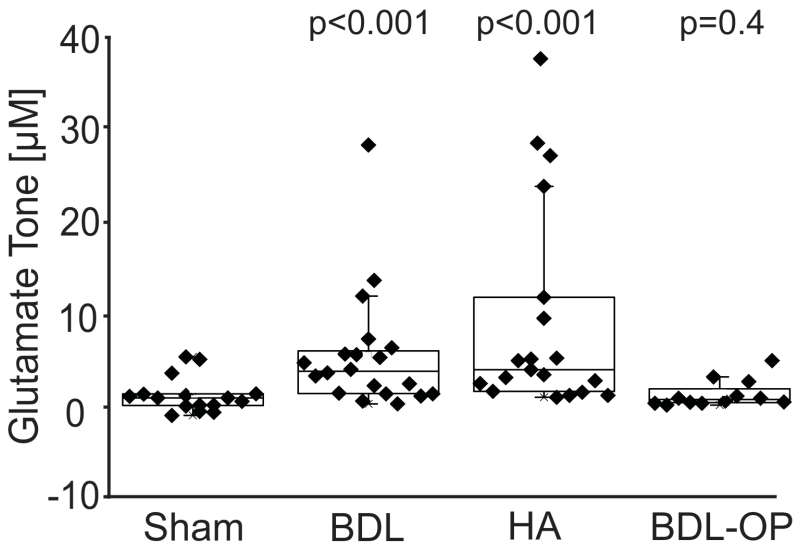

Figure 23: HE is associated with markedly higher glutamate tone in slices of the cerebral cortex. Summary data illustrating tonic release of glutamate in cortical slices of Sham operated, BDL, HA, and BDL-OP treated rats. *p* values indicate differences from the Sham-operated rats.

Increasing the permeability of connexin hemichannels by lowering $[Ca^{2+}]_e$ did not trigger glutamate release in Sham-operated rats (by Δ0.3±0.1 μM, n=24), BDL (by Δ0.5±0.1 μM, p=0.7, n=27) or HA animals (by Δ0.3±0.2 μM, p=0.5, n=22) (Figure 24). Hypoxia had a significant effect on extracellular glutamate only in cortical slices prepared from the brains of BDL (1.6±0.1 μM, p=0.02, n=28) and HA animals (5±0.3 μM, p<0.001, n=27), but not in slices of Sham-operated rats (Δ0.3±0.03 μM, n=28) (Figure 25).

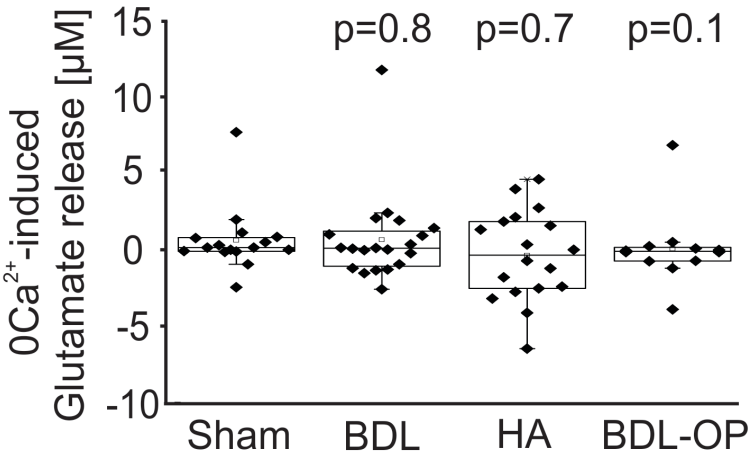

Figure 24: Glutamate release is not affected by lowering extracellular [Ca^{2+}]. Summary data illustrating peak changes in glutamate release in response to lowering $[Ca^{2+}]_e$ in cortical slices of Sham-operated, BDL, HA, and BDL-OP treated rats. *p* values indicate differences from the responses recorded in Sham-operated rats.

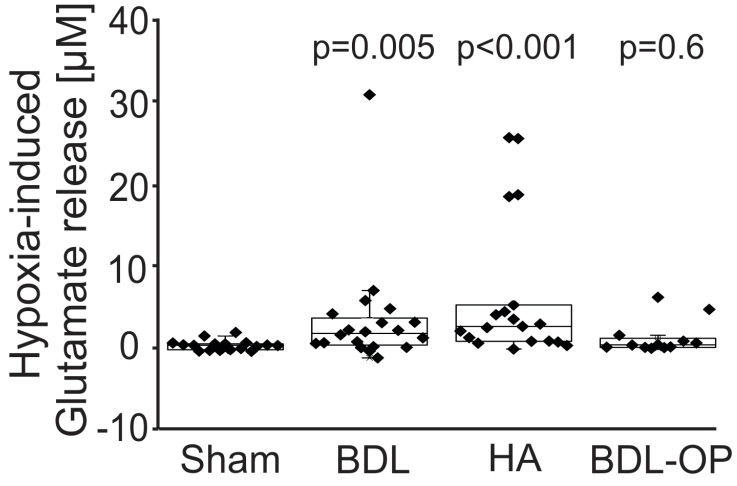

Figure 25: Hypoxia increases the level of extracellular glutamate in the cerebral cortex in animal models of HE. Summary data illustrating peak changes in glutamate release in response to hypoxia (aCSF saturated with 95% N_2/5% CO_2) in cortical slices of Sham-operated, BDL, HA, and BDL-OP treated rats. *p* values show differences from the responses recorded in Sham-operated rats.

The same protocol was applied in cerebellar slices to record glutamate levels in Sham-operated, BDL and HA animals. In Sham-operated animals biosensors detected tonic glutamate efflux of 26±2 μM (n=13). In BDL and HA rats, the glutamate tone recorded was 12±0.6 μM (n=16, p=0.3) and 18±1 μM (n=16, p=0.7) respectively (Figure 26A). Hypoxia-induced glutamate release in cerebellar slices of Sham-operated rats (20±2 μM, n=12), was significantly higher than that recorded in the cortex. However, it was not significantly different from the glutamate release measured in slices of BDL (10±0.8 μM; p=0.1, n=16) and HA animals (10±0.7 μM; p=0.2, n=14) (Figure 26B). Finally, increasing the permeability of connexin hemichannels by lowering $[Ca^{2+}]_e$ had no effect on the release of glutamate in Sham-operated rats (by Δ0.1±0.4 μM, n=12), BDL (by Δ0.01±0.2 μM; p=0.9, n=16) and HA animals (by Δ0.03±0.4 μM; p=0.7, n=16) (Figure 26C). These results demonstrated that extracellular level of glutamate is not affected in the cerebellum of both animal models of HE. Since no differences in glutamate level were observed in the cerebellum, the subsequent experiments focused on the glutamate recordings in the cerebral cortex.

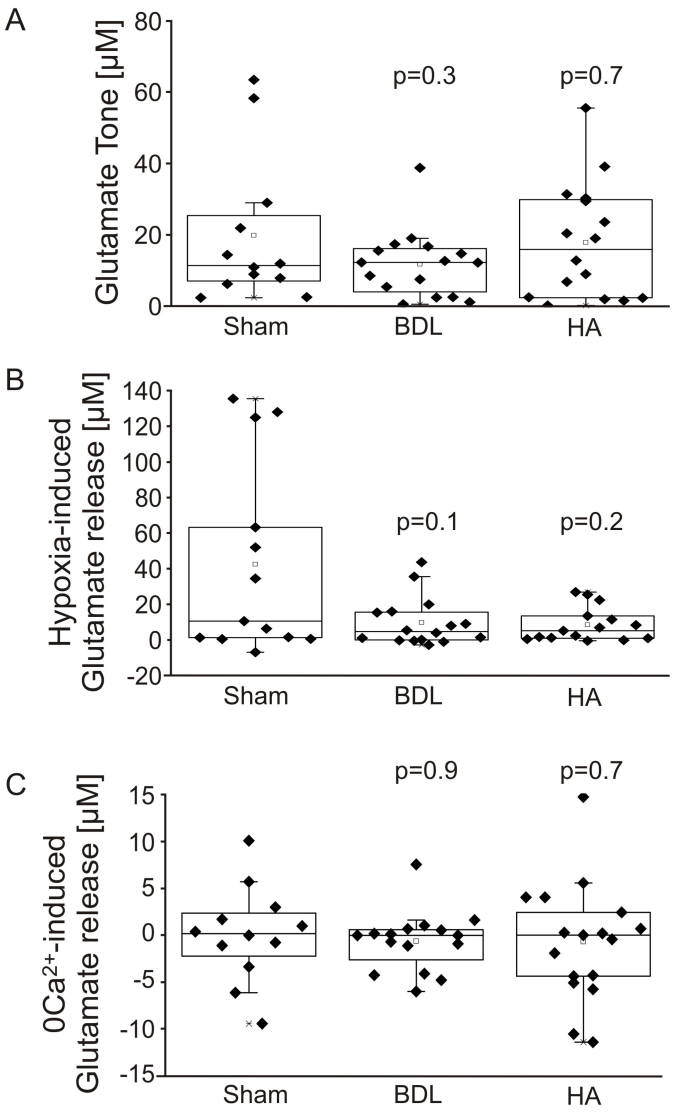

Figure 26: HE is not associated with significant alterations in extracellular glutamate concentrations in the cerebellum. A. Summary data illustrating tonic release of glutamate in cerebellar slices of Sham-operated, BDL and HA rats. **B.** Summary data illustrating peak changes in glutamate release in response to hypoxia (perfusion of the slice with aCSF saturated with 95% N_2/5% CO_2) in cerebellar slices of Sham-operated, BDL and HA rats. **C.** Summary data illustrating peak changes in glutamate release in response to lowering $[Ca^{2+}]_e$ in cerebellar slices of Sham-operated, BDL and HA rats. *p* values indicate differences from the Sham-operated rats.

4.2.3 Ammonia lowering treatment restores cortical glutamate release

OP treatment of BDL rats lowered tonic (1.1±0.09 μM, p=0.4 [compared to Sham-operated animals], n=15) and hypoxia-induced (Δ0.7±0.1 μM, p=0.4, n=15) glutamate release to concentrations similar to that recorded in Sham-operated animals (Figure 23, 25). Glutamate was not released due to lowering of $[Ca^{2+}]_e$ (Δ0.40±0.14 μM, p=0.08, n=14) (Figure 24). These results suggest that high ammonia levels are responsible for the increase in glutamate release in the cerebral cortex of BDL animals.

4.2.4 Cortical glutamate transporter expression in animal models of HE

The expression of the main astrocytic glutamate transporters was next evaluated in animal models of HE used in this study. RT-qPCR was performed on mRNA extracted from the cerebral cortices of BDL and Sham-operated animals (Figure 27). The data were normalised against the housekeeping gene Ubiquitin C. The relative expression of GLT-1 was not significantly different between the BDL- (1.16, CI 0.23-0.28, n=6) and Sham-operated animals (1, CI 0.24-0.31, n=5). No difference in GLAST expression was observed between the BDL- (1.23, CI 0.25-0.23, n=6) and Sham-operated rats (1, CI 0.03-0.02, n=5).

Western blots were performed on proteins extracted from the cerebral cortices of Sham, BDL and HA animals and no differences in cortical GLT-1 protein expression were observed between the groups (Figure 27).

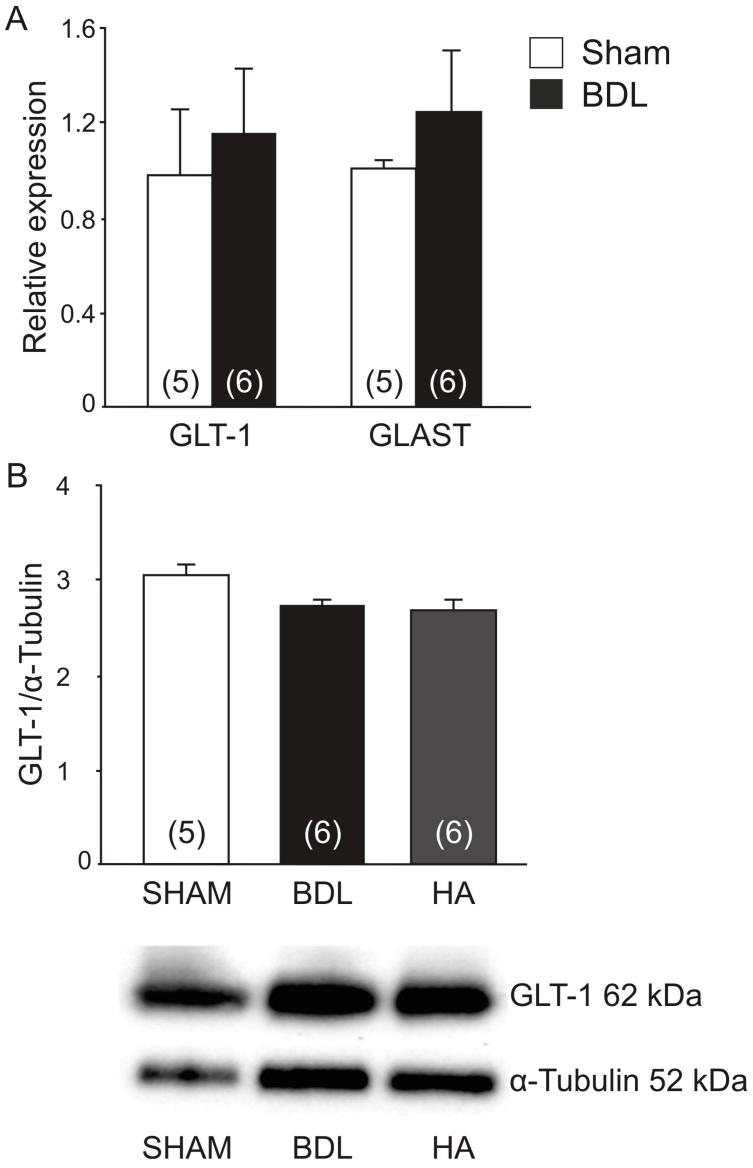

Figure 27: Cortical glutamate transporter expression in animal models of HE. A. Relative expression ($2^{-\Delta\Delta Ct}$) of GLT-1 and GLAST mRNA normalised to the housekeeping gene, Ubiquitin C, in the cortex of Sham-operated and BDL animals. **B. Top:** Summary data illustrating means±SEM of the densitometry of GLT-1 expression normalised to the expression of α-Tubulin in cell lysates of the cerebral cortices of Sham-operated, BDL and HA rats. **Bottom:** Representative immunoblots showing GLT-1 protein expression in cerebral cortices of Sham-operated, BDL and HA rats.

4.3 Discussion

Glutamate is the major excitatory neurotransmitter in the mammalian brain and can be released from astrocytes via various mechanisms. Glutamate metabolism is highly compartmentalised and can be influenced by several factors (Orellana et al., 2011). Glutamate is also used as a precursor for other neurotransmitters, such as GABA. As a result an alteration in glutamate metabolism could lead to transmitter imbalance in the brain as well as extracellular accumulation of glutamate and therefore excitotoxicity and neuronal death.

Under pathological conditions, the parameters that can change include: a) the content (expression, synthesis, degradation) of the main proteins involved in glutamate neurotransmission, such as the enzyme glutamate synthase or GS, b) spatial membrane concentrations of receptors and transporters, c) the function of receptor and transporters which is modulated in different ways including phosphorylation and dephosphorylation, d) alterations in the release and uptake of glutamate; and finally e) alterations in any of the steps of signal transduction pathways associated with different types of glutamate receptors (Monfort et al., 2002). There is evidence indicating that high levels of ammonia inhibit glutamate uptake (Chan et al., 2000), which could be caused by the reversal of glutamate transporters (Kosenko et al., 1994) or the involvement of other factors such as oxidative stress (Blanc et al., 1998b) or manganese (Rose et al., 1999) interfering with glutamate transport even in the absence of changes in transporter expression.

In the experiments described in this Chapter, an increase in tonic glutamate concentration was observed in the cortex (but not the cerebellum) of BDL and HA rats compared to the Sham-operated controls. Some differences between the cortex and cerebellum in terms of the extracellular glutamate concentrations recorded are expected as discussed in **Chapter 3**. Additionally, Bergmann cells express GLAST at very high levels, while cortical glial mainly express GLT-1. The different glutamate transporters could be associated with some differences in glutamate affinity or overall kinetics (Drejer et al., 1982), resulting in moderate regional differences in extracellular glutamate as shown here. The data illustrated in this Chapter are in agreement with the results of human studies showing increased glutamate in the CSF of patients with liver cirrhosis and HE (Weiss et al., 2016, Watanabe et al., 1984). Astrocytes are essential players in both the glutamate recycling and metabolism, and the removal of ammonia via the enzyme GS (Michalak et al., 1997). In HE, astroglial GS pathway is saturated by excess ammonia while its activity is further limited by oxidative and nitrosative stress developed due to hyperammonemia (Bobermin et al., 2015). As a result, this alters the efficacy of the astroglial glutamate-glutamine shuttle, causing a significant increase in intracellular glutamine and therefore glutamate, which then leads to an increase in release and extracellular glutamate (from neurons).

Due to my interest in hemichannels and the parallel work described in **Chapter 3**, $0Ca^{2+}$-aCSF, a common stimulus used to increase hemichannel permeability was applied but had no effect on glutamate release in cortical slices of BDL or HA animals. Interestingly, hypoxia, which is also known to increase the permeability of astrocytic hemichannels (Orellana et al., 2010), resulted in a significantly higher

glutamate release in the BDL and HA animals compared to healthy controls. However, this observation is unlikely to be due to altered activity of hemichannels, since **Chapter 3,** has already provided evidence of an impaired hemichannel functionality in the cortex of HE animals.

While there is evidence depicting that astroglial glutamate reuptake is altered in hyperammonemic conditions, resulting in increased extracellular concentrations of glutamate (Chan et al., 2000, Norenberg et al., 1997), the expression of GLT-1 and GLAST was not altered in animal models of HE used in this study.

Certain ions are essential for the correct function of glutamate transporters (Vandenberg and Ryan, 2013). Glutamate can therefore be transported in an outward direction when extracellular Na+/intracellular K^+ decreases and intracellular Na^+/extracellular K^+ increases. During severe ischemia, the activity of the Na^+/K^+ ATPase is markedly supressed and the ionic gradient of Na^+ (extracellular [Na^+]) decreases resulting in reversal of astrocytic and neuronal glutamate transporters. Interestingly, in the BDL animals a hypoxic cerebral environment has been shown (**Chapter 2**), which could be resulting in the stated phenotype of ionic imbalance and transporter reversal. During the *in vitro* slice experiments, the oxygenation level at rest is expected to be similar. However, the reversal of the transports could persist resulting in the reported phenotype. Furthermore, the application of the hypoxic stimulus could be exacerbating this, resulting in more glutamate release than the already high basal concentration. Interestingly, co-transport of Na^+ and glutamate via reversed glutamate transporters (during ischemia), contributes to the

suppression of the reversed Na^+/Ca^+ exchanger-induced rise in $[Ca^{2+}]_i$ by maintaining Na^+ gradient across astrocytic plasma membranes, contributing to the survival of astrocytes (Kosugi and Kawahara, 2006).

Finally, high ammonia concentration may lead to a reduction in transmembrane electrochemical gradients of Na^+ and H^+ (usually changes are minor), which impair the driving force of astrocytic glutamate transporters, inhibiting glutamate uptake (Bobermin et al., 2015, Kelly et al., 2009). Additionally, a recent study by Rangroo Thrane et al., (Rangroo Thrane et al., 2013) reported that ammonia results in an increase in extracellular K^+ which in combination with external acidification accompanied by the elevated ammonia concentrations, would greatly reduce glutamate transport. Thus, significant available evidence suggests that ammonia plays a key role in altering the glutamate transporter activity (but not expression), and in triggering elevations in extracellular glutamate concentrations. This hypothesis is strongly supported by the significant improvement in glutamate concentration back to normal levels, observed in the brains of animals that have been treated with the ammonia-lowering agent OP.

To conclude the results of experimental studies described in this Chapter demonstrate that HE is associated with significant changes in the extracellular concentration of glutamate in the cerebral cortex, with ammonia playing the key role in mediating this dysfunction.

Chapter 5: Impaired brain glymphatic flow in a rodent model of chronic liver disease with minimal hepatic encephalopathy

5.0 Introduction

The mechanisms underlying the pathogenesis of HE in patients with cirrhosis are not completely understood. The data available in the literature suggest that noxious substances and metabolites such as lactate, glutamate, bile acids and drugs accumulate in the brain of HE patients (Weiss et al., 2016). The currently prevailing hypothesis proposes that this occurs due to the metabolic and signalling defects induced by hyperammonemia, inflammation and alterations in BBB function (Shawcross et al., 2010, Hadjihambi et al., 2017).

In the periphery, the lymphatic system is responsible for ISF clearance, a critical mechanism of maintaining tissue homeostasis. Metabolic rate of the brain is very high, accounting for ~20% of body energy expenditure. Although neuronal function is exquisitely sensitive to alterations in the extracellular environment, until recently, the brain was believed to be devoid of the lymphatic drainage/clearance system. Recent studies identified a brain-wide paravascular pathway that facilitates the efficient clearance of various molecules, including toxic interstitial proteins, lactate and others (Iliff et al., 2013a, Iliff et al., 2012). Subarachnoid CSF recirculates through the brain parenchyma along the paravascular spaces surrounding penetrating arteries, exchanging with the surrounding ISF, facilitating the clearance of interstitial solutes

via convective bulk flow. ISF is then cleared along paravascular spaces surrounding large caliber cerebral veins, which reach the recently discovered CNS lymphatic vessels (Louveau et al., 2015) and eventually enter systemic circulation. This pathway has been termed the “glymphatic system”, due to its dependence on glial water channels and its clearance function similar to that of the lymphatic system. In addition to clearing the brain, it also contributes to the distribution of growth factors, neuromodulators, carrier proteins and other solutes within the brain (Kress et al., 2014). Failure of the glymphatic system may have critical adverse consequences and has been linked to the pathogenesis of neurodegenerative disease(s) (Iliff et al., 2012, Peng et al., 2016).

Experimental studies described in this Chapter tested the hypothesis that the glymphatic clearance mechanisms are impaired in cirrhosis, potentially contributing to the development of neurochemical phenotype observed in HE.

5.1 Material and methods

All the experiments were performed in accordance with the Animals (Scientific Procedures) Act 1986 (ASPA) revised according to the European Directive 2010/63/EU and the UK Home Office (Scientific Procedures) Act (1986) with project approval from the Institutional Animal Care and Use Committee.

5.1.1 Animal models

Male Sprague-Dawley rats (body weight ~350-400g) were obtained from a commercial supplier (Charles Rivers Laboratories, Inc.).

BDL surgery: 16 rats underwent BDL surgery as described in detail in section 2.1.1.

Blood and brain tissue were collected under terminal isoflurane anaesthesia. Plasma biochemistry was performed using a Cobas Integra II system (Roche Diagnostics).

5.1.2 Dynamic Contrast-Enhanced MRI

The MRI experiments were conducted in collaboration with Dr. Ian Harrison (CABI, UCL), who helped with image acquisition and analysis.

I. *Surgical Preparation*

28 days after the surgery, 5 Sham-operated and 5 BDL rats were anaesthetized with 5% isoflurane in pure oxygen for induction, followed by 2% isoflurane in oxygen for maintenance, and positioned in a stereotaxic frame with the head flexed to 50°. A midline incision was made at a midpoint between the skull base and the occipital margin to the first vertebrae. The underlying muscles were parted to expose the atlanto-occipital membrane and dura mater overlaying the cisterna magna. An intrathecal 24-gauge infusion catheter (0.7 x 19 mm, B|Braun, Melsungen, Germany) was advanced 1 mm into the cisternal space. The cannula was sealed and anchored in place using superglue and fast setting resin (Araldite) and the needle was then removed without depressurising the system. It was then attached to polyethylene tubing (0.4 mm x 0.8 mm, Portex) and a 100 µL glass Hamilton syringe connected to a microinfusion pump (PHD 2000 syringe pump, Harvard Apparatus, Cambridge, UK), which were all prefilled with low molecular weight paramagnetic contrast agent Magnevist® (21 mM Gd-DTPA, MW 938 Da; Schering Health Care Ltd., in saline solution).

II. *MR Image Acquisition*

Following surgery, animals were transferred to an MRI compatible cradle with head held prone and a snout mask positioned to deliver 1.5% isoflurane in oxygen. Core temperature and respiratory rate were monitored using a rectal probe and pressure pad respectively (SA Instruments). Rats were maintained at 37°C using heated water tubing and feedback loop controlled warm air delivery system (SA Instruments). Respiratory rate was maintained between 70 and 100 breaths per minute by incrementally adjusting isoflurane dose. All imaging was performed with a 9.4T VNMRS horizontal bore MR scanner (Agilent Inc., Santa Clara, California, USA). A 72 mm inner diameter volume coil (Rapid Biomedical, Rimpar, Germany) was used for radiofrequency (RF) transmission and signal was received using a 4-channel array head coil (Rapid Biomedical). A 3D T1-weighted gradient echo sequence was employed to detect the motion of the Gd-DTPA with parameters: TR = 15 ms, TE = 3.4 ms, flip angle = 15°, NA = 3, FOV = 1.5 × 3.0 × 2.6 cm, scanning time = 12 min, acquisition matrix size of 128 × 128 × 128, yielding an image resolution of 0.12 × 0.23 × 0.20 mm. A baseline scan was acquired prior to intrathecal infusion of Gd-DTPA via the pre-implanted catheter (80 µl at 1.6 µl/min, total time 50 min). MR images were continually acquired throughout and after intrathecal infusion for a total time of 144 min. At the end of the experiment the animal was euthanized by sodium pentobarbital overdose (200 mg/kg).

III. *Image Processing and Analysis*

For presentation of images, a difference image was calculated for each time point using the following expression:

$$D(i,j,k) = [I(i,j,k) - B(i,j,k)]$$

Where D is the difference image, I is the time series image post Gd-DTPA infusion, B is the average baseline image, and (i, j, k) represent the voxel position. Signal intensity measured on the T1 weighted MR images over time in preselected anatomical areas were used to obtain intensity measurements. Both the T1-weighted averaged baseline images and the contrast-enhanced T1-weighted MR images were used to anatomically guide placement of 3D ROIs and extract volumes. The intensity signal for each ROI on each time point image was extracted and expressed as a % change from the average baseline image.

5.1.3 Intracranial pressure measurements

In a separate group of BDL (n=6) and Sham-operated (n=8) animals (4-weeks after the surgery), resting ICP was determined. Under general anaesthesia (5% isoflurane in pure oxygen for induction, 2% isoflurane in air for maintenance), the femoral artery was cannulated for blood pressure measurements. The rats were then positioned in a stereotaxic frame with the head flexed to 50° and a midline incision was made at a midpoint between the skull base and the occipital margin to the first vertebrae. The underlying muscles were parted to expose the atlanto-occipital membrane and dura

mater overlaying the cisterna magna. A 23-gauge needle attached to a cannula connected to a pressure transducer was inserted in the cisterna magna and the system was sealed immediately using surgical glue. The animal was allowed to recover for 15 min and the ICP was recorded. Data from previous studies have already shown no significant alterations in ICP during the chosen volume and rate of contrast agent infusion (Yang et al., 2013).

5.1.4 Behavioral experiments

The behavioral experiments were conducted in collaboration with Dr. Natalia Arias (Department of Liver and Digestive health, UCL).

I. *Evaluation of Prefrontal Cortex function: Spatial working memory*

Spatial working memory in separate groups of Sham-operated (n=5) and BDL rats (n=5) was evaluated in the Barnes Maze. The training consisted of one day for habituation in which each rat was gently placed into the escape box, which was then covered for 2 min. After that 2 min habituation period, the rat was placed into the start box located in the centre of the maze, the box was opened and the rat was allowed 300 s to locate the escape box. If the rat did not locate and enter the escape box during that allotted time, it was gently guided to and allowed to remain in the escape box for 15 s prior to being returned to its home cage. If the rat located the escape box, it was also allowed 15 s inside before being returned to its home cage.

The working memory training involved a paired sample task during the following six days of training. Each daily session consisted of two identical trials (sample and retention). During both trials, the escape box was in a fixed position every day, changing between days in a pseudorandom order. Each trial began with the start box positioned in the centre of the maze and the rat placed inside it. The rat remained in the start box for 30 s, providing a standard starting context for each trial and ensuring that initial orientation of the rat on the maze varied randomly from trial to trial. On each training trial, 11 of the 12 holes were blocked. The remaining hole provided access to the escape box, which was positioned on the underside of the maze. The ramp leading to the escape box was the same colour and texture as the doors blocking the holes, so that from the centre of the maze it could not be distinguished visually from the other 11 holes. Each rat was permitted to explore the maze freely. If the rat did not enter the escape box within 300 s, it was gently picked up by the experimenter and placed over the target hole and allowed to enter the escape box. The rat remained in the escape box for 15 s before it was returned to its home cage. The maze and escape box were cleaned carefully with a 10% alcohol solution to dissipate odour cues and provide a standard olfactory context for each trial.

II. *Evaluation of Hippocampal function: Spatial Reference Memory*

To test the reference memory in the Barnes Maze, an escape box was placed underneath one of the holes on the maze and remained in the same position during the training session for five days. Visual cues of different colours and shapes were

placed above four quadrants of the maze. In the acclimation period, each rat was placed by the edge of the escape box. The rat was gently put into the box if it had not entered the escape box within 1 min. During the training period, the rat was placed in the centre of the maze and covered by an opaque plastic box. After 15 s, the box was removed and the rat was allowed to walk around the maze for 3 min to find and enter the escape box. If the rat failed to enter the escape box within 3 min, it was gently guided to the box. At the end of the session, a probe test was applied in which the escape box was removed and the rat was introduced to the maze for 2 min in order to check whether the animal remembers the position of the escape box. Immediately after the probe test, the animals were subjected to an additional trial with the escape box placed in its usual position to avoid any possible interference with the probe test. Four trials were performed per day for five days. Time spent to find the target hole where the escape box used to be located (latency), distance travelled, speed and path efficiency were recorded and analysed by ANY-maze software (Stoelting Co). Path efficiency is a measure, which represents an index of the efficiency of the path taken by the animal to get from the starting position to the escape box. A value of 1 indicates perfect efficiency- the animal moved in a straight line- less than 1 indicates decreasing in efficiency. The maze was wiped thoroughly with 10% alcohol solution to avoid olfactory cues.

5.1.5 ***Statistical analysis***

Statistical comparisons between MR time course data from Sham-operated and BDL groups were performed using two-way ANOVA with Bonferroni post-hoc test.

ICP recorded in Sham-operated and BDL animals was compared using a Student's t test and biochemistry data was analysed using one-way ANOVA.

For the neurobehavioral experiments, normality test for each group and parameter was performed. Statistical comparisons of data between Sham-operated and BDL animals were performed via two-way ANOVA with Bonferroni post-hoc test. For comparison of data within animal groups along training days, two-way ANOVA was applied followed by Tukey post-hoc test.

Statistical tests were performed using GraphPad Prism (v6 for Windows, San Diego, CA, USA), and all data were reported as mean±SEM. Differences with p value of <0.05 were considered to be significant.

5.2 Results

5.2.1 Biochemistry

Plasma biochemistry and ammonia concentration were assessed in all groups of animals, showing the same changes as described in **Chapter 2** (Table 2).

5.2.2 Glymphatic flow evaluated using dynamic contrast-enhanced MRI

Dynamic contrast-enhanced MRI was used to visualize brain-wide subarachnoid CSF-ISF exchange in anesthetized BDL rats (n=5), and Sham-operated control animals (n=5). Time course of parenchymal distribution of the paramagnetic contrast agent, gadolinium (Gd-DTPA) throughout the brain was assessed as a measure of glymphatic flow (Iliff et al., 2013a, Iliff et al., 2012). Following an intra-cisternal infusion of gadolinium, serial acquisition of T1-weighted MR images was performed (Figure 28A). The integrity of the skull was confirmed by monitoring the temporalis muscle for the presence of gadolinium, to ensure a sealed and intact system, which is essential for the glymphatic flow (Figure 29E).

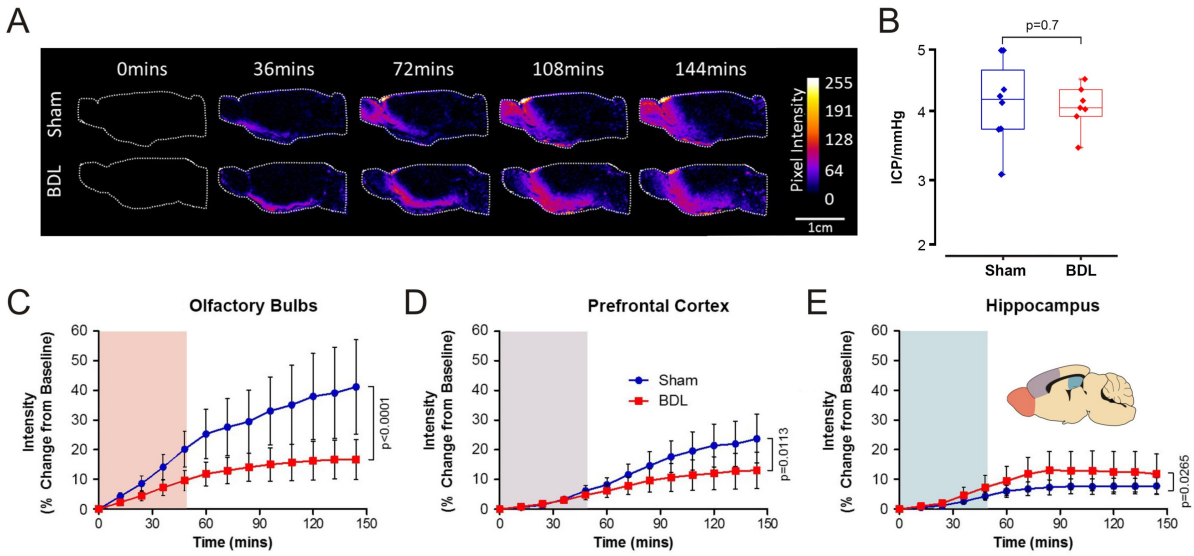

Figure 28: Impaired contrast agent penetration in the brain of animals with HE. A. Representative images of dynamic contrast-enhanced MRI of Sham-operated and BDL animals. Pseudocolour scaling illustrates distribution of gadolinium throughout the brain over the 144 min of the recording, with the BDL brain showing reduced contrast agent and therefore glymphatic inflow in rostral areas. **B.** Summary data illustrating resting intracranial pressure (ICP) in Sham-operated and BDL animals. Summary data showing MR contrast intensity changes in **C.** the olfactory bulb **D.** the prefrontal cortex and, **E.** the hippocampus of Sham-operated and BDL rats. *Inset*: Schematic drawing illustrating the brain regions of interest. Shading indicates period of contrast agent infusion. *p* values indicate the level of significant differences between the sham-operated and BDL groups.

In order to assess the ability of the brain to distribute the infused contrast agent, the brain was compartmentalized (on analysis) and the quantification of signal intensity *vs*. time of inflow was compared between the experimental (BDL) and control (Sham-operated) animal groups. CSF filled compartments, including the aqueduct, third and lateral ventricles, showed no significant differences in flow between Sham-operated and BDL animals (Figure 30A-D). Similarly, time-course of the parenchymal distribution of the contrast agent in the striatum ($p=0.4$), midbrain ($p=0.7$), caudal cortex ($p=0.1$), thalamus ($p=0.06$) and hypothalamus ($p=0.2$) was not different between the two animal groups (Figure 29A-D, F).

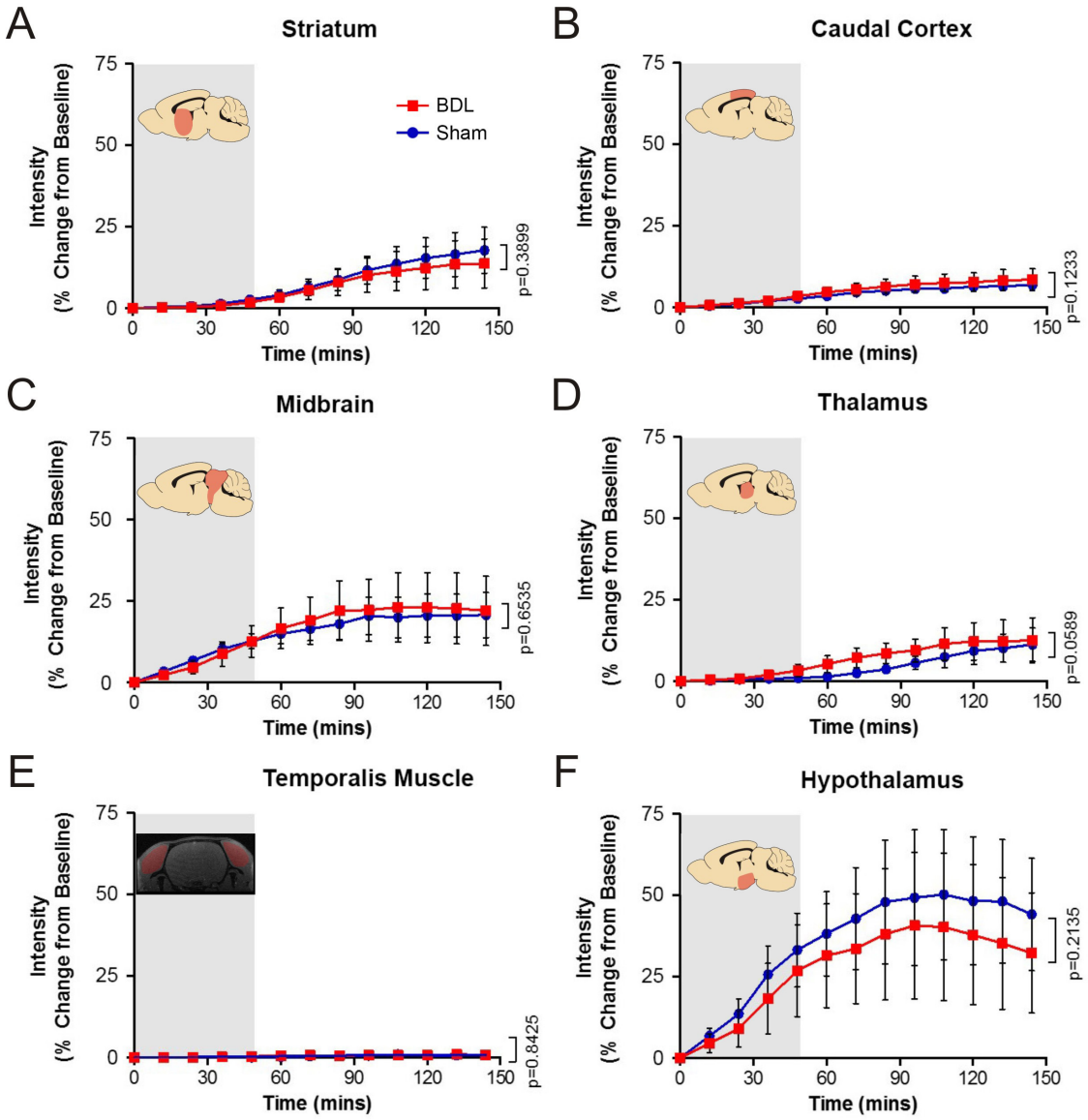

Figure 29: Unchanged contrast agent penetration in the striatum, caudal cortex, midbrain, thalamus, and hypothalamus of animals with HE. A. Intensity (% change from the baseline) vs. time plots of contrast agent penetration in the striatum showing no difference between Sham-operated and BDL rats. **B.** Intensity (% change from baseline) vs. time plots of contrast agent penetration indicating no difference in the caudal cortex of Sham-operated and BDL rats. **C.** Intensity (% change from baseline) vs. time plots of contrast agent penetration indicating no difference in the midbrain of Sham-operated and BDL rats. **D.** Intensity (% change from baseline) vs. time plots of contrast agent penetration

indicating no difference in the thalamus of Sham-operated and BDL rats. **E.** Intensity (% change from baseline) vs. time plots of contrast agent penetration in the temporalis muscle of Sham-operated and BDL rats acting as negative control. Lack of contrast agent in the temporalis muscle represents a sealed system and no CSF leakage due to the cannula implantation. **F.** Intensity (% change from baseline) vs. time plots of contrast agent penetration indicating no difference in the hypothalamus of Sham-operated and BDL rats. Grey shading indicates period of contrast agent infusion. *p* values indicate the level of differences between the Sham-operated and BDL groups.

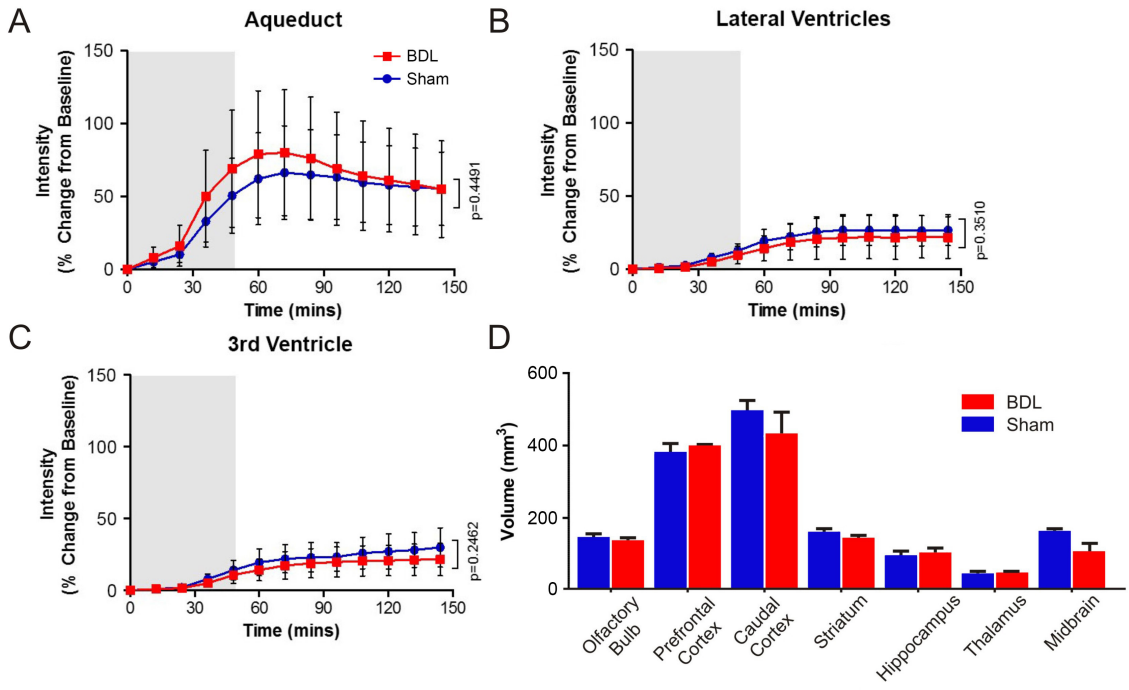

Figure 30: Contrast agent inflow in CSF filled compartments (aqueduct, lateral ventricles and third ventricle) and volumes of select brain regions are not altered in HE. A. Intensity (% change from baseline) vs. time plots of contrast agent penetration indicating no difference in the aqueduct of Sham-operated and BDL rats. **B.** Intensity (% change from baseline) vs. time plots of contrast agent penetration indicating no difference in the lateral ventricles of Sham-operated and BDL rats. **C.** Intensity (% change from baseline) vs. time plots of contrast agent penetration indicating no difference in the 3rd ventricle of Sham-operated and BDL rats. Grey shading indicates period of contrast agent infusion. **D.** Summary data illustrating volume (mm^3) of the brain regions of interest obtained from 3D ROI measurements of contrast-enhanced MR images from Sham-operated and BDL animals, with no significant differences reported. *p* values indicate the level of differences between the sham and BDL groups.

Parenchymal penetration of the contrast agent in the olfactory bulb ($p<0.0001$) and prefrontal cortex ($p=0.01$) was dramatically reduced in BDL rats compared to Sham-operated animals, indicating that the efficacy of glymphatic flow in these areas is compromised (Figure 28C-D). In contrast, facilitated inflow of contrast agent was observed in the hippocampus ($p=0.03$) of BDL rats (Figure 28E), further suggesting that glymphatic flow is altered in this model of mHE.

5.2.3 Measurement of intracranial pressure and volume of the brain regions of interest in Sham-operated and BDL animals

Impairment of parenchymal contrast agent penetration could be due to altered ICP in BDL animals. Therefore, volumes of select brain regions obtained from 3D ROI measurements of contrast-enhanced MR images (Figure 30D) and recorded ICP from the cisterna magna (Figure 28B) were next determined in Sham-operated (n=8) and BDL (n=6) animals.

The results obtained demonstrated that the observed contrast agent inflow impairment cannot be attributed to altered pressure in the brain, as the volumes of brain regions ($p>0.05$ for all regions) and the ICP recorded from the cisterna magna ($p=0.7$) were not different between Sham-operated and BDL animals.

5.2.4 Evaluation of Prefrontal Cortex function: Spatial working memory

To determine the functional consequences of altered glymphatic flow, an array of behavioral and cognitive tests were performed in BDL (n=5) and Sham-operated (n=5) animals. The prefrontal cortex and hippocampus are involved in learning and memory (Damasio, 1989, Squire et al., 1992). Prefrontal cortex is critically involved in cognitive functions such as working memory, a process of maintaining an active representation of information available for use, as well as organization and planning of responses (Fuster, 1990). Testing spatial working memory in the Barnes Maze was then used to assess the function of prefrontal cortex. While there was no difference between the animal groups in time required to reach the escape box during the sample trial (p=3) (training on the day to learn the new location of the escape box), significant differences between the BDL and Sham-operated animals in the retention trial (p=0.02) were recorded (Figure 31A-B). These data suggest that the BDL animals are unable to retain an active representation of information indicating an impairment of the prefrontal cortex function.

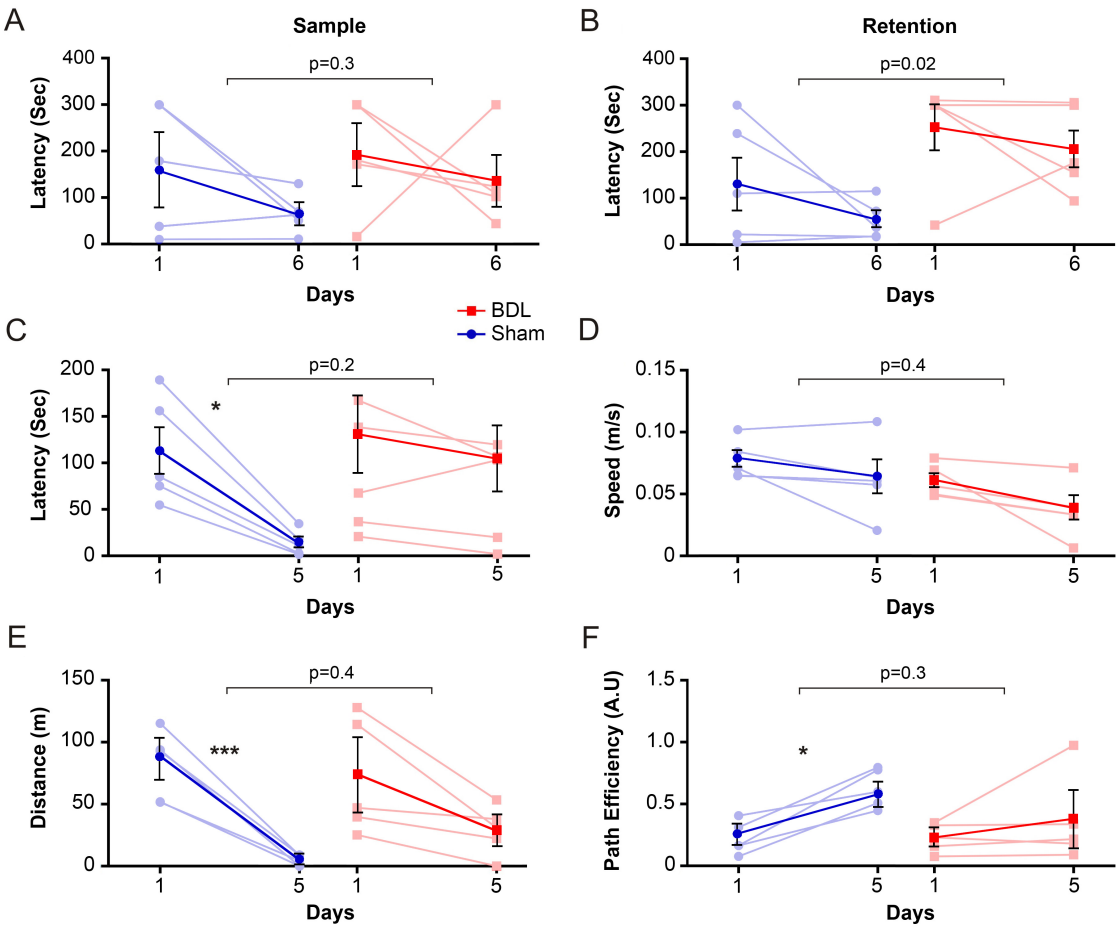

Figure 31: Cognitive/behavioral deficits in HE. A. Summary data illustrating time latency required to reach the escape box in the working memory task in Sham-operated and BDL rats. Summary data illustrating **B.** retention latency in the working memory task, **C.** latency, in the spatial reference memory task, **D.** speed of animal during the reference memory task, **E.** distance travelled during the reference memory task and **F.** path efficiency from the starting point to the escape box during the reference memory task comparing sham and BDL rats. *p* values indicate the level of significant differences between the sham-operated and BDL groups. For within group comparison $^{*}p<0.05$, $^{***}p<0.001$.

5.2.5 Evaluation of Hippocampal function: Spatial Reference Memory

As the hippocampus is important in the acquisition of spatial reference memory (Li et al., 2013), further tests to assess its function were performed in the Barnes Maze. Although no differences were observed in escape latencies between BDL and Sham-operated animals ($p=0.2$), the control group showed a progressive and significant improvement in the task acquisition during the training days ($p=0.01$), which was not observed in the BDL animals ($p>0.05$) (Figure 31C). This indicates the inability of BDL animals to learn how to use the reference cues in order to reach the escape box, suggesting potential impairment of hippocampal function. There were no differences in the speed ($p=0.4$) and distance travelled ($p=0.4$) between the two groups of animals, suggesting that the observed differences in latency were not due to the potential locomotor deficiency in the BDL rats (Figure 31D-E). Moreover, the learning ability of Sham-operated, but not of BDL animals was observed through the significant decrease in distance covered (within the group, $p<0.001$), which was also reflected in the increase of path efficiency ($p=0.01$) along training days (Figure 31F). These results demonstrate a functional correlate to the observed alteration in glymphatic flow in the hippocampus.

5.3 Discussion

Many diseases, mainly neurodegenerative, are associated with accumulation of cellular waste products (such as by-products of cellular respiration). Intracellular proteasomal degradation and autophagy are considered the principal means for removing proteins in the CNS and the dysfunction of these processes has been associated with neurodegeneration (Nedelsky et al., 2008). Yet, many cytosolic proteins are released into the interstitial space of the brain, suggesting that effective disposal routes should exist in order to eliminate waste. Preliminary evidence exists showing bile acid accumulation in the CSF (not included in this thesis) and excessive release of glutamate in the brain of rodent models of HE (**Chapter 4**), which add to the human data indicating the accumulation of many noxious substances and metabolites in the ISF and CSF collected from the brain of HE patients (Weiss et al., 2016). These data therefore points to a possible impairment of the glymphatic flow, which results in the lack of brain clearance observed.

This study demonstrates impaired CSF penetration and parenchymal clearance of the contrast agent in the olfactory bulb and prefrontal cortex of HE rats, indicating a clear dysfunction of the glymphatic clearance system in an animal model of mHE. The reasons underlying increased contrast agent inflow in the hippocampus are unclear at the moment, but may be due to cell loss/neurodegeneration, also seen in animal models of Alzheimer's disease or regional glial alterations that may occur in HE (Hernandez-Rabaza et al., 2016). Cytotoxic oedema and energy depletion, which are known features of HE, enhance glymphatic CSF influx while suppressing ISF

efflux (Thrane et al., 2014) may also contribute to the increased contrast inflow in the hippocampus. The data showing memory deficits in this model of HE provide a functional correlate for these findings indicating impairment of the prefrontal cortex function as well as a potential derangement in hippocampal-prefrontal cortex connections. The pathophysiological mechanisms underlying impaired glymphatic flow reported here are unclear. However, several factors, some known to be deranged in HE, such as reactive astrogliosis (Iliff et al., 2014), hemichannel dysfunction (Hadjihambi et al., 2017), loss of perivascular astroglial AQP4 water channel polarization (Kress et al., 2014), altered neuronal activity (Thrane et al., 2014), arterial pulse-pressure (Iliff et al., 2013b), CNS inflammation (Erickson et al., 2012) may play a role. Interestingly, many of these factors are prominent during other diseases (Kress et al., 2014) and could represent important therapeutic targets to restore paravascular CSF-ISF exchange.

Connexin hemichannel dysfunction in animal models of HE has been reported in **Chapter 3**. These porous channels are vastly expressed on astrocytes and allow the (controlled) passage of various ions and molecules as well as water (Beyer and Berthoud, 2014). Impairment of the opening of these channels, as seen in HE, can potentially compromise water transport across astrocytes and therefore convective bulk flow, which will then compromise the process of CSF-ISF exchange, resulting in the reported glymphatic flow impairment.

Volume homeostasis of cells requires energy in order to be maintained. Energy depletion, (evidence of potential neuronal energy deficit in HE reported in **Chapter 3)** (Hadjihambi et al., 2017), can cause brain cell swelling termed cytotoxic oedema. From extensive studies on HE rodent models, it is known that ammonia plays a direct role in the development of this oedema and it is mainly observed in astrocytes, although this is mild in mHE. Astrocytic end-feet interpose a high-resistance barrier to fluid-solute flux between paravascular and interstitial compartments. Pericyte and microglial processes are also scattered in between the vascular wall and astrocyte end-feet, which creates a filter size of glial barrier large enough for nearly all-mammalian proteins (~35kDa and diameter 2-3 nm, including serum albumin ~70kDa and 4-6 nm diameter). Astrocytic swelling (extending to the end-feet) can therefore largely interfere with the clearance of the brain by obstructing the paravascular CSF-ISF exchange and solute clearance.

An interesting idea reported by Thrane et al (Thrane et al., 2014), was that GJ connections between astrocytes might rapidly distribute Na^+-influx across the glial syncytium (Ezan et al., 2012, Rose and Ransom, 1997). Na^+ and Cl^- redistribution would in turn make ISF slightly hypo-osmolar relative to CSF (Ishimaru et al., 1993), which would build an osmotic ISF-CSF gradient that in theory will pull CSF into the ISF compartment. Results of the experiments described in **Chapter 3** demonstrated functional hemichannel dysfunction in the cerebral cortex of BDL animals. This dysfunction could also extend to the GJ level, preventing the distribution of these ions and therefore the development of an osmotic gradient, which will consequently diminish the efficacy of the glymphatic clearance pathway as demonstrated in this Chapter.

In conclusion, this study provides the first experimental evidence of impaired glymphatic clearance in HE.

Chapter 6: General Discussion and Summary

The experimental studies described in this thesis aimed to determine whether during HE, chronic exposure to elevated ammonia concentrations interferes with cerebral oxygenation, compromises lactate transport between cells and affects uptake of neurotransmitters. Additionally, experimental studies were aimed to test the hypothesis that HE impairs glymphatic clearance mechanisms, either as a cause or a consequence of the disease, which contributes to the cognitive impairment. HE is a serious syndrome, which has detrimental effects on the socioeconomic status and quality of life of patients. It is, therefore, necessary to have a very clear and in depth understanding, of how the contributing pathogenic factors involved, affect the brain on the molecular, membrane, cellular and neuronal/astroglial network level. This study used contemporary neuroscience methods applied in carefully designed and executed experiments conducted (*in vivo* and *in vitro*) in animal (rat) models. Collectively, this thesis demonstrates that in animal models of HE, chronic hyperammonemia compromises cerebral oxygenation without affecting cerebrovascular reactivity and it is associated with cortical hemichannel dysfunction, impaired lactate release, as well as significant increases in cortical extracellular glutamate concentrations, which is exacerbated under hypoxic conditions. Finally, glymphatic function is altered at discrete regions of the brain, which aligns with specific cognitive impairments observed in these animals.

Experiments described in **Chapter 2** were designed to determine whether cerebral oxygenation is impaired in HE and, if so, explore the potential underlying mechanisms. The data obtained demonstrate that HE is associated with reduced brain tissue PO_2, which is independent of systemic hypotension. Ammonia lowering treatment prevented this decrease in cerebral PO_2 suggesting that ammonia plays a key role in this phenotype. The exact mechanism leading to the compromised brain oxygenation in HE is still unclear, although the results of this thesis in combination with the current literature suggest that ammonia may act by reducing brain metabolic activity, as well as by indirectly increasing vascular tone with secondary effects on CBF.

These findings provide the first insights into an ammonia-triggered mechanism involving compromised CBF, which results in decreased brain tissue oxygenation, and is hypothesised to contribute to the pathogenesis of HE. Further experiments are required to unravel the exact mechanism. CBF will be further investigated in an MRI study, examining baseline perfusion, effectiveness of ACTZ and sildenafil in increasing CBF, as well as integrity of neurovascular coupling in animal models of HE. Additionally, cognitive tests will be performed in BDL and Sham-operated animals treated with ACTZ or vehicle in order to assess the role of reduced cerebral oxygenation in cognitive decline observed in animal models of HE. Finally, the role of pericytes have yet to be investigated in the field of HE and it will be an important area of study due to the increasing evidence pointing towards their active control of the capillary blood flow and CBF regulation in health and disease.

Having established the presence of compromised cerebral oxygenation in HE, the experiments described in **Chapter 3** were designed to determine whether chronic ammonia exposure alters brain extracellular lactate concentration and, if so, study the potential underlying mechanisms.

It was found that HE is associated with a significant reduction in both tonic and hypoxia-induced lactate release in the cerebral cortex, which was normalised by ammonia-lowering treatment. Cortical dye loading experiments revealed hemichannel dysfunction in HE with improvement following OP treatment, while the expression of key connexins was unaffected. These results demonstrate that HE is associated with cortical hemichannel dysfunction, with ammonia playing a key role. The data provide evidence of a potential neuronal energy deficit due to impaired hemichannel-mediated lactate transport between astrocytes and neurons as a possible mechanism underlying pathogenesis of HE.

Subsequent experiments described in **Chapter 4** were designed to test the hypothesis that chronic ammonia exposure may also alter the extracellular concentration of neurotransmitters. To test this hypothesis glutamate concentrations were assessed in the cerebral cortex of BDL and Sham-operated animals. The data obtained demonstrate an increase in tonic glutamate concentration in the cortex (but not the cerebellum) of BDL and HA rats compared to Sham-operated controls. Evidence suggests that ammonia plays a key role in compromising the glutamate transporter activity and therefore glutamate uptake, but not the expression of the transporters as seen by the unaltered expression of GLT-1 and GLAST in the animal

models of HE used in this study. The hypothesis of ammonia mediating this change is strongly reinforced by the significant improvement in glutamate concentration back to normal concentrations, observed in the brains of animals that have been treated with ammonia-lowering agent. Thus, these results demonstrate that HE is associated with significant changes in the extracellular concentration of glutamate in the cerebral cortex, with ammonia playing the key role.

Having established the ammonia-mediated increase in extracellular glutamate concentration, the experiments described in **Chapter 5** were aimed to evaluate whether the glymphatic flow and therefore clearance is impaired in HE, and if so, determine whether the affected brain regions correlate with cognitive alterations. In this study, a dynamic contrast-enhanced MRI technique was used to assess the efficacy of the glymphatic clearance, which facilitates clearance of solutes from the brain. Discrete brain regions (olfactory bulb, prefrontal cortex and hippocampus) of altered glymphatic flow were identified, which aligned with behavioral deficits. Although the underlying pathophysiological mechanisms remain unclear, this study provides the first experimental evidence of impaired glymphatic clearance in HE.

Reduced efficacy of glymphatic clearance has been seen in several diseases including Alzheimer as well as during normal aging (Iliff et al., 2012, Peng et al., 2016). In Alzheimer's disease there is a gradual build-up of amyloid beta peptides in the brain parenchyma, likely due the impairment of glymphatic clearance. This leads to impaired neurovascular coupling inducing decrease in CBF, BBB disruption and altered vascular structure (Kyrtsos and Baras, 2015). Similarly, reduction in ISF flow

as a consequence of aging, induces vascular abnormalities such as compromised vascular tone and vessel wall pulsatility (Kyrtsos and Baras, 2015, Kress et al., 2014). This suggests that an impaired glymphatic pathway could be responsible for the phenotypes reported throughout this study and therefore the progression of HE. However, since the glymphatic impairment in HE is a very recent observation, not enough evidence exists regarding the timeline and sequence of events (glymphatic impairment resulting in altered neurochemical phenotype or visa versa). Nevertheless, it is possible that this is a result of hyperammonemia (a consequence rather than a cause) and could be reversed by ammonia-lowering treatment(s).

Potential areas for further investigation

It is well known that sleep improves memory and maintains metabolic balance of the body, while sleep deprivation impairs cognitive performance and is a common cause of seizures. A recent study has proposed that during sleep glymphatic clearance is facilitated while its efficacy is suppressed during wakefulness (Xie et al., 2013). This suggests that one of the major functions of sleep could be to promote glymphatic clearance of metabolic waste products produced during wakefulness. Interestingly, CLD and HE conditions are always accompanied by dyssomnia (Bajaj et al., 2011), (Liu et al., 2015).

mHE patients suffer from poor sleep quality, take longer to fall asleep, exhibit lower sleep efficiency and show daytime functional disturbances (Liu et al., 2015). Aside

from anxiety and depression other psychiatric factors tend to have a negative impact on sleep quality, which results in a vicious cycle and further health deteriorations.

A study by Lundgaard et al., (Lundgaard et al., 2016) has proposed that the glymphatic system is responsible for state-dependent changes in brain lactate concentration with lactate being high during wakefulness and declines within minutes of sleep. The authors have suggested that brain lactate is a good biomarker of sleep-wake cycle and increases further during sleep deprivation, since brain extracellular lactate concentration is inversely correlated with glymphatic-lymphatic clearance. Based on this observation and the hypothesis that lactate may have an excitatory effect (through the activation of neurons releasing norepinephrine) (Tang et al., 2014), it would be interesting to investigate the possibility that impairment of glymphatic pathway in HE, results in lactate accumulation, which exerts an excitatory effect on arousal-promoting neurons and therefore prevents sleep.

The experimental plan proposed for investigating this hypothesis is as follows: Sleep activity will be monitored in Sham-operated and BDL animals through electromyogram (EMG) recordings achieved by bilateral placement of wires in both neck muscles. During sleep EMG activity decreases while wakefulness is characterised by significant increase in EMG activity. If more accurate monitoring of sleep is required then an electroencephalogram will also be recorded. A decrease in lactate release during HE was reported in **Chapter 3**. This could still result in a significant extracellular accumulation of if the glymphatic pathway is impaired.

Once the sleeping pattern of animals is established, the effect of L-lactate can be investigated. Implantation of EMG electrodes will be repeated in another group of animals, in combination with viral microinjection, which mediate the conversion of L-lactate to D-lactate. D-lactate, is the stereoisomer of L-lactate and is believed to antagonize its actions (Gibbs and Hertz, 2008). This will allow us to study the effect of lactate accumulation (proposed to be due to a glymphatic impairment) on the sleeping pattern of animals with HE. If an improvement in sleep is observed, further glymphatic system manipulations can be applied in these animals (e.g. cisterna magna puncture) to ensure that the observed effect depends on the glymphatic activity. Therefore, this study might be able to propose alternative treatments for HE patients who suffer from sleep disturbances and cognitive decline.

Finally, another possible area of study would be the investigation of astrocytic volume and interstitial space during sleep and wakefulness. Xie et al., (Xie et al., 2013) have shown that during sleep the interstitial space increases, improving the efficiency of glymphatic clearance, as a result of astrocytic shrinkage at sleep. It would therefore be interesting to investigate whether in HE the “swollen” astrocytes or the interstitial space are able to adapt their volume during sleep. This could be another factor contributing to the impaired glymphatic activity and sleep disturbances observed in HE.

To conclude, the data obtained in this study provide the first evidence of a critical pathophysiological role of ammonia in inducing neuronal energy deficit in HE due to

impaired cerebral oxygenation, compromised hemichannel-mediated lactate transport between astrocytes and neurons and affected glymphatic clearance. Additionally, while most literature in the field is focused on astrocytes and their morphological alterations during the disease, it has been unclear what this means in terms of their functionality. During this thesis, data indicated a functional contribution of astrocytes in the development of the disease and introduced the important concept of an altered astrocyte-neuron communication, which has not been looked at before in HE. While studies of other factors potentially involved in the progression of the disease, such as inflammation, have been beyond the scope of this study, they are not excluded as possible contributors. However, the results obtained indicate reversible phenotypes when treated with an ammonia-lowering agent (such as OP), which holds great therapeutic potential in the field of HE.

Bibliography

ALBRECHT, J. & JONES, E. A. 1999. Hepatic encephalopathy: molecular mechanisms underlying the clinical syndrome. *J Neurol Sci,* 170**,** 138-46.

AMERICAN ASSOCIATION FOR THE STUDY OF LIVER, D. & EUROPEAN ASSOCIATION FOR THE STUDY OF THE, L. 2014. Hepatic encephalopathy in chronic liver disease: 2014 practice guideline by the European Association for the Study of the Liver and the American Association for the Study of Liver Diseases. *J Hepatol,* 61**,** 642-59.

ANGELOVA, P. R., KASYMOV, V., CHRISTIE, I., SHEIKHBAHAEI, S., TUROVSKY, E., MARINA, N., KORSAK, A., ZWICKER, J., TESCHEMACHER, A. G., ACKLAND, G. L., FUNK, G. D., KASPAROV, S., ABRAMOV, A. Y. & GOURINE, A. V. 2015. Functional Oxygen Sensitivity of Astrocytes. *J Neurosci,* 35**,** 10460-73.

ARAQUE, A., PARPURA, V., SANZGIRI, R. P. & HAYDON, P. G. 1999. Tripartite synapses: glia, the unacknowledged partner. *Trends Neurosci,* 22**,** 208-15.

ATTWELL, D., BUCHAN, A. M., CHARPAK, S., LAURITZEN, M., MACVICAR, B. A. & NEWMAN, E. A. 2010. Glial and neuronal control of brain blood flow. *Nature,* 468**,** 232-43.

BAJAJ, J. S., SAEIAN, K., SCHUBERT, C. M., FRANCO, R., FRANCO, J. & HEUMAN, D. M. 2011. Disruption of sleep architecture in minimal hepatic encephalopathy and ghrelin secretion. *Aliment Pharmacol Ther,* 34**,** 103-5.

BALASUBRAMANIYAN, V., WRIGHT, G., SHARMA, V., DAVIES, N. A., SHARIFI, Y., HABTESION, A., MOOKERJEE, R. P. & JALAN, R. 2012. Ammonia

reduction with ornithine phenylacetate restores brain eNOS activity via the DDAH-ADMA pathway in bile duct-ligated cirrhotic rats. *Am J Physiol Gastrointest Liver Physiol,* 302**,** G145-52.

BALATA, S., OLDE DAMINK, S. W., FERGUSON, K., MARSHALL, I., HAYES, P. C., DEUTZ, N. E., WILLIAMS, R., WARDLAW, J. & JALAN, R. 2003. Induced hyperammonemia alters neuropsychology, brain MR spectroscopy and magnetization transfer in cirrhosis. *Hepatology,* 37**,** 931-9.

BALLABH, P., BRAUN, A. & NEDERGAARD, M. 2004. The blood-brain barrier: an overview: structure, regulation, and clinical implications. *Neurobiol Dis,* 16**,** 1-13.

BANASIAK, K. J. & HADDAD, G. G. 1998. Hypoxia-induced apoptosis: effect of hypoxic severity and role of p53 in neuronal cell death. *Brain Res,* 797**,** 295-304.

BAO, X., CHEN, Y., LEE, S. H., LEE, S. C., REUSS, L. & ALTENBERG, G. A. 2005. Membrane transport proteins with complete replacement of transmembrane helices with polyalanine sequences remain functional. *J Biol Chem,* 280**,** 8647-50.

BATRA, N., BURRA, S., SILLER-JACKSON, A. J., GU, S., XIA, X., WEBER, G. F., DESIMONE, D., BONEWALD, L. F., LAFER, E. M., SPRAGUE, E., SCHWARTZ, M. A. & JIANG, J. X. 2012. Mechanical stress-activated integrin alpha5beta1 induces opening of connexin 43 hemichannels. *Proc Natl Acad Sci U S A,* 109**,** 3359-64.

BELANGER, M., ALLAMAN, I. & MAGISTRETTI, P. J. 2011. Brain energy metabolism: focus on astrocyte-neuron metabolic cooperation. *Cell Metab,* 14**,** 724-38.

BELANGER, M., DESJARDINS, P., CHATAURET, N. & BUTTERWORTH, R. F. 2006. Selectively increased expression of the astrocytic/endothelial glucose transporter protein GLUT1 in acute liver failure. *Glia,* 53**,** 557-62.

BEMEUR, C., QU, H., DESJARDINS, P. & BUTTERWORTH, R. F. 2010. IL-1 or TNF receptor gene deletion delays onset of encephalopathy and attenuates brain edema in experimental acute liver failure. *Neurochem Int,* 56**,** 213-5.

BENDER, A. S. & NORENBERG, M. D. 1998. Effect of benzodiazepines and neurosteroids on ammonia-induced swelling in cultured astrocytes. *J Neurosci Res,* 54**,** 673-80.

BENDER AS, R. I. N. M. 1992. Tumor necrosis factor a induces astrocyte swelling. *Trans Am Neurochem,* 23**,** 113.

BENJAMIN, A. M., OKAMOTO, K. & QUASTEL, J. H. 1978. Effects of ammonium ions on spontaneous action potentials and on contents of sodium, potassium, ammonium and chloride ions in brain in vitro. *J Neurochem,* 30**,** 131-43.

BENNETT, M. V., CONTRERAS, J. E., BUKAUSKAS, F. F. & SAEZ, J. C. 2003. New roles for astrocytes: gap junction hemichannels have something to communicate. *Trends Neurosci,* 26**,** 610-7.

BERNAL, W. 2010. Lactate is important in determining prognosis in acute liver failure. *J Hepatol,* 53**,** 209-10.

BERNAL, W., HALL, C., KARVELLAS, C. J., AUZINGER, G., SIZER, E. & WENDON, J. 2007. Arterial ammonia and clinical risk factors for encephalopathy and intracranial hypertension in acute liver failure. *Hepatology,* 46**,** 1844-52.

BEYER, E. C. & BERTHOUD, V. M. 2014. Connexin hemichannels in the lens. *Front Physiol,* 5**,** 20.

BEZZI, P., DOMERCQ, M., VESCE, S. & VOLTERRA, A. 2001. Neuron-astrocyte cross-talk during synaptic transmission: physiological and neuropathological implications. *Prog Brain Res,* 132**,** 255-65.

BLANC, E. M., BRUCE-KELLER, A. J. & MATTSON, M. P. 1998a. Astrocytic gap junctional communication decreases neuronal vulnerability to oxidative stress-induced disruption of Ca2+ homeostasis and cell death. *J Neurochem,* 70**,** 958-70.

BLANC, E. M., KELLER, J. N., FERNANDEZ, S. & MATTSON, M. P. 1998b. 4-hydroxynonenal, a lipid peroxidation product, impairs glutamate transport in cortical astrocytes. *Glia,* 22**,** 149-60.

BOBERMIN, L. D., HANSEL, G., SCHERER, E. B., WYSE, A. T., SOUZA, D. O., QUINCOZES-SANTOS, A. & GONCALVES, C. A. 2015. Ammonia impairs glutamatergic communication in astroglial cells: protective role of resveratrol. *Toxicol In Vitro,* 29**,** 2022-9.

BOSOI, C. R., PARENT-ROBITAILLE, C., ANDERSON, K., TREMBLAY, M. & ROSE, C. F. 2011. AST-120 (spherical carbon adsorbent) lowers ammonia levels and attenuates brain edema in bile duct-ligated rats. *Hepatology,* 53**,** 1995-2002.

BOSOI, C. R. & ROSE, C. F. 2009. Identifying the direct effects of ammonia on the brain. *Metab Brain Dis,* 24**,** 95-102.

BOSOI, C. R. & ROSE, C. F. 2013a. Brain edema in acute liver failure and chronic liver disease: similarities and differences. *Neurochem Int,* 62**,** 446-57.

BOSOI, C. R. & ROSE, C. F. 2013b. Oxidative stress: a systemic factor implicated in the pathogenesis of hepatic encephalopathy. *Metab Brain Dis,* 28**,** 175-8.

BOSOI, C. R., ZWINGMANN, C., MARIN, H., PARENT-ROBITAILLE, C., HUYNH, J., TREMBLAY, M. & ROSE, C. F. 2014. Increased brain lactate is central to the development of brain edema in rats with chronic liver disease. *J Hepatol,* 60**,** 554-60.

BROER, S. & BROOKES, N. 2001. Transfer of glutamine between astrocytes and neurons. *J Neurochem,* 77**,** 705-19.

BROOKES, N. 2000. Functional integration of the transport of ammonium, glutamate and glutamine in astrocytes. *Neurochem Int,* 37**,** 121-9.

BUKAUSKAS, F. F. & PERACCHIA, C. 1997. Two distinct gating mechanisms in gap junction channels: CO2-sensitive and voltage-sensitive. *Biophys J,* 72**,** 2137-42.

BURTON, B. K. 2000. Urea cycle disorders. *Clin Liver Dis,* 4**,** 815-30, vi.

BUSHONG, E. A., MARTONE, M. E., JONES, Y. Z. & ELLISMAN, M. H. 2002. Protoplasmic astrocytes in CA1 stratum radiatum occupy separate anatomical domains. *J Neurosci,* 22**,** 183-92.

BUTT, A. M. & KALSI, A. 2006. Inwardly rectifying potassium channels (Kir) in central nervous system glia: a special role for Kir4.1 in glial functions. *J Cell Mol Med,* 10**,** 33-44.

BUTTERWORTH, R. 2007. Neuronal cell death in hepatic encephalopathy. *Metab Brain Dis,* 22**,** 309-20.

BUTTERWORTH, R. F. 2000. The astrocytic ("peripheral-type") benzodiazepine receptor: role in the pathogenesis of portal-systemic encephalopathy. *Neurochem Int,* 36**,** 411-6.

BUTTERWORTH, R. F. 2002. Pathophysiology of hepatic encephalopathy: a new look at ammonia. *Metab Brain Dis,* 17**,** 221-7.

BUTTERWORTH, R. F. 2011. Neuroinflammation in acute liver failure: mechanisms and novel therapeutic targets. *Neurochem Int,* 59**,** 830-6.

BUTTERWORTH, R. F. 2014. Pathophysiology of brain dysfunction in hyperammonemic syndromes: The many faces of glutamine. *Mol Genet Metab,* 113**,** 113-7.

BUTTERWORTH, R. F., NORENBERG, M. D., FELIPO, V., FERENCI, P., ALBRECHT, J., BLEI, A. T. & MEMBERS OF THE, I. C. O. E. M. O. H. E. 2009. Experimental models of hepatic encephalopathy: ISHEN guidelines. *Liver Int,* 29**,** 783-8.

CATALDO, A. M. & BROADWELL, R. D. 1986. Cytochemical identification of cerebral glycogen and glucose-6-phosphatase activity under normal and experimental conditions. II. Choroid plexus and ependymal epithelia, endothelia and pericytes. *J Neurocytol,* 15**,** 511-24.

CAULI, O., RODRIGO, R., LLANSOLA, M., MONTOLIU, C., MONFORT, P., PIEDRAFITA, B., EL MLILI, N., BOIX, J., AGUSTI, A. & FELIPO, V. 2009. Glutamatergic and gabaergic neurotransmission and neuronal circuits in hepatic encephalopathy. *Metab Brain Dis,* 24**,** 69-80.

CHAN, H., HAZELL, A. S., DESJARDINS, P. & BUTTERWORTH, R. F. 2000. Effects of ammonia on glutamate transporter (GLAST) protein and mRNA in cultured rat cortical astrocytes. *Neurochem Int,* 37**,** 243-8.

CHAPMAN, M. H., TIDSWELL, R., DOOLEY, J. S., SANDANAYAKE, N. S., CEREC, V., DEHERAGODA, M., LEE, A. J., SWANTON, C., ANDREOLA, F. & PEREIRA, S. P. 2012. Whole genome RNA expression profiling of endoscopic biliary brushings provides data suitable for biomarker discovery in cholangiocarcinoma. *J Hepatol,* 56**,** 877-85.

CHEN, J. R., WANG, B. N., TSENG, G. F., WANG, Y. J., HUANG, Y. S. & WANG, T. J. 2014. Morphological changes of cortical pyramidal neurons in hepatic encephalopathy. *BMC Neurosci,* 15**,** 15.

CLEMMESEN, J. O., LARSEN, F. S., KONDRUP, J., HANSEN, B. A. & OTT, P. 1999. Cerebral herniation in patients with acute liver failure is correlated with arterial ammonia concentration. *Hepatology,* 29**,** 648-53.

CONTRERAS, J. E., SAEZ, J. C., BUKAUSKAS, F. F. & BENNETT, M. V. 2003. Gating and regulation of connexin 43 (Cx43) hemichannels. *Proc Natl Acad Sci U S A,* 100**,** 11388-93.

COOPER, A. J. 2001. Role of glutamine in cerebral nitrogen metabolism and ammonia neurotoxicity. *Ment Retard Dev Disabil Res Rev,* 7**,** 280-6.

COOPER, A. J. & PLUM, F. 1987. Biochemistry and physiology of brain ammonia. *Physiol Rev,* 67**,** 440-519.

CORDOBA, J., RAGUER, N., FLAVIA, M., VARGAS, V., JACAS, C., ALONSO, J. & ROVIRA, A. 2003. T2 hyperintensity along the cortico-spinal tract in cirrhosis relates to functional abnormalities. *Hepatology,* 38**,** 1026-33.

CORNELL-BELL, A. H., FINKBEINER, S. M., COOPER, M. S. & SMITH, S. J. 1990. Glutamate induces calcium waves in cultured astrocytes: long-range glial signaling. *Science,* 247**,** 470-3.

DAM, G., KEIDING, S., MUNK, O. L., OTT, P., VILSTRUP, H., BAK, L. K., WAAGEPETERSEN, H. S., SCHOUSBOE, A. & SORENSEN, M. 2013. Hepatic encephalopathy is associated with decreased cerebral oxygen metabolism and blood flow, not increased ammonia uptake. *Hepatology,* 57**,** 258-65.

DAMASIO, A. R. 1989. Time-locked multiregional retroactivation: a systems-level proposal for the neural substrates of recall and recognition. *Cognition,* 33**,** 25-62.

DAVIES, N. A., WRIGHT, G., YTREBO, L. M., STADLBAUER, V., FUSKEVAG, O. M., ZWINGMANN, C., DAVIES, D. C., HABTESION, A., HODGES, S. J. & JALAN, R. 2009. L-ornithine and phenylacetate synergistically produce sustained reduction in ammonia and brain water in cirrhotic rats. *Hepatology,* 50**,** 155-64.

DE VRIES, H. E., BLOM-ROOSEMALEN, M. C., VAN OOSTEN, M., DE BOER, A. G., VAN BERKEL, T. J., BREIMER, D. D. & KUIPER, J. 1996. The influence of cytokines on the integrity of the blood-brain barrier in vitro. *J Neuroimmunol,* 64**,** 37-43.

DE WOLF, E., COOK, J. & DALE, N. 2017. Evolutionary adaptation of the sensitivity of connexin26 hemichannels to CO2. *Proc Biol Sci,* 284.

DEJONG, C. H., DEUTZ, N. E. & SOETERS, P. B. 1993. Renal ammonia and glutamine metabolism during liver insufficiency-induced hyperammonemia in the rat. *J Clin Invest,* 92**,** 2834-40.

DREJER, J., LARSSON, O. M. & SCHOUSBOE, A. 1982. Characterization of L-glutamate uptake into and release from astrocytes and neurons cultured from different brain regions. *Exp Brain Res,* 47**,** 259-69.

DUCHINI, A., GOVINDARAJAN, S., SANTUCCI, M., ZAMPI, G. & HOFMAN, F. M. 1996. Effects of tumor necrosis factor-alpha and interleukin-6 on fluid-phase permeability and ammonia diffusion in CNS-derived endothelial cells. *J Investig Med,* 44**,** 474-82.

DUFFY, H. S., SORGEN, P. L., GIRVIN, M. E., O'DONNELL, P., COOMBS, W., TAFFET, S. M., DELMAR, M. & SPRAY, D. C. 2002. pH-dependent intramolecular binding and structure involving Cx43 cytoplasmic domains. *J Biol Chem,* 277**,** 36706-14.

DZHALA, V. I., KUCHIBHOTLA, K. V., GLYKYS, J. C., KAHLE, K. T., SWIERCZ, W. B., FENG, G., KUNER, T., AUGUSTINE, G. J., BACSKAI, B. J. & STALEY, K. J. 2010. Progressive NKCC1-dependent neuronal chloride accumulation during neonatal seizures. *J Neurosci,* 30**,** 11745-61.

ERCEG, S., MONFORT, P., HERNANDEZ-VIADEL, M., RODRIGO, R., MONTOLIU, C. & FELIPO, V. 2005. Oral administration of sildenafil restores learning ability in rats with hyperammonemia and with portacaval shunts. *Hepatology,* 41**,** 299-306.

ERICKSON, M. A., HARTVIGSON, P. E., MOROFUJI, Y., OWEN, J. B., BUTTERFIELD, D. A. & BANKS, W. A. 2012. Lipopolysaccharide impairs amyloid beta efflux from brain: altered vascular sequestration, cerebrospinal fluid reabsorption, peripheral clearance and transporter function at the blood-brain barrier. *J Neuroinflammation,* 9**,** 150.

ESTRELA, H. F., DAMASIO, E. S., FONSECA, E. K., BERGAMASCHI, C. T. & CAMPOS, R. R. 2016. Differential Sympathetic Vasomotor Activation Induced by Liver Cirrhosis in Rats. *PLoS One,* 11**,** e0152512.

EZAN, P., ANDRE, P., CISTERNINO, S., SAUBAMEA, B., BOULAY, A. C., DOUTREMER, S., THOMAS, M. A., QUENECH'DU, N., GIAUME, C. & COHEN-SALMON, M. 2012. Deletion of astroglial connexins weakens the blood-brain barrier. *J Cereb Blood Flow Metab,* 32**,** 1457-67.

FAUL, F., ERDFELDER, E., BUCHNER, A. & LANG, A. G. 2009. Statistical power analyses using G*Power 3.1: tests for correlation and regression analyses. *Behav Res Methods,* 41**,** 1149-60.

FELIPO, V. & BUTTERWORTH, R. F. 2002a. Mitochondrial dysfunction in acute hyperammonemia. *Neurochem Int,* 40**,** 487-91.

FELIPO, V. & BUTTERWORTH, R. F. 2002b. Neurobiology of ammonia. *Prog Neurobiol,* 67**,** 259-79.

FERNANDEZ-KLETT, F., OFFENHAUSER, N., DIRNAGL, U., PRILLER, J. & LINDAUER, U. 2010. Pericytes in capillaries are contractile in vivo, but arterioles mediate functional hyperemia in the mouse brain. *Proc Natl Acad Sci U S A,* 107**,** 22290-5.

FIORI, M. C., REUSS, L., CUELLO, L. G. & ALTENBERG, G. A. 2014. Functional analysis and regulation of purified connexin hemichannels. *Front Physiol,* 5**,** 71.

FUSTER, J. M. 1990. Behavioral electrophysiology of the prefrontal cortex of the primate. *Prog Brain Res,* 85**,** 313-23; discussion 323-4.

GIAUME, C., KOULAKOFF, A., ROUX, L., HOLCMAN, D. & ROUACH, N. 2010. Astroglial networks: a step further in neuroglial and gliovascular interactions. *Nat Rev Neurosci,* 11**,** 87-99.

GIAUME, C., LEYBAERT, L., NAUS, C. C. & SAEZ, J. C. 2013. Connexin and pannexin hemichannels in brain glial cells: properties, pharmacology, and roles. *Front Pharmacol,* 4**,** 88.

GIAUME, C., ORELLANA, J. A., ABUDARA, V. & SAEZ, J. C. 2012. Connexin-based channels in astrocytes: how to study their properties. *Methods Mol Biol,* 814**,** 283-303.

GIBBS, M. E. & HERTZ, L. 2008. Inhibition of astrocytic energy metabolism by D-lactate exposure impairs memory. *Neurochem Int,* 52**,** 1012-8.

GLASS, C. K., SAIJO, K., WINNER, B., MARCHETTO, M. C. & GAGE, F. H. 2010. Mechanisms underlying inflammation in neurodegeneration. *Cell,* 140**,** 918-34.

GORDON, G. R., CHOI, H. B., RUNGTA, R. L., ELLIS-DAVIES, G. C. & MACVICAR, B. A. 2008. Brain metabolism dictates the polarity of astrocyte control over arterioles. *Nature,* 456**,** 745-9.

GORG, B., MORWINSKY, A., KEITEL, V., QVARTSKHAVA, N., SCHROR, K. & HAUSSINGER, D. 2010. Ammonia triggers exocytotic release of L-glutamate from cultured rat astrocytes. *Glia,* 58**,** 691-705.

GORG, B., QVARTSKHAVA, N., KEITEL, V., BIDMON, H. J., SELBACH, O., SCHLIESS, F. & HAUSSINGER, D. 2008. Ammonia induces RNA oxidation in cultured astrocytes and brain in vivo. *Hepatology,* 48**,** 567-79.

GOURINE, A. V., DALE, N., KORSAK, A., LLAUDET, E., TIAN, F., HUCKSTEPP, R. & SPYER, K. M. 2008. Release of ATP and glutamate in the nucleus tractus solitarii mediate pulmonary stretch receptor (Breuer-Hering) reflex pathway. *J Physiol,* 586**,** 3963-78.

GOURINE, A. V. & FUNK, G. D. 2017. On the existence of a central respiratory oxygen sensor. *J Appl Physiol (1985)***,** jap 00194 2017.

GOURINE, A. V., KASYMOV, V., MARINA, N., TANG, F., FIGUEIREDO, M. F., LANE, S., TESCHEMACHER, A. G., SPYER, K. M., DEISSEROTH, K. & KASPAROV, S. 2010. Astrocytes control breathing through pH-dependent release of ATP. *Science,* 329**,** 571-5.

GOURINE, A. V., LLAUDET, E., DALE, N. & SPYER, K. M. 2005. Release of ATP in the ventral medulla during hypoxia in rats: role in hypoxic ventilatory response. *J Neurosci,* 25**,** 1211-8.

GOURINE, A. V., LLAUDET, E., THOMAS, T., DALE, N. & SPYER, K. M. 2002. Adenosine release in nucleus tractus solitarii does not appear to mediate hypoxia-induced respiratory depression in rats. *J Physiol,* 544**,** 161-70.

GREEN, K. N., BOYLE, J. P. & PEERS, C. 2002. Hypoxia potentiates exocytosis and Ca2+ channels in PC12 cells via increased amyloid beta peptide formation and reactive oxygen species generation. *J Physiol,* 541**,** 1013-23.

GUEVARA, M., BRU, C., GINES, P., FERNANDEZ-ESPARRACH, G., SORT, P., BATALLER, R., JIMENEZ, W., ARROYO, V. & RODES 1998. Increased cerebrovascular resistance in cirrhotic patients with ascites. *Hepatology,* 28**,** 39-44.

GUPTA, R. K., YADAV, S. K., RANGAN, M., RATHORE, R. K., THOMAS, M. A., PRASAD, K. N., PANDEY, C. M. & SARASWAT, V. A. 2010. Serum proinflammatory cytokines correlate with diffusion tensor imaging derived metrics and 1H-MR spectroscopy in patients with acute liver failure. *Metab Brain Dis,* 25**,** 355-61.

H. K. KIMELBERG, E. R. O. C., HELMUT KETTENMANN 1993. Advances in Comparative and Environmental Physiology. *Effects of Swelling on Glial Cell Function.* Springer Berlin Heidelberg.

HADJIHAMBI, A., DE CHIARA, F., HOSFORD, P. S., HABTETION, A., KARAGIANNIS, A., DAVIES, N., GOURINE, A. V. & JALAN, R. 2017. Ammonia mediates cortical hemichannel dysfunction in rodent models of chronic liver disease. *Hepatology,* 65**,** 1306-1318.

HADJIHAMBI, A., KHETAN, V. & JALAN, R. 2014a. Pharmacotherapy for hyperammonemia. *Expert Opin Pharmacother,* 15**,** 1685-95.

HADJIHAMBI, A., ROSE, C. F. & JALAN, R. 2014b. Novel insights into ammonia-mediated neurotoxicity pointing to potential new therapeutic strategies. *Hepatology,* 60**,** 1101-3.

HAHN M, M. O., NENCKI M, PAVLOV J. 1893. Die Eck'sche fistel zwischen der unteren hohlvene und der pfortadre und ihre folgen fu¨r den organismus. *Archiv fuer Experimentelle Pathologie und Pharmakologie* 32**,** 161–210.

HALASSA, M. M., FELLIN, T. & HAYDON, P. G. 2007a. The tripartite synapse: roles for gliotransmission in health and disease. *Trends Mol Med,* 13**,** 54-63.

HALASSA, M. M., FELLIN, T., TAKANO, H., DONG, J. H. & HAYDON, P. G. 2007b. Synaptic islands defined by the territory of a single astrocyte. *J Neurosci,* 27**,** 6473-7.

HALL, C. N., REYNELL, C., GESSLEIN, B., HAMILTON, N. B., MISHRA, A., SUTHERLAND, B. A., O'FARRELL, F. M., BUCHAN, A. M., LAURITZEN, M. & ATTWELL, D. 2014. Capillary pericytes regulate cerebral blood flow in health and disease. *Nature,* 508**,** 55-60.

HARRY, D., ANAND, R., HOLT, S., DAVIES, S., MARLEY, R., FERNANDO, B., GOODIER, D. & MOORE, K. 1999. Increased sensitivity to endotoxemia in the bile duct-ligated cirrhotic Rat. *Hepatology,* 30**,** 1198-205.

HAUCK, E. F., APOSTEL, S., HOFFMANN, J. F., HEIMANN, A. & KEMPSKI, O. 2004. Capillary flow and diameter changes during reperfusion after global cerebral ischemia studied by intravital video microscopy. *J Cereb Blood Flow Metab,* 24**,** 383-91.

HAUSSINGER, D., KIRCHEIS, G., FISCHER, R., SCHLIESS, F. & VOM DAHL, S. 2000. Hepatic encephalopathy in chronic liver disease: a clinical manifestation of astrocyte swelling and low-grade cerebral edema? *J Hepatol,* 32**,** 1035-8.

HAYDON, P. G., BLENDY, J., MOSS, S. J. & ROB JACKSON, F. 2009. Astrocytic control of synaptic transmission and plasticity: a target for drugs of abuse? *Neuropharmacology,* 56 Suppl 1**,** 83-90.

HE Y, L. G., SONG H, LUO T, GAO B, XU J. 2011. Partial pressure of NH_3 in cirrhotic patients with and without hepatic encephalopathy.

. *J Gastrointestin Liver Dis.,* 20**,** 169-74.

HEIN, T. W., XU, W. & KUO, L. 2006. Dilation of retinal arterioles in response to lactate: role of nitric oxide, guanylyl cyclase, and ATP-sensitive potassium channels. *Invest Ophthalmol Vis Sci,* 47**,** 693-9.

HENNEBERGER, C., PAPOUIN, T., OLIET, S. H. & RUSAKOV, D. A. 2010. Long-term potentiation depends on release of D-serine from astrocytes. *Nature,* 463**,** 232-6.

HERNANDEZ-RABAZA, V., CABRERA-PASTOR, A., TAORO-GONZALEZ, L., MALAGUARNERA, M., AGUSTI, A., LLANSOLA, M. & FELIPO, V. 2016. Hyperammonemia induces glial activation, neuroinflammation and alters neurotransmitter receptors in hippocampus, impairing spatial learning: reversal by sulforaphane. *J Neuroinflammation,* 13**,** 41.

HOSOI, T., OKUMA, Y. & NOMURA, Y. 2002. The mechanisms of immune-to-brain communication in inflammation as a drug target. *Curr Drug Targets Inflamm Allergy,* 1**,** 257-62.

HUCKSTEPP, R. T., EASON, R., SACHDEV, A. & DALE, N. 2010. CO2-dependent opening of connexin 26 and related beta connexins. *J Physiol,* 588**,** 3921-31.

IADECOLA, C. 2004. Neurovascular regulation in the normal brain and in Alzheimer's disease. *Nat Rev Neurosci,* 5**,** 347-60.

ILIFF, J. J., CHEN, M. J., PLOG, B. A., ZEPPENFELD, D. M., SOLTERO, M., YANG, L., SINGH, I., DEANE, R. & NEDERGAARD, M. 2014. Impairment of glymphatic pathway function promotes tau pathology after traumatic brain injury. *J Neurosci,* 34**,** 16180-93.

ILIFF, J. J., LEE, H., YU, M., FENG, T., LOGAN, J., NEDERGAARD, M. & BENVENISTE, H. 2013a. Brain-wide pathway for waste clearance captured by contrast-enhanced MRI. *J Clin Invest,* 123**,** 1299-309.

ILIFF, J. J., WANG, M., LIAO, Y., PLOGG, B. A., PENG, W., GUNDERSEN, G. A., BENVENISTE, H., VATES, G. E., DEANE, R., GOLDMAN, S. A., NAGELHUS, E. A. & NEDERGAARD, M. 2012. A paravascular pathway facilitates CSF flow through the brain parenchyma and the clearance of interstitial solutes, including amyloid beta. *Sci Transl Med,* 4**,** 147ra111.

ILIFF, J. J., WANG, M., ZEPPENFELD, D. M., VENKATARAMAN, A., PLOG, B. A., LIAO, Y., DEANE, R. & NEDERGAARD, M. 2013b. Cerebral arterial pulsation drives paravascular CSF-interstitial fluid exchange in the murine brain. *J Neurosci,* 33**,** 18190-9.

ISHIMARU, S., OKADA, Y., MIES, G. & HOSSMANN, K. A. 1993. Relationship between blood flow and blood-brain barrier permeability of sodium and albumin in focal ischaemia of rats: a triple tracer autoradiographic study. *Acta Neurochir (Wien),* 120**,** 72-80.

IVERSEN, P., SORENSEN, M., BAK, L. K., WAAGEPETERSEN, H. S., VAFAEE, M. S., BORGHAMMER, P., MOURIDSEN, K., JENSEN, S. B., VILSTRUP, H., SCHOUSBOE, A., OTT, P., GJEDDE, A. & KEIDING, S. 2009. Low cerebral

oxygen consumption and blood flow in patients with cirrhosis and an acute episode of hepatic encephalopathy. *Gastroenterology,* 136**,** 863-71.

JALAN, R., OLDE DAMINK, S. W., DEUTZ, N. E., HAYES, P. C. & LEE, A. 2004a. Moderate hypothermia in patients with acute liver failure and uncontrolled intracranial hypertension. *Gastroenterology,* 127**,** 1338-46.

JALAN, R., OLDE DAMINK, S. W., HAYES, P. C., DEUTZ, N. E. & LEE, A. 2004b. Pathogenesis of intracranial hypertension in acute liver failure: inflammation, ammonia and cerebral blood flow. *J Hepatol,* 41**,** 613-20.

JALAN, R., WRIGHT, G., DAVIES, N. A. & HODGES, S. J. 2007. L-Ornithine phenylacetate (OP): a novel treatment for hyperammonemia and hepatic encephalopathy. *Med Hypotheses,* 69**,** 1064-9.

JALAN, R., YURDAYDIN, C., BAJAJ, J. S., ACHARYA, S. K., ARROYO, V., LIN, H. C., GINES, P., KIM, W. R., KAMATH, P. S. & WORLD GASTROENTEROLOGY ORGANIZATION WORKING, P. 2014. Toward an improved definition of acute-on-chronic liver failure. *Gastroenterology,* 147**,** 4-10.

JAYAKUMAR, A. R., RUIZ-CORDERO, R., TONG, X. Y. & NORENBERG, M. D. 2013. Brain edema in acute liver failure: role of neurosteroids. *Arch Biochem Biophys,* 536**,** 171-5.

JIANG, W., DESJARDINS, P. & BUTTERWORTH, R. F. 2009a. Cerebral inflammation contributes to encephalopathy and brain edema in acute liver failure: protective effect of minocycline. *J Neurochem,* 109**,** 485-93.

JIANG, W., DESJARDINS, P. & BUTTERWORTH, R. F. 2009b. Direct evidence for central proinflammatory mechanisms in rats with experimental acute liver

failure: protective effect of hypothermia. *J Cereb Blood Flow Metab,* 29**,** 944-52.

JOHNSTON, W. H. & LATTA, H. 1977. Glomerular mesangial and endothelial cell swelling following temporary renal ischemia and its role in the no-reflow phenomenon. *Am J Pathol,* 89**,** 153-66.

KARAGIANNIS, A., SYLANTYEV, S., HADJIHAMBI, A., HOSFORD, P. S., KASPAROV, S. & GOURINE, A. V. 2016. Hemichannel-mediated release of lactate. *J Cereb Blood Flow Metab,* 36**,** 1202-11.

KATO, M., HUGHES, R. D., KEAYS, R. T. & WILLIAMS, R. 1992. Electron microscopic study of brain capillaries in cerebral edema from fulminant hepatic failure. *Hepatology,* 15**,** 1060-6.

KELLY, T., KAFITZ, K. W., RODERIGO, C. & ROSE, C. R. 2009. Ammonium-evoked alterations in intracellular sodium and pH reduce glial glutamate transport activity. *Glia,* 57**,** 921-34.

KETTENMANN, H. & VERKHRATSKY, A. 2011. [Neuroglia--living nerve glue]. *Fortschr Neurol Psychiatr,* 79**,** 588-97.

KHOT, S. & TIRSCHWELL, D. L. 2006. Long-term neurological complications after hypoxic-ischemic encephalopathy. *Semin Neurol,* 26**,** 422-31.

KIM, Y., DAVIDSON, J. O., GREEN, C. R., NICHOLSON, L. F., O'CARROLL, S. J. & ZHANG, J. 2017. Connexins and Pannexins in cerebral ischemia. *Biochim Biophys Acta*.

KIMELBERG, H. K. 2005. Astrocytic swelling in cerebral ischemia as a possible cause of injury and target for therapy. *Glia,* 50**,** 389-97.

KIMELBERG, H. K., ANDERSON, E. & KETTENMANN, H. 1990. Swelling-induced changes in electrophysiological properties of cultured astrocytes and oligodendrocytes. II. Whole-cell currents. *Brain Res,* 529**,** 262-8.

KIMELBERG HK, O. C. E., KETTENMANN H 1993. Advances in Comparative and Environmental Physiology. *In:* LANG F, H. (ed.) *Effects of Swelling on Glial Cell Function.* Springer Berlin Heidelberg.

KISLER, K., NELSON, A. R., MONTAGNE, A. & ZLOKOVIC, B. V. 2017. Cerebral blood flow regulation and neurovascular dysfunction in Alzheimer disease. *Nat Rev Neurosci*.

KOFUJI, P. & NEWMAN, E. A. 2004. Potassium buffering in the central nervous system. *Neuroscience,* 129**,** 1045-56.

KOSENKO, E., KAMINSKY, Y., GRAU, E., MINANA, M. D., MARCAIDA, G., GRISOLIA, S. & FELIPO, V. 1994. Brain ATP depletion induced by acute ammonia intoxication in rats is mediated by activation of the NMDA receptor and Na+,K(+)-ATPase. *J Neurochem,* 63**,** 2172-8.

KOSUGI, T. & KAWAHARA, K. 2006. Reversed actrocytic GLT-1 during ischemia is crucial to excitotoxic death of neurons, but contributes to the survival of astrocytes themselves. *Neurochem Res,* 31**,** 933-43.

KRESS, B. T., ILIFF, J. J., XIA, M., WANG, M., WEI, H. S., ZEPPENFELD, D., XIE, L., KANG, H., XU, Q., LIEW, J. A., PLOG, B. A., DING, F., DEANE, R. & NEDERGAARD, M. 2014. Impairment of paravascular clearance pathways in the aging brain. *Ann Neurol,* 76**,** 845-61.

KYRTSOS, C. R. & BARAS, J. S. 2015. Modeling the Role of the Glymphatic Pathway and Cerebral Blood Vessel Properties in Alzheimer's Disease Pathogenesis. *PLoS One,* 10**,** e0139574.

LAI, J. C. & COOPER, A. J. 1986. Brain alpha-ketoglutarate dehydrogenase complex: kinetic properties, regional distribution, and effects of inhibitors. *J Neurochem,* 47**,** 1376-86.

LARSEN, F. S., ADEL HANSEN, B., POTT, F., EJLERSEN, E., SECHER, N. H., PAULSON, O. B. & KNUDSEN, G. M. 1996. Dissociated cerebral vasoparalysis in acute liver failure. A hypothesis of gradual cerebral hyperaemia. *J Hepatol,* 25**,** 145-51.

LARSEN, F. S., OLSEN, K. S., EJLERSEN, E., HANSEN, B. A., PAULSON, O. B. & KNUDSEN, G. M. 1995. Cerebral blood flow autoregulation and transcranial Doppler sonography in patients with cirrhosis. *Hepatology,* 22**,** 730-6.

LERCHUNDI, R., FERNANDEZ-MONCADA, I., CONTRERAS-BAEZA, Y., SOTELO-HITSCHFELD, T., MACHLER, P., WYSS, M. T., STOBART, J., BAEZA-LEHNERT, F., ALEGRIA, K., WEBER, B. & BARROS, L. F. 2015. NH4(+) triggers the release of astrocytic lactate via mitochondrial pyruvate shunting. *Proc Natl Acad Sci U S A,* 112**,** 11090-5.

LI, L., SASE, A., PATIL, S., SUNYER, B., HOGER, H., SMALLA, K. H., STORK, O. & LUBEC, G. 2013. Distinct set of kinases induced after retrieval of spatial memory discriminate memory modulation processes in the mouse hippocampus. *Hippocampus,* 23**,** 672-83.

LIU, C., ZHOU, J., YANG, X., LV, J., SHI, Y. & ZENG, X. 2015. Changes in sleep architecture and quality in minimal hepatic encephalopathy patients and relationship to psychological dysfunction. *Int J Clin Exp Med,* 8**,** 21541-8.

LLAUDET, E., BOTTING, N. P., CRAYSTON, J. A. & DALE, N. 2003. A three-enzyme microelectrode sensor for detecting purine release from central nervous system. *Biosens Bioelectron,* 18**,** 43-52.

LOCKWOOD, A. H., YAP, E. W. & WONG, W. H. 1991. Cerebral ammonia metabolism in patients with severe liver disease and minimal hepatic encephalopathy. *J Cereb Blood Flow Metab,* 11**,** 337-41.

LOURENCO, C. F., LEDO, A., DIAS, C., BARBOSA, R. M. & LARANJINHA, J. 2015. Neurovascular and neurometabolic derailment in aging and Alzheimer's disease. *Front Aging Neurosci,* 7**,** 103.

LOUVEAU, A., SMIRNOV, I., KEYES, T. J., ECCLES, J. D., ROUHANI, S. J., PESKE, J. D., DERECKI, N. C., CASTLE, D., MANDELL, J. W., LEE, K. S., HARRIS, T. H. & KIPNIS, J. 2015. Structural and functional features of central nervous system lymphatic vessels. *Nature,* 523**,** 337-41.

LUNDGAARD, I., LU, M. L., YANG, E., PENG, W., MESTRE, H., HITOMI, E., DEANE, R. & NEDERGAARD, M. 2016. Glymphatic clearance controls state-dependent changes in brain lactate concentration. *J Cereb Blood Flow Metab***,** 271678X16661202.

MAGISTRETTI, P. J. 2011. Neuron-glia metabolic coupling and plasticity. *Exp Physiol,* 96**,** 407-10.

MARCAGGI, P. & COLES, J. A. 2001. Ammonium in nervous tissue: transport across cell membranes, fluxes from neurons to glial cells, and role in signalling. *Prog Neurobiol,* 64**,** 157-83.

MARCU, R., WICZER, B. M., NEELEY, C. K. & HAWKINS, B. J. 2014. Mitochondrial matrix Ca(2)(+) accumulation regulates cytosolic NAD(+)/NADH metabolism, protein acetylation, and sirtuin expression. *Mol Cell Biol,* 34**,** 2890-902.

MARINA, N., ANG, R., MACHHADA, A., KASYMOV, V., KARAGIANNIS, A., HOSFORD, P. S., MOSIENKO, V., TESCHEMACHER, A. G., VIHKO, P., PATON, J. F., KASPAROV, S. & GOURINE, A. V. 2015. Brainstem hypoxia

contributes to the development of hypertension in the spontaneously hypertensive rat. *Hypertension,* 65**,** 775-83.

MATYASH, V. & KETTENMANN, H. 2010. Heterogeneity in astrocyte morphology and physiology. *Brain Res Rev,* 63**,** 2-10.

MCCOY, M. K. & TANSEY, M. G. 2008. TNF signaling inhibition in the CNS: implications for normal brain function and neurodegenerative disease. *J Neuroinflammation,* 5**,** 45.

MEIGH, L., GREENHALGH, S. A., RODGERS, T. L., CANN, M. J., ROPER, D. I. & DALE, N. 2013. CO(2)directly modulates connexin 26 by formation of carbamate bridges between subunits. *Elife,* 2**,** e01213.

MICHALAK, A., KNECHT, K. & BUTTERWORTH, R. F. 1997. Hepatic encephalopathy in acute liver failure: role of the glutamate system. *Adv Exp Med Biol,* 420**,** 35-43.

MICHALAK, A., ROSE, C., BUTTERWORTH, J. & BUTTERWORTH, R. F. 1996. Neuroactive amino acids and glutamate (NMDA) receptors in frontal cortex of rats with experimental acute liver failure. *Hepatology,* 24**,** 908-13.

MISHRA, A., REYNOLDS, J. P., CHEN, Y., GOURINE, A. V., RUSAKOV, D. A. & ATTWELL, D. 2016. Astrocytes mediate neurovascular signaling to capillary pericytes but not to arterioles. *Nat Neurosci,* 19**,** 1619-1627.

MONFORT, P., MUNOZ, M. D., ELAYADI, A., KOSENKO, E. & FELIPO, V. 2002. Effects of hyperammonemia and liver failure on glutamatergic neurotransmission. *Metab Brain Dis,* 17**,** 237-50.

MONTANA, V., VERKHRATSKY, A. & PARPURA, V. 2014. Pathological role for exocytotic glutamate release from astrocytes in hepatic encephalopathy. *Curr Neuropharmacol,* 12**,** 324-33.

MONTOLIU, C., PIEDRAFITA, B., SERRA, M. A., DEL OLMO, J. A., URIOS, A., RODRIGO, J. M. & FELIPO, V. 2009. IL-6 and IL-18 in blood may discriminate cirrhotic patients with and without minimal hepatic encephalopathy. *J Clin Gastroenterol,* 43**,** 272-9.

MOSER, H. 1987. Electrophysiological evidence for ammonium as a substitute for potassium in activating the sodium pump in a crayfish sensory neuron. *Can J Physiol Pharmacol,* 65**,** 141-5.

MOSKOWITZ, M. A., LO, E. H. & IADECOLA, C. 2010. The science of stroke: mechanisms in search of treatments. *Neuron,* 67**,** 181-98.

MULLER, D. J., HAND, G. M., ENGEL, A. & SOSINSKY, G. E. 2002. Conformational changes in surface structures of isolated connexin 26 gap junctions. *EMBO J,* 21**,** 3598-607.

NAGARAJA, T. N. & BROOKES, N. 1998. Intracellular acidification induced by passive and active transport of ammonium ions in astrocytes. *Am J Physiol,* 274**,** C883-91.

NAVARRETE, M., PEREA, G., FERNANDEZ DE SEVILLA, D., GOMEZ-GONZALO, M., NUNEZ, A., MARTIN, E. D. & ARAQUE, A. 2012. Astrocytes mediate in vivo cholinergic-induced synaptic plasticity. *PLoS Biol,* 10**,** e1001259.

NEDELSKY, N. B., TODD, P. K. & TAYLOR, J. P. 2008. Autophagy and the ubiquitin-proteasome system: collaborators in neuroprotection. *Biochim Biophys Acta,* 1782**,** 691-9.

NEDERGAARD, M. 2013. Neuroscience. Garbage truck of the brain. *Science,* 340**,** 1529-30.

NICCHIA, G. P., SRINIVAS, M., LI, W., BROSNAN, C. F., FRIGERI, A. & SPRAY, D. C. 2005. New possible roles for aquaporin-4 in astrocytes: cell cytoskeleton and functional relationship with connexin43. *FASEB J,* 19**,** 1674-6.

NICOLAO, F., EFRATI, C., MASINI, A., MERLI, M., ATTILI, A. F. & RIGGIO, O. 2003. Role of determination of partial pressure of ammonia in cirrhotic patients with and without hepatic encephalopathy. *J Hepatol,* 38**,** 441-6.

NORENBERG, M. D. 1977. A light and electron microscopic study of experimental portal-systemic (ammonia) encephalopathy. Progression and reversal of the disorder. *Lab Invest,* 36**,** 618-27.

NORENBERG, M. D. 1998. Astroglial dysfunction in hepatic encephalopathy. *Metab Brain Dis,* 13**,** 319-35.

NORENBERG, M. D., HUO, Z., NEARY, J. T. & ROIG-CANTESANO, A. 1997. The glial glutamate transporter in hyperammonemia and hepatic encephalopathy: relation to energy metabolism and glutamatergic neurotransmission. *Glia,* 21**,** 124-33.

O'GRADY, J. G., SCHALM, S. W. & WILLIAMS, R. 1993. Acute liver failure: redefining the syndromes. *Lancet,* 342**,** 273-5.

OBERHEIM, N. A., GOLDMAN, S. A. & NEDERGAARD, M. 2012. Heterogeneity of astrocytic form and function. *Methods Mol Biol,* 814**,** 23-45.

OJA, S. S., SARANSAARI, P. & KORPI, E. R. 2017. Neurotoxicity of Ammonia. *Neurochem Res,* 42**,** 713-720.

OLDE DAMINK, S. W., JALAN, R. & DEJONG, C. H. 2009. Interorgan ammonia trafficking in liver disease. *Metab Brain Dis,* 24**,** 169-81.

ORELLANA, J. A., FROGER, N., EZAN, P., JIANG, J. X., BENNETT, M. V., NAUS, C. C., GIAUME, C. & SAEZ, J. C. 2011. ATP and glutamate released via

astroglial connexin 43 hemichannels mediate neuronal death through activation of pannexin 1 hemichannels. *J Neurochem,* 118**,** 826-40.

ORELLANA, J. A., HERNANDEZ, D. E., EZAN, P., VELARDE, V., BENNETT, M. V., GIAUME, C. & SAEZ, J. C. 2010. Hypoxia in high glucose followed by reoxygenation in normal glucose reduces the viability of cortical astrocytes through increased permeability of connexin 43 hemichannels. *Glia,* 58**,** 329-43.

ORIA, M., ROMERO-GIMENEZ, J., ARRANZ, J. A., RIUDOR, E., RAGUER, N. & CORDOBA, J. 2012. Ornithine phenylacetate prevents disturbances of motor-evoked potentials induced by intestinal blood in rats with portacaval anastomosis. *J Hepatol,* 56**,** 109-14.

OSTERGAARD, L., ENGEDAL, T. S., AAMAND, R., MIKKELSEN, R., IVERSEN, N. K., ANZABI, M., NAESS-SCHMIDT, E. T., DRASBEK, K. R., BAY, V., BLICHER, J. U., TIETZE, A., MIKKELSEN, I. K., HANSEN, B., JESPERSEN, S. N., JUUL, N., SORENSEN, J. C. & RASMUSSEN, M. 2014. Capillary transit time heterogeneity and flow-metabolism coupling after traumatic brain injury. *J Cereb Blood Flow Metab,* 34**,** 1585-98.

PATET, C., QUINTARD, H., SUYS, T., BLOCH, J., DANIEL, R. T., PELLERIN, L., MAGISTRETTI, P. J. & ODDO, M. 2015. Neuroenergetic Response to Prolonged Cerebral Glucose Depletion after Severe Brain Injury and the Role of Lactate. *J Neurotrauma,* 32**,** 1560-6.

PELLERIN, L. & MAGISTRETTI, P. J. 1994. Glutamate uptake into astrocytes stimulates aerobic glycolysis: a mechanism coupling neuronal activity to glucose utilization. *Proc Natl Acad Sci U S A,* 91**,** 10625-9.

PELLERIN, L. & MAGISTRETTI, P. J. 2012. Sweet sixteen for ANLS. *J Cereb Blood Flow Metab,* 32**,** 1152-66.

PENG, W. G., ACHARIYAR, T. M., LI, B. M., LIAO, Y. H., MESTRE, H., HITOMI, E., REGAN, S., KASPER, T., PENG, S. S., DING, F. F., BENVENISTE, H., NEDERGAARD, M. & DEANE, R. 2016. Suppression of glymphatic fluid transport in a mouse model of Alzheimer's disease. *Neurobiology of Disease,* 93**,** 215-225.

PETERSON, C., GIGUERE, J. F., COTMAN, C. W. & BUTTERWORTH, R. F. 1990. Selective loss of N-methyl-D-aspartate-sensitive L-[3H]glutamate binding sites in rat brain following portacaval anastomosis. *J Neurochem,* 55**,** 386-90.

PHILIPS, B. J., ARMSTRONG, I. R., POLLOCK, A. & LEE, A. 1998. Cerebral blood flow and metabolism in patients with chronic liver disease undergoing orthotopic liver transplantation. *Hepatology,* 27**,** 369-76.

POPE, A. 1978. **Neuroglia: quantitative aspects. In (E. Schoffeniels, G. Franck, L. Hertz and D.B. Tower, eds.)** ***Dynamic Properties of Glia Cells, Pergamon Press, London,*****,** 13-20.

PRAKASH, R. & MULLEN, K. D. 2010. Mechanisms, diagnosis and management of hepatic encephalopathy. *Nat Rev Gastroenterol Hepatol,* 7**,** 515-25.

QUIST, A. P., RHEE, S. K., LIN, H. & LAL, R. 2000. Physiological role of gap-junctional hemichannels. Extracellular calcium-dependent isosmotic volume regulation. *J Cell Biol,* 148**,** 1063-74.

RACKAYOVA, V., BRAISSANT, O., MCLIN, V. A., BERSET, C., LANZ, B. & CUDALBU, C. 2016. 1H and 31P magnetic resonance spectroscopy in a rat model of chronic hepatic encephalopathy: in vivo longitudinal measurements of brain energy metabolism. *Metab Brain Dis,* 31**,** 1303-1314.

RAMA RAO, K. V., CHEN, M., SIMARD, J. M. & NORENBERG, M. D. 2003. Increased aquaporin-4 expression in ammonia-treated cultured astrocytes. *Neuroreport,* 14**,** 2379-82.

RAMA RAO, K. V. & NORENBERG, M. D. 2012. Brain energy metabolism and mitochondrial dysfunction in acute and chronic hepatic encephalopathy. *Neurochem Int,* 60**,** 697-706.

RAMON Y, C. S. 1909. Histologie du systeme nerveux de l'homme et des vertebres. *Maloine, Paris*.

RANGROO THRANE, V., THRANE, A. S., WANG, F., COTRINA, M. L., SMITH, N. A., CHEN, M., XU, Q., KANG, N., FUJITA, T., NAGELHUS, E. A. & NEDERGAARD, M. 2013. Ammonia triggers neuronal disinhibition and seizures by impairing astrocyte potassium buffering. *Nat Med,* 19**,** 1643-8.

RAO, K. V., MAWAL, Y. R. & QURESHI, I. A. 1997. Progressive decrease of cerebral cytochrome C oxidase activity in sparse-fur mice: role of acetyl-L-carnitine in restoring the ammonia-induced cerebral energy depletion. *Neurosci Lett,* 224**,** 83-6.

RAO, K. V. & NORENBERG, M. D. 2001. Cerebral energy metabolism in hepatic encephalopathy and hyperammonemia. *Metab Brain Dis,* 16**,** 67-78.

RETAMAL, M. A. 2014. Connexin and Pannexin hemichannels are regulated by redox potential. *Front Physiol,* 5**,** 80.

RIGGS, A. 1963. The Amino Acid Composition of Some Mammalian Hemoglobins: Mouse, Guinea Pig, and Elephant. *J Biol Chem,* 238**,** 2983-7.

RODRIGO, R., CAULI, O., GOMEZ-PINEDO, U., AGUSTI, A., HERNANDEZ-RABAZA, V., GARCIA-VERDUGO, J. M. & FELIPO, V. 2010. Hyperammonemia induces neuroinflammation that contributes to cognitive

impairment in rats with hepatic encephalopathy. *Gastroenterology,* 139**,** 675-84.

ROLANDO, N., WADE, J., DAVALOS, M., WENDON, J., PHILPOTT-HOWARD, J. & WILLIAMS, R. 2000. The systemic inflammatory response syndrome in acute liver failure. *Hepatology,* 32**,** 734-9.

ROS, J., PECINSKA, N., ALESSANDRI, B., LANDOLT, H. & FILLENZ, M. 2001. Lactate reduces glutamate-induced neurotoxicity in rat cortex. *J Neurosci Res,* 66**,** 790-4.

ROSE, C. 2002. Increased extracellular brain glutamate in acute liver failure: decreased uptake or increased release? *Metab Brain Dis,* 17**,** 251-61.

ROSE, C. 2006. Effect of ammonia on astrocytic glutamate uptake/release mechanisms. *J Neurochem,* 97 Suppl 1**,** 11-5.

ROSE, C., BUTTERWORTH, R. F., ZAYED, J., NORMANDIN, L., TODD, K., MICHALAK, A., SPAHR, L., HUET, P. M. & POMIER-LAYRARGUES, G. 1999. Manganese deposition in basal ganglia structures results from both portal-systemic shunting and liver dysfunction. *Gastroenterology,* 117**,** 640-4.

ROSE, C., KRESSE, W. & KETTENMANN, H. 2005. Acute insult of ammonia leads to calcium-dependent glutamate release from cultured astrocytes, an effect of pH. *J Biol Chem,* 280**,** 20937-44.

ROSE, C., YTREBO, L. M., DAVIES, N. A., SEN, S., NEDREDAL, G. I., BELANGER, M., REVHAUG, A. & JALAN, R. 2007. Association of reduced extracellular brain ammonia, lactate, and intracranial pressure in pigs with acute liver failure. *Hepatology,* 46**,** 1883-92.

ROSE, C. F. 2010. Increase brain lactate in hepatic encephalopathy: cause or consequence? *Neurochem Int,* 57**,** 389-94.

ROSE, C. F. 2012. Ammonia-lowering strategies for the treatment of hepatic encephalopathy. *Clin Pharmacol Ther,* 92**,** 321-31.

ROSE, C. R. & RANSOM, B. R. 1997. Gap junctions equalize intracellular Na+ concentration in astrocytes. *Glia,* 20**,** 299-307.

ROSSELLI, M., MACNAUGHTAN, J., JALAN, R. & PINZANI, M. 2013. Beyond scoring: a modern interpretation of disease progression in chronic liver disease. *Gut,* 62**,** 1234-41.

ROUACH, N., AVIGNONE, E., MEME, W., KOULAKOFF, A., VENANCE, L., BLOMSTRAND, F. & GIAUME, C. 2002. Gap junctions and connexin expression in the normal and pathological central nervous system. *Biol Cell,* 94**,** 457-75.

ROUACH, N., GLOWINSKI, J. & GIAUME, C. 2000. Activity-dependent neuronal control of gap-junctional communication in astrocytes. *J Cell Biol,* 149**,** 1513-26.

S. R. MCIVER, M. F., P. G. HAYDON, 2013. Neural-Immune Interactions in Brain Function and Alcohol Related Disorders. *In:* CUI, C., GRANDISON, LINDSEY, NORONHA, ANTONIO (ed.) *Astrocyte–Neuron Communications* New York: Springer Science+Business Media.

SAEZ, P. J., SHOJI, K. F., RETAMAL, M. A., HARCHA, P. A., RAMIREZ, G., JIANG, J. X., VON BERNHARDI, R. & SAEZ, J. C. 2013. ATP is required and advances cytokine-induced gap junction formation in microglia in vitro. *Mediators Inflamm,* 2013**,** 216402.

SAWHNEY, R., HOLLAND-FISCHER, P., ROSSELLI, M., MOOKERJEE, R. P., AGARWAL, B. & JALAN, R. 2016. Role of ammonia, inflammation, and

cerebral oxygenation in brain dysfunction of acute-on-chronic liver failure patients. *Liver Transpl,* 22**,** 732-42.

SCHLIESS, F., GORG, B., FISCHER, R., DESJARDINS, P., BIDMON, H. J., HERRMANN, A., BUTTERWORTH, R. F., ZILLES, K. & HAUSSINGER, D. 2002. Ammonia induces MK-801-sensitive nitration and phosphorylation of protein tyrosine residues in rat astrocytes. *FASEB J,* 16**,** 739-41.

SCHLIESS, F., SINNING, R., FISCHER, R., SCHMALENBACH, C. & HAUSSINGER, D. 1996. Calcium-dependent activation of Erk-1 and Erk-2 after hypo-osmotic astrocyte swelling. *Biochem J,* 320 (Pt 1)**,** 167-71.

SCHMIDT, W., WOLF, G., GRUNGREIFF, K., MEIER, M. & REUM, T. 1990. Hepatic encephalopathy influences high-affinity uptake of transmitter glutamate and aspartate into the hippocampal formation. *Metab Brain Dis,* 5**,** 19-31.

SCHOUSBOE, A., BAK, L. K. & WAAGEPETERSEN, H. S. 2013. Astrocytic Control of Biosynthesis and Turnover of the Neurotransmitters Glutamate and GABA. *Front Endocrinol (Lausanne),* 4**,** 102.

SCHURR, A., PAYNE, R. S., MILLER, J. J. & RIGOR, B. M. 1997. Brain lactate is an obligatory aerobic energy substrate for functional recovery after hypoxia: further in vitro validation. *J Neurochem,* 69**,** 423-6.

SHAWCROSS, D. & JALAN, R. 2005. The pathophysiologic basis of hepatic encephalopathy: central role for ammonia and inflammation. *Cell Mol Life Sci,* 62**,** 2295-304.

SHAWCROSS, D. L., DAVIES, N. A., WILLIAMS, R. & JALAN, R. 2004. Systemic inflammatory response exacerbates the neuropsychological effects of induced hyperammonemia in cirrhosis. *J Hepatol,* 40**,** 247-54.

SHAWCROSS, D. L., SHABBIR, S. S., TAYLOR, N. J. & HUGHES, R. D. 2010. Ammonia and the neutrophil in the pathogenesis of hepatic encephalopathy in cirrhosis. *Hepatology,* 51**,** 1062-9.

SHAWCROSS, D. L., WRIGHT, G., OLDE DAMINK, S. W. & JALAN, R. 2007. Role of ammonia and inflammation in minimal hepatic encephalopathy. *Metab Brain Dis,* 22**,** 125-38.

SKOWRONSKA, M., ZIELINSKA, M., WOJCIK-STANASZEK, L., RUSZKIEWICZ, J., MILATOVIC, D., ASCHNER, M. & ALBRECHT, J. 2012. Ammonia increases paracellular permeability of rat brain endothelial cells by a mechanism encompassing oxidative/nitrosative stress and activation of matrix metalloproteinases. *J Neurochem,* 121**,** 125-34.

SOBEL, R. A., DEARMOND, S. J., FORNO, L. S. & ENG, L. F. 1981. Glial fibrillary acidic protein in hepatic encephalopathy. An immunohistochemical study. *J Neuropathol Exp Neurol,* 40**,** 625-32.

SOFRONIEW, M. V. & VINTERS, H. V. 2010. Astrocytes: biology and pathology. *Acta Neuropathol,* 119**,** 7-35.

SOHL, G. & WILLECKE, K. 2004. Gap junctions and the connexin protein family. *Cardiovasc Res,* 62**,** 228-32.

SQUIRE, L. R., OJEMANN, J. G., MIEZIN, F. M., PETERSEN, S. E., VIDEEN, T. O. & RAICHLE, M. E. 1992. Activation of the hippocampus in normal humans: a functional anatomical study of memory. *Proc Natl Acad Sci U S A,* 89**,** 1837-41.

STRAUSS, G. I., HANSEN, B. A., HERZOG, T. & LARSEN, F. S. 2000. Cerebral autoregulation in patients with end-stage liver disease. *Eur J Gastroenterol Hepatol,* 12**,** 767-71.

SUAREZ, I., BODEGA, G. & FERNANDEZ, B. 2000. Modulation of glutamate transporters (GLAST, GLT-1 and EAAC1) in the rat cerebellum following portocaval anastomosis. *Brain Res,* 859**,** 293-302.

SUN, M. K. & REIS, D. J. 1994. Hypoxia selectively excites vasomotor neurons of rostral ventrolateral medulla in rats. *Am J Physiol,* 266**,** R245-56.

TANG, F., LANE, S., KORSAK, A., PATON, J. F., GOURINE, A. V., KASPAROV, S. & TESCHEMACHER, A. G. 2014. Lactate-mediated glia-neuronal signalling in the mammalian brain. *Nat Commun,* 5**,** 3284.

THRANE, A. S., RANGROO THRANE, V. & NEDERGAARD, M. 2014. Drowning stars: reassessing the role of astrocytes in brain edema. *Trends Neurosci,* 37**,** 620-8.

TIAN, F., GOURINE, A. V., HUCKSTEPP, R. T. & DALE, N. 2009. A microelectrode biosensor for real time monitoring of L-glutamate release. *Anal Chim Acta,* 645**,** 86-91.

TREXLER, E. B., BUKAUSKAS, F. F., BENNETT, M. V., BARGIELLO, T. A. & VERSELIS, V. K. 1999. Rapid and direct effects of pH on connexins revealed by the connexin46 hemichannel preparation. *J Gen Physiol,* 113**,** 721-42.

TSACOPOULOS, M. & MAGISTRETTI, P. J. 1996. Metabolic coupling between glia and neurons. *J Neurosci,* 16**,** 877-85.

TUETTENBERG, J., HEIMANN, A. & KEMPSKI, O. 2001. Nitric oxide modulates cerebral blood flow stimulation by acetazolamide in the rat cortex: a laser Doppler scanning study. *Neurosci Lett,* 315**,** 65-8.

TUROVSKY, E., KARAGIANNIS, A., ABDALA, A. P. & GOURINE, A. V. 2015. Impaired CO2 sensitivity of astrocytes in a mouse model of Rett syndrome. *J Physiol,* 593**,** 3159-68.

VANDENBERG, R. J. & RYAN, R. M. 2013. Mechanisms of glutamate transport. *Physiol Rev,* 93**,** 1621-57.

VAQUERO, J. & BUTTERWORTH, R. F. 2006. The brain glutamate system in liver failure. *J Neurochem,* 98**,** 661-9.

VENKAT, P., CHOPP, M. & CHEN, J. 2016. New insights into coupling and uncoupling of cerebral blood flow and metabolism in the brain. *Croat Med J,* 57**,** 223-8.

VORSTRUP, S., HENRIKSEN, L. & PAULSON, O. B. 1984. Effect of acetazolamide on cerebral blood flow and cerebral metabolic rate for oxygen. *J Clin Invest,* 74**,** 1634-9.

WAKIM-FLEMING, J. 2011. Hepatic encephalopathy: suspect it early in patients with cirrhosis. *Cleve Clin J Med,* 78**,** 597-605.

WALLRAFF, A., KOHLING, R., HEINEMANN, U., THEIS, M., WILLECKE, K. & STEINHAUSER, C. 2006. The impact of astrocytic gap junctional coupling on potassium buffering in the hippocampus. *J Neurosci,* 26**,** 5438-47.

WANG, K., SMITH, Z. M., BUXTON, R. B., SWENSON, E. R. & DUBOWITZ, D. J. 2015. Acetazolamide during acute hypoxia improves tissue oxygenation in the human brain. *J Appl Physiol (1985),* 119**,** 1494-500.

WATANABE, A., TAKEI, N., HIGASHI, T., SHIOTA, T., NAKATSUKASA, H., FUJIWARA, M., SAKATA, T. & NAGASHIMA, H. 1984. Glutamic acid and glutamine levels in serum and cerebrospinal fluid in hepatic encephalopathy. *Biochem Med,* 32**,** 225-31.

WEISS, N., BARBIER SAINT HILAIRE, P., COLSCH, B., ISNARD, F., ATTALA, S., SCHAEFER, A., AMADOR, M. D., RUDLER, M., LAMARI, F., SEDEL, F., THABUT, D. & JUNOT, C. 2016. Cerebrospinal fluid metabolomics highlights

dysregulation of energy metabolism in overt hepatic encephalopathy. *J Hepatol,* 65**,** 1120-1130.

WILLEBRORDS, J., CRESPO YANGUAS, S., MAES, M., DECROCK, E., WANG, N., LEYBAERT, L., KWAK, B. R., GREEN, C. R., COGLIATI, B. & VINKEN, M. 2016. Connexins and their channels in inflammation. *Crit Rev Biochem Mol Biol,* 51**,** 413-439.

WRIGHT, G., DAVIES, N. A., SHAWCROSS, D. L., HODGES, S. J., ZWINGMANN, C., BROOKS, H. F., MANI, A. R., HARRY, D., STADLBAUER, V., ZOU, Z., WILLIAMS, R., DAVIES, C., MOORE, K. P. & JALAN, R. 2007. Endotoxemia produces coma and brain swelling in bile duct ligated rats. *Hepatology,* 45**,** 1517-26.

XIE, L., KANG, H., XU, Q., CHEN, M. J., LIAO, Y., THIYAGARAJAN, M., O'DONNELL, J., CHRISTENSEN, D. J., NICHOLSON, C., ILIFF, J. J., TAKANO, T., DEANE, R. & NEDERGAARD, M. 2013. Sleep drives metabolite clearance from the adult brain. *Science,* 342**,** 373-7.

YANG, L., KRESS, B. T., WEBER, H. J., THIYAGARAJAN, M., WANG, B., DEANE, R., BENVENISTE, H., ILIFF, J. J. & NEDERGAARD, M. 2013. Evaluating glymphatic pathway function utilizing clinically relevant intrathecal infusion of CSF tracer. *J Transl Med,* 11**,** 107.

YAO, H., SADOSHIMA, S., FUJII, K., KUSUDA, K., ISHITSUKA, T., TAMAKI, K. & FUJISHIMA, M. 1987. Cerebrospinal fluid lactate in patients with hepatic encephalopathy. *Eur Neurol,* 27**,** 182-7.

YE, Z. C., OBERHEIM, N., KETTENMANN, H. & RANSOM, B. R. 2009. Pharmacological "cross-inhibition" of connexin hemichannels and swelling activated anion channels. *Glia,* 57**,** 258-69.

YEMISCI, M., GURSOY-OZDEMIR, Y., VURAL, A., CAN, A., TOPALKARA, K. & DALKARA, T. 2009. Pericyte contraction induced by oxidative-nitrative stress impairs capillary reflow despite successful opening of an occluded cerebral artery. *Nat Med,* 15**,** 1031-7.

YTREBO, L. M., KRISTIANSEN, R. G., MAEHRE, H., FUSKEVAG, O. M., KALSTAD, T., REVHAUG, A., COBOS, M. J., JALAN, R. & ROSE, C. F. 2009. L-ornithine phenylacetate attenuates increased arterial and extracellular brain ammonia and prevents intracranial hypertension in pigs with acute liver failure. *Hepatology,* 50**,** 165-74.

ZEMTSOVA, I., GORG, B., KEITEL, V., BIDMON, H. J., SCHROR, K. & HAUSSINGER, D. 2011. Microglia activation in hepatic encephalopathy in rats and humans. *Hepatology,* 54**,** 204-15.

ZHANG, C., BELANGER, S., POULIOT, P. & LESAGE, F. 2015. Measurement of Local Partial Pressure of Oxygen in the Brain Tissue under Normoxia and Epilepsy with Phosphorescence Lifetime Microscopy. *PLoS One,* 10**,** e0135536.

ZHANG, L. J., YANG, G., YIN, J., LIU, Y. & QI, J. 2007. Neural mechanism of cognitive control impairment in patients with hepatic cirrhosis: a functional magnetic resonance imaging study. *Acta Radiol,* 48**,** 577-87.

ZWINGMANN, C. 2007. The anaplerotic flux and ammonia detoxification in hepatic encephalopathy. *Metab Brain Dis,* 22**,** 235-49.